PHASE 1 WIND STUDIES REPORT

ENVIRONMENTAL STUDIES AND PRELIMINARY DESIGN
FOR A SUICIDE DETERRENT SYSTEM

Contract 2006-B-17

24 MAY 2007

Golden Gate Bridge
Highway and Transportation District

This report was developed by the following organizations with much support from the Golden Gate Bridge, Highway and Transportation District:

DMJM Harris
Oakland CA

Maunsell
Hong Kong China

CirclePoint
San Franciso CA

JRP Historical Consultants
Davis CA

Macdonald Architects
San Francisco CA

West Wind Laboratory
Marina CA

24 May 2007

TABLE OF CONTENTS

ENVIRONMENTAL STUDIES AND PRELIMINARY DESIGN FOR A SUICIDE DETERRENT SYSTEM ON THE GOLDEN GATE BRIDGE

PHASE 1 WIND STUDIES REPORT EXECUTIVE SUMMARY

Introduction

On September 22, 2006, the Golden Gate Bridge, Highway and Transportation District (District) Board of Directors (Board) authorized the commencement of environmental studies and preliminary design work for a Suicide Deterrent System on the Golden Gate Bridge (Bridge). This is a two-phased effort.

Phase 1 of this effort is wind tunnel testing and analysis of generic suicide deterrent concepts. Phase 1 is now complete and the results are contained herein.

Phase 2 will take the Phase 1 generic concepts that passed the wind test and develop potential alternatives for further evaluation. Phase 2 will include both the required federal and state environmental review processes of each potential alternative and will include preliminary engineering of the potential alternatives. The potential alternatives will also be evaluated against each of the Suicide Deterrent Study Criteria that was adopted by the Board, and for the anticipated environmental affects. The required evaluation of potential alternatives will consider both a "no-build" alternative as well as several "build" alternatives.

Wind and Long-Span Bridges

Long span suspension bridges are flexible structures that respond dynamically and potentially dramatically to wind. The original design of the Golden Gate Bridge provides

for the roadway deck of the Bridge to move a considerable amount. At the mid-point between the towers the deck was designed to move approximately six feet down, ten feet up and sideways about twenty-seven feet. This flexibility allows the Bridge to move during wind and earthquake events.

The cross section of the Bridge at the roadway consists of a stiffening truss, roadway deck and railing as depicted in the photographs above. The shape of the Bridge cross section has a significant impact on the Bridge's aerodynamic stability during high winds. Minor alterations to the shape of the Bridge including changes to the stiffening truss, roadway deck or railing will affect the aerodynamic form of the Bridge which changes how it moves during strong wind.

The movement of long span suspension bridges due to wind was most memorably demonstrated by the Tacoma-Narrows Bridge failure. On the day of its collapse in 1940, a 40 mph sustained wind applied at just the right angle caused the bridge to vibrate, resulting in wave motions and twisting of the deck that far exceeded the normal movement of the bridge. This motion grew continuously over a period of a few hours, ultimately leading to the collapse of the bridge.

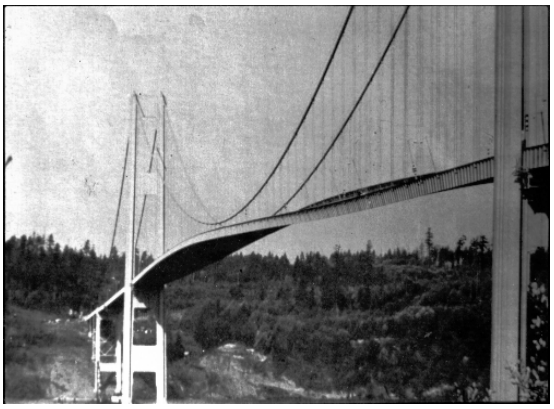

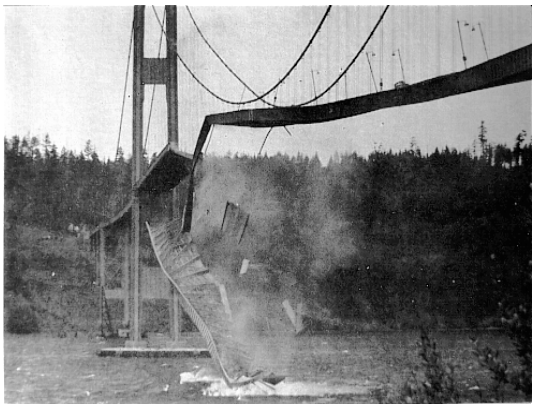

Tacoma-Narrows Bridge Failure

The sensitivity of a suspension bridge to wind is most pronounced between the two main towers, where the bridge is most flexible, as evidenced in the above two photographs of the Tacoma-Narrows Bridge. The flexibility of the Tacoma-Narrows Bridge and the shape of its roadway cross section combined to make it highly unstable to relatively low wind speeds.

As a result of the ensuing studies after the Tacoma-Narrows collapse, engineers have a greater understanding of how wind affects long span bridges like the Golden Gate Bridge, and what factors will determine whether or not a particular bridge will remain stable when subjected to high winds. Wind tunnel testing is now performed on models of all new long span suspension bridges to determine how sensitive the proposed bridge cross

section is to wind and ensure that an event such as the Tacoma-Narrows Bridge failure does not occur.

Golden Gate Bridge Wind Testing – Overview

Any modifications to the existing railings or any additional netting added on the Golden Gate Bridge will affect how the Bridge responds to strong wind. Wind tunnel testing and complex computer analyses were performed on potential modifications to the Golden Gate Bridge to determine which modifications do not result in problems during strong winds. Wind tunnel testing was performed using a geometrically accurate 1:50 scale model of a portion of the Bridge deck.

Golden Gate Bridge Test Model - West Wind Laboratory

The District has established the wind design criteria for the Golden Gate Bridge consistent with that used in the design of new long span bridges. That is the Bridge, with any contemplated suicide deterrent system installed, should remain stable for wind speeds that are expected to occur once every 10,000 years. Previous meteorological studies of high winds in the San Francisco area and the bridge site in particular determined the wind speeds associated with this probability as 100 mph for winds blowing from the west, and 66 mph for winds from the east. These wind speeds are an average wind speed over a ten minute interval. The prevailing wind direction at the Bridge is from the west, so this is why the speed is higher from the west for the 10,000 year wind.

The wind tunnel testing considered a range of variables for three different generic concepts. The generic concepts consisted of the following:

1. Add on to the existing railing
2. Replace the existing railing
3. Add a netting system that extends out horizontally from the Bridge

The variables included:

1. Different heights (8 feet to 14 feet)
2. Different "solids ratios"
3. Different types of "wind devices" to achieve the wind design criteria

In total, over 70 different variations of these generic concepts were tested. In accordance with the Board criteria, each of these generic concepts that met the design criteria was also tested with a moveable median barrier in all possible lane configurations (7 lane configurations per concept). This resulted in the performance of approximately 200 individual wind tunnel tests.

The heights tested varied from 8 ft to 14 ft for generic concepts in the first two categories (tall railing systems); extensions of 10 ft were considered for horizontal netting concepts. These dimensions were selected after reviewing barriers that have been implemented at other facilities.

Wind Tunnel Testing indicated that each generic concept has a different maximum solid ratio that satisfies the wind criteria.

Solid ratio is defined as the total area of all solid components of the railing, divided by the total area of the railing (length x height); an example depicting this calculation is shown below.

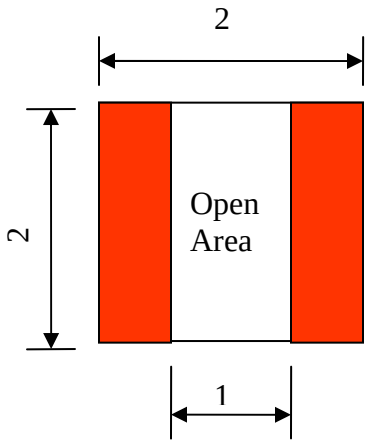

Solid Ratio % = (Solid Area) / (Total Area) x 100

Solid Area = 2 x 1 = 2
Total Area = 2 x 2 = 4

Solid Ratio = 2/4 x 100 = **50%**

The wind tunnel testing confirmed that additions to the Bridge were very susceptible to wind since the solid ratio of acceptable generic concepts varied from between 12 and 23 percent.

Initial testing of generic concepts revealed that all concepts require the installation of a wind device in order to meet the stated wind criteria. Wind devices are components that are added to the Bridge so the various concepts can achieve the wind design criteria. From the perspective of bridge users there are two types of wind devices: visible and hidden from view; while technically, there are two different types of wind devices which work in fundamentally different ways: “fairings” and “winglets”.

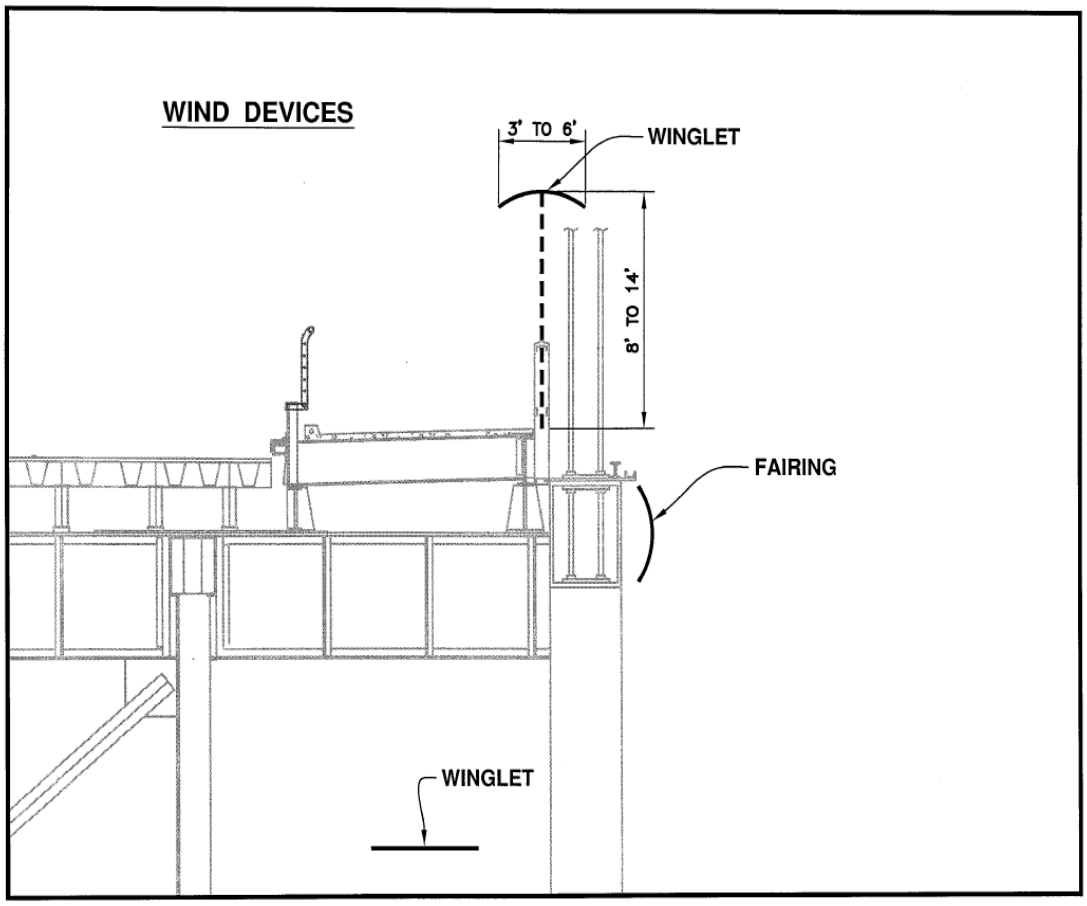

Cross Section Depicting Wind Devices

Fairings are wind devices that are added to the side of the Bridge and work in concert with a replacement railing that is less solid and more aerodynamically efficient. The fairings act to bring the airflow around and over the top of the stiffening truss more efficiently and in a streamlined fashion which reduces the energy input into the Bridge due to wind and lessens the resulting movement of the Bridge.

Winglets are in essence airfoils or small wings. They are non-adjustable surfaces that generate lift. As the wind speed increases, the generated lift increases. The force of the

lift resists the tendency of the bridge to twist in strong wind. This is referred to as aerodynamic damping. When winglets are used they must minimally be positioned between the towers where there is the greatest twisting in strong wind.

Results & Conclusions

Wind tunnel testing and analysis has determined the combinations of height, solid ratio and wind devices for all three generic concepts that will comply with the established wind stability criteria for the Golden Gate Bridge. Testing has further confirmed that these concepts will not prevent the future installation of a moveable median barrier system, meaning that wind stability will still be achieved if and when a moveable median barrier is implemented.

The parameters defining each generic concept are summarized below. Sketches and examples illustrating these concepts are immediately following this Executive Summary.

Generic Concept Type 1 – Add on to the Existing Railing

The existing railing is comprised of pickets between a top and bottom rail. Though it appears that the existing railing is open and will allow wind to pass through, in actuality the railing is 60 percent solid. This presents a challenge for concepts that add on to the existing railing.

In order to satisfy the wind criteria while keeping the existing railing it is necessary to have a winglet on top of the railing as depicted in Figure 1.1. Hidden wind devices do not work.

The width of the winglet decreases as the height of the railing increases. This arises because the air at a higher level above the deck is less disturbed and is more streamlined which results in the winglet being more efficient.

A range of heights between 10 and 14 feet tall was satisfactorily tested.

The testing indicated that any addition to the existing railing must be very open so that the wind can easily pass through. The testing determined that the addition must have no more than 12 percent solids.

Figures 1.2a through 1.4b provide illustrative examples of how this concept might look, using various components.

Generic Concept Type 2 – Existing Railing replaced with New Railing

The removal of the existing railing provides much greater latitude in the design for this concept as compared to the first concept. The replacement concept can have a solid ratio of up to 23 percent. A sensitivity analysis was performed which indicates that the "vertical" replacement railing can be tilted 20 degrees inboard or outboard from the vertical upright position with no appreciable change in the wind response of the Bridge.

The removal of the existing railing provides more options for acceptable wind devices. Testing has confirmed that this concept can be implemented in combination with any one of the wind devices developed:

- Two below deck winglets, positioned underneath the east sidewalk and a winglet that functions as a "catwalk" (or maintenance walkway) positioned under the west sidewalk. This is depicted in Figure 2.1; Figures 2.2a through 2.4b provide illustrative examples of how this concept might look with this wind device.
- Wind fairings placed on the outer vertical face of the west stiffening truss and on the outside face of the west sidewalk as depicted in Figure 2.5; Figures 2.6a and 2.6b show an example that incorporates vertical glass blades.
- Above deck "winglets" (the width of the winglet varies with the height above deck) as depicted in Figure 2.7; Figures 2.8a through 2.9b show examples depicting this concept and wind device.

A range of heights between 8 and 14 feet tall was tested with satisfactory results with the above mentioned wind devices and maximum solid ratio.

Generic Concept Type 3 – Add a Netting System that extends out Horizontally from the Bridge

It was surprisingly difficult to arrive at acceptable net options. Netting systems that extend out horizontally disturb the airflow as it approaches the top of the stiffening truss and railing. To satisfy the wind criteria with horizontal netting it is necessary to replace the existing railing between the main towers with a less solid and more aerodynamically efficient railing and it is necessary to add winglets. The addition of fairings to this concept did not satisfy the wind design criteria.

Previously, the District performed studies in order to incorporate modifications to enhance the wind stability of the Bridge in the seismic retrofit program. As part of this effort the District developed a design for a "replicated" railing. The replicated railing uses the same structural elements as the existing railing for the support posts and top rail cap, but with new ¼ inch plate verticals spaced 6 inches on center replacing the existing pickets. The Phase 3 Seismic Retrofit design incorporates the replacement of the railing on the west sidewalk between the two main towers with the replicated railing and adds fairings on the west side between the two main towers.

This replicated railing, which has a maximum solid ratio of 23 percent, was successfully tested with a net system that had a maximum solid ratio of 16 percent coupled with winglets. Both above deck and below deck winglets worked with this combination. Both the replicated railing and the winglets are only necessary between the two main towers, not along the entire length of the Bridge. Figure 3.1 depicts the acceptable net parameters with the below deck winglets.

Figure 3.2a through Figure 3.3b illustrate net concepts with hidden wind devices. Sketches of net options that incorporate an above deck winglet were not prepared, because any visual advantage of a net option would be obviated by the above deck winglets.

EXECUTIVE SUMMARY – CONCEPT FIGURES

CONCEPT 1: ADDING TO THE EXISTING RAILING TO INCREASE ITS HEIGHT

CONCEPT 2: AN ALL NEW VERTICAL BARRIER/RAILING SYSTEM

Concepts with no above deck aerodynamic elements

# # # # #

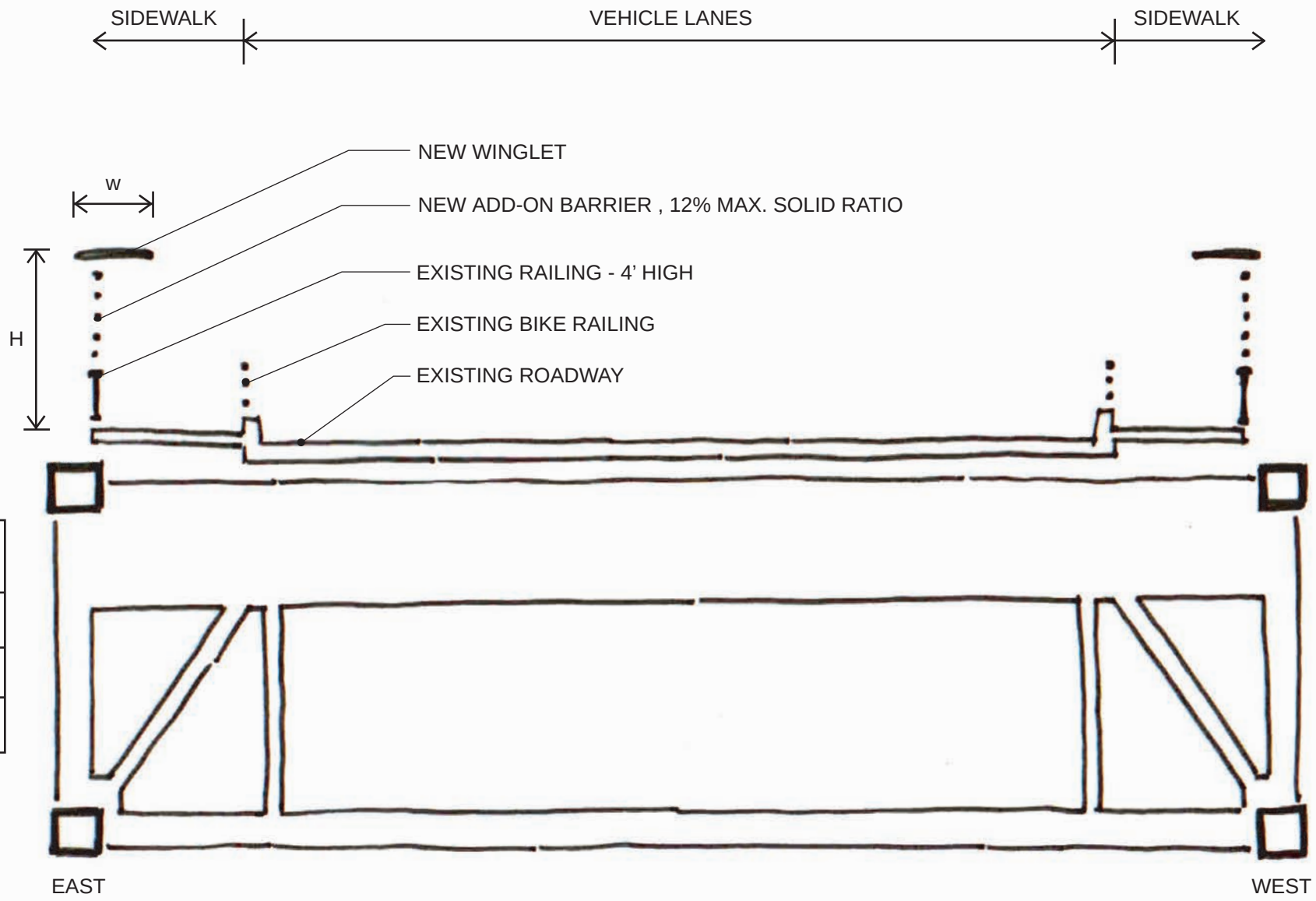

H (FT.)	W (IN.)
10	72
12	64
14	64

FIGURE 1.1 - CONCEPT 1 : ADDING TO THE EXISTING RAILING
SCALE : NOT TO SCALE

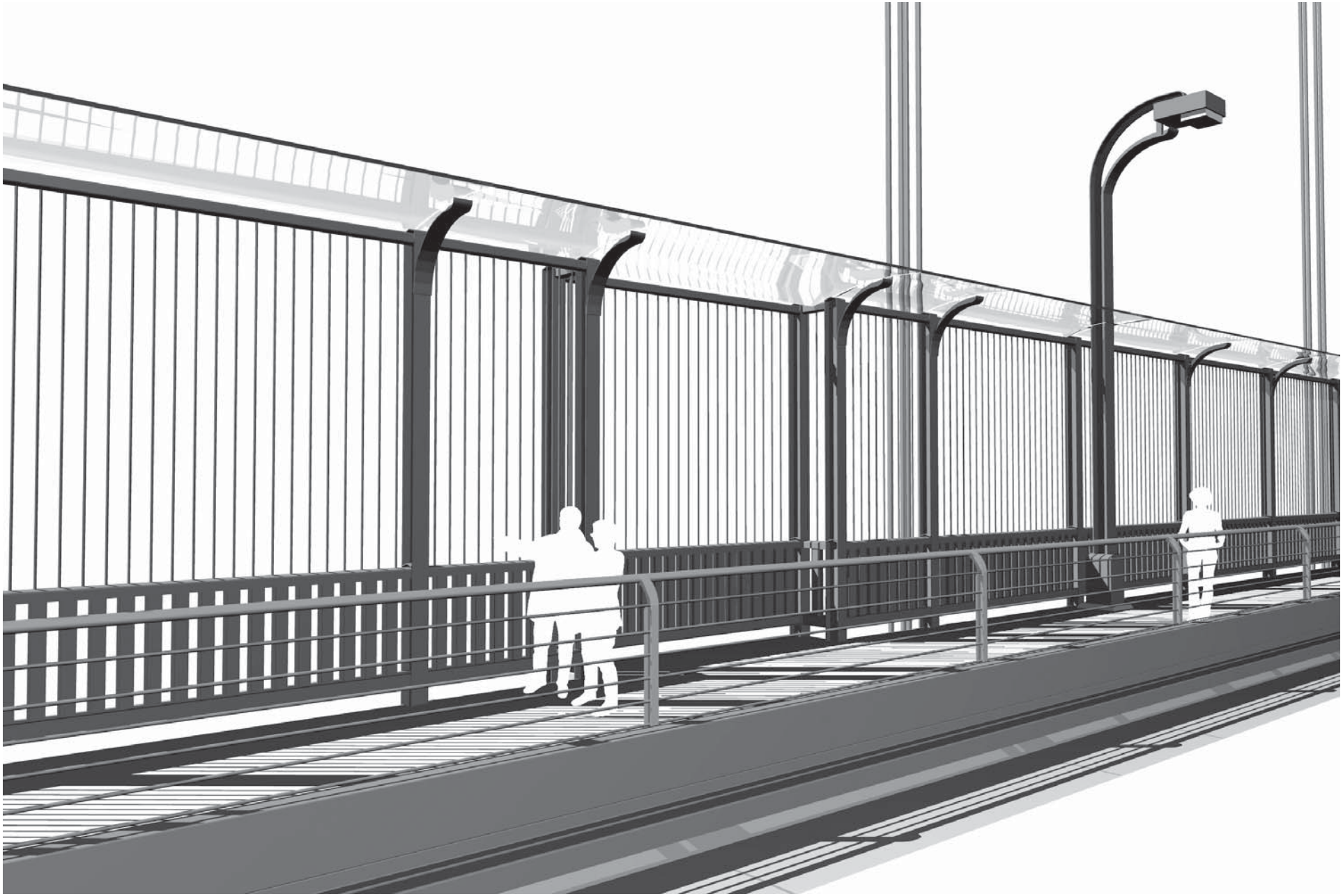

FIGURE 1.2a - EXAMPLE OF CONCEPT 1 (EXAMPLE SHOWN WITH HEIGHT OF 14’-0” TRANSPARENT WINGLET OF 64”, VERTICAL MEMBERS SPACED AT 6”, SOLID RATIO OF 12%) *VIEW FROM ROADWAY*

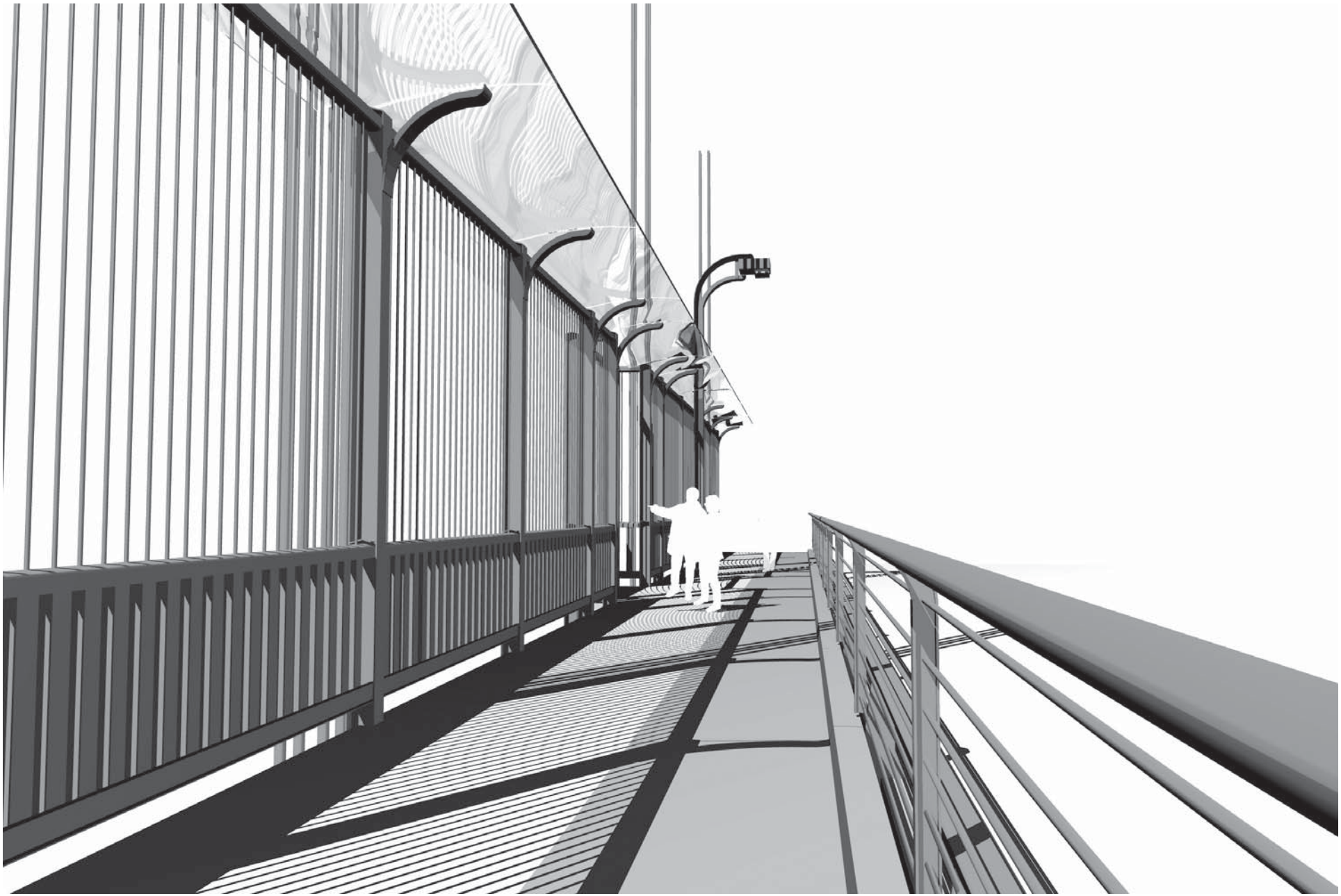

FIGURE 1.2b - EXAMPLE OF CONCEPT 1 (EXAMPLE SHOWN WITH HEIGHT OF 14’-0” TRANSPARENT WINGLET OF 64”, VERTICAL MEMBERS SPACED AT 6”, SOLID RATIO OF 12%) *VIEW FROM SIDEWALK*

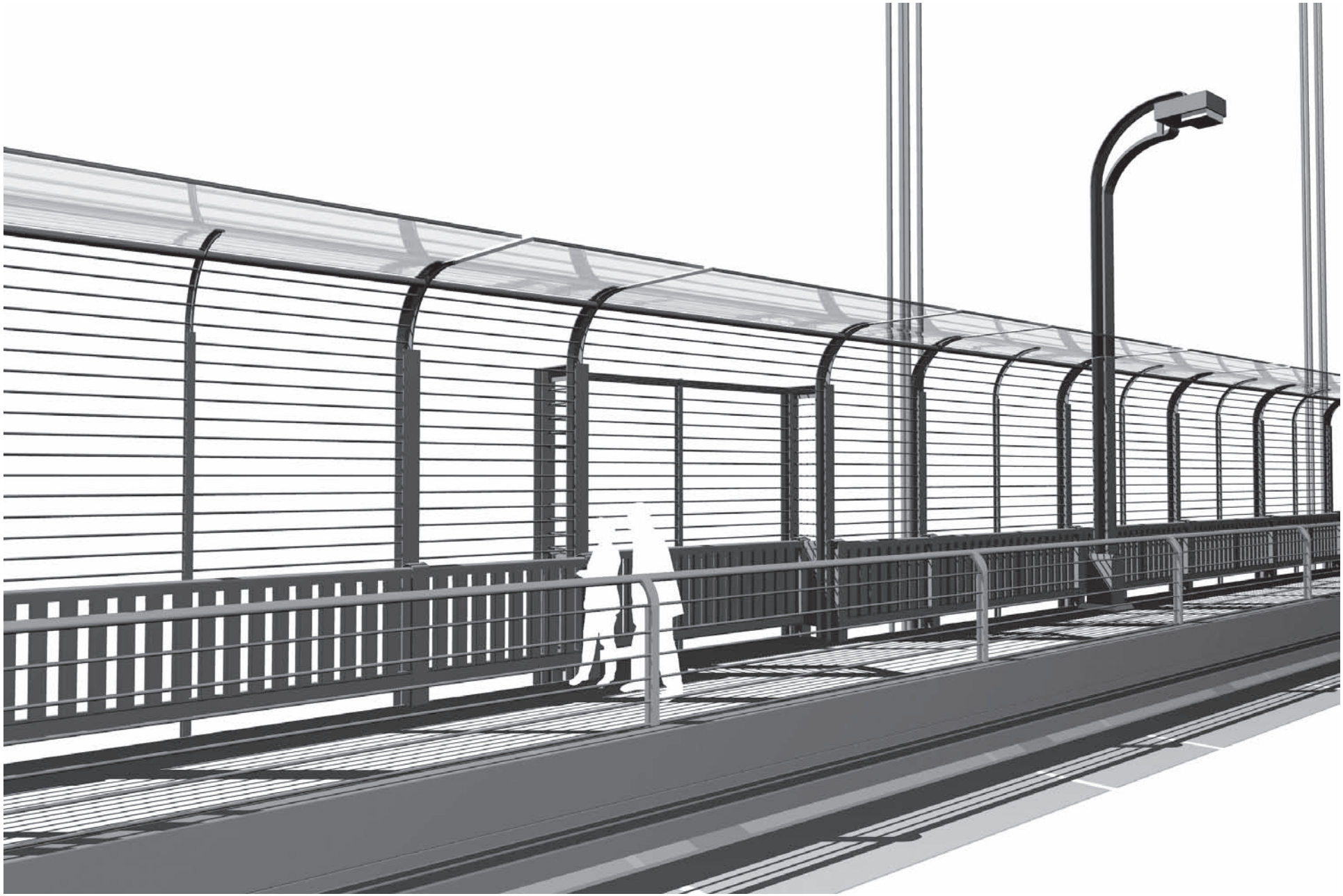

FIGURE 1.3a - EXAMPLE OF CONCEPT 1 (EXAMPLE SHOWN WITH HEIGHT OF 12’-0” TRANSPARENT WINGLET OF 64”, HORIZONTAL MEMBERS SPACED AT 6”, SOLID RATIO OF 9%) *VIEW FROM ROADWAY*

FIGURE 1.3b - EXAMPLE OF CONCEPT 1 (EXAMPLE SHOWN WITH HEIGHT OF 12’-0” TRANSPARENT WINGLET OF 64”, HORIZONTAL MEMBERS SPACED AT 6”, SOLID RATIO OF 9%) *VIEW FROM SIDEWALK*

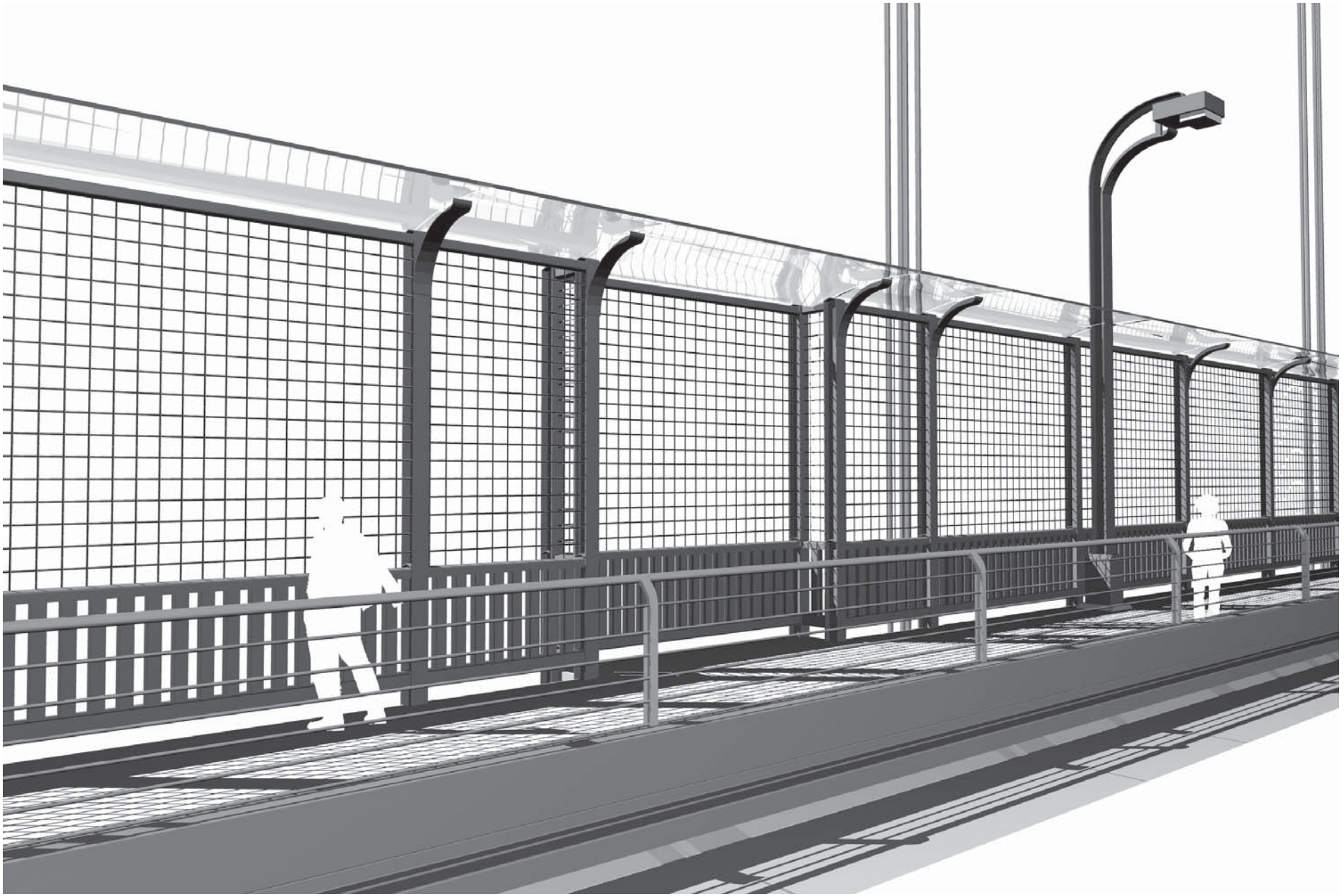

FIGURE 1.4a - EXAMPLE OF CONCEPT 1 (EXAMPLE SHOWN WITH HEIGHT OF 14’-0” TRANSPARENT WINGLET OF 64”, VERTICAL AND HORIZONTAL WIRE MESH OF 6”, SOILD RATIO OF 11%) *VIEW FROM ROADWAY*

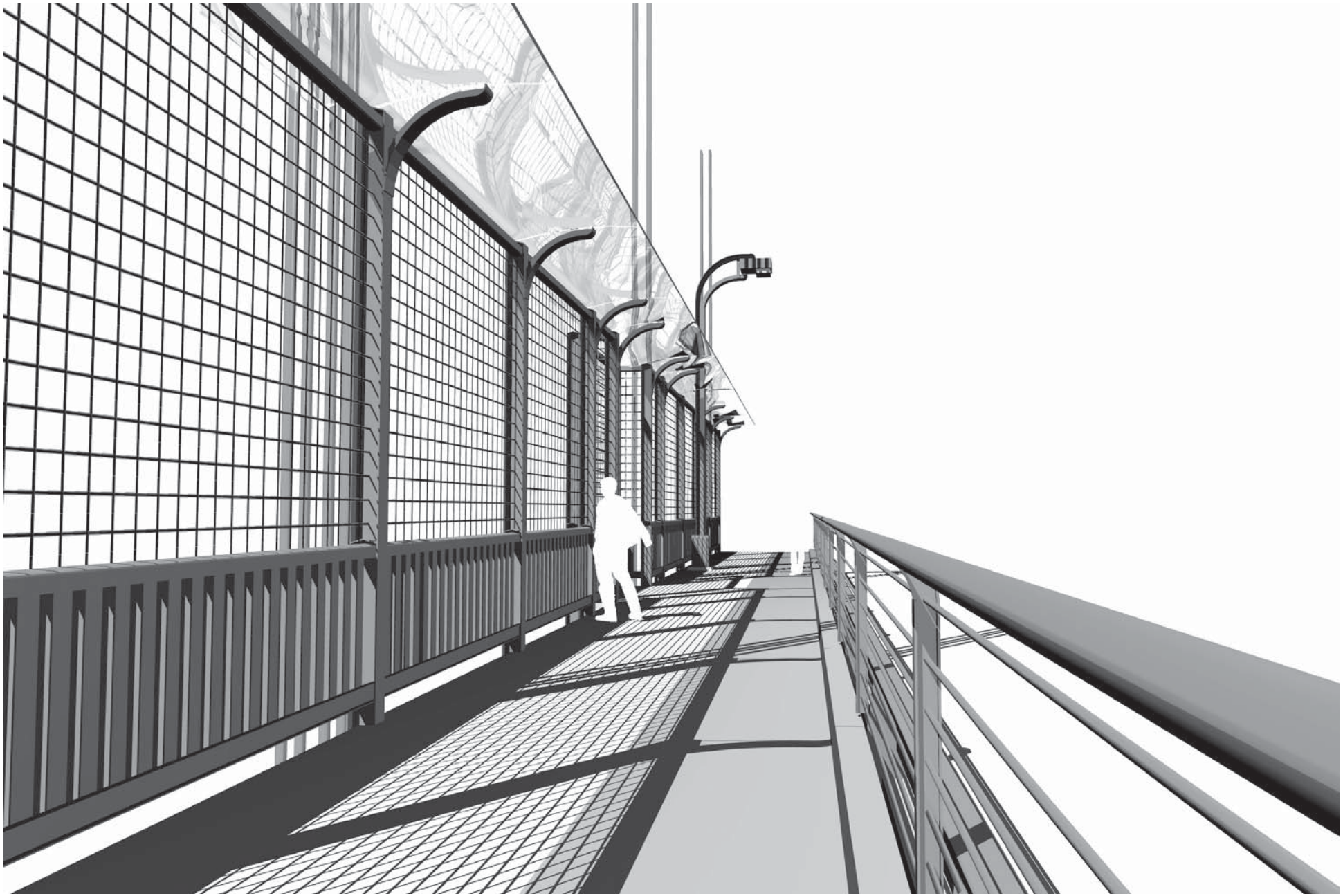

FIGURE 1.4b - EXAMPLE OF CONCEPT 1 (EXAMPLE SHOWN WITH HEIGHT OF 14’-0” TRANSPARENT WINGLET OF 64”, VERTICAL AND HORIZONTAL WIRE MESH OF 6”, SOILD RATIO OF 11%) *VIEW FROM SIDEWALK*

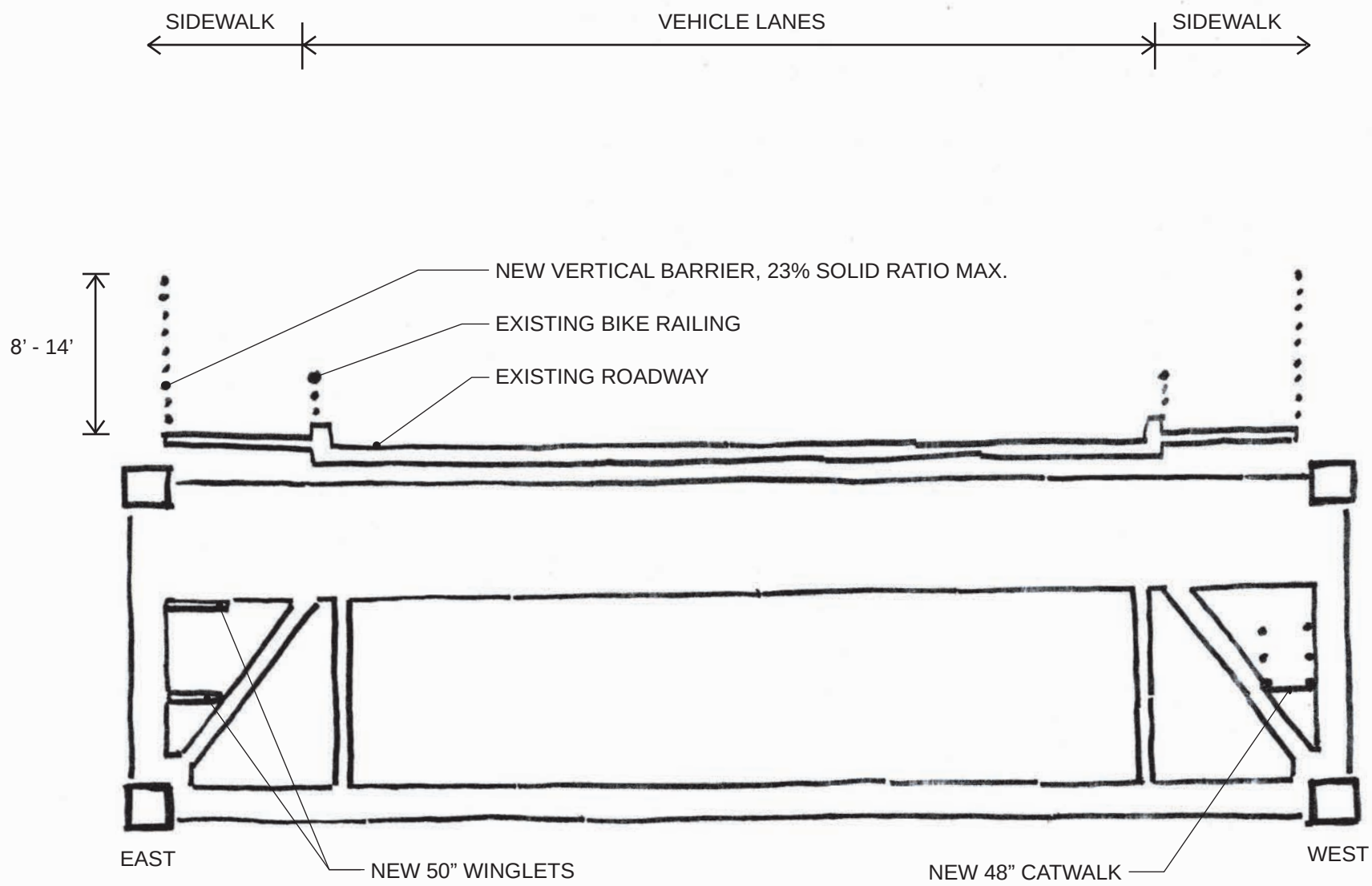

FIGURE 2.1 - CONCEPT 2 : REPLACING THE EXISTING RAILING; WINGLETS UNDER DECK

SCALE : NOT TO SCALE8

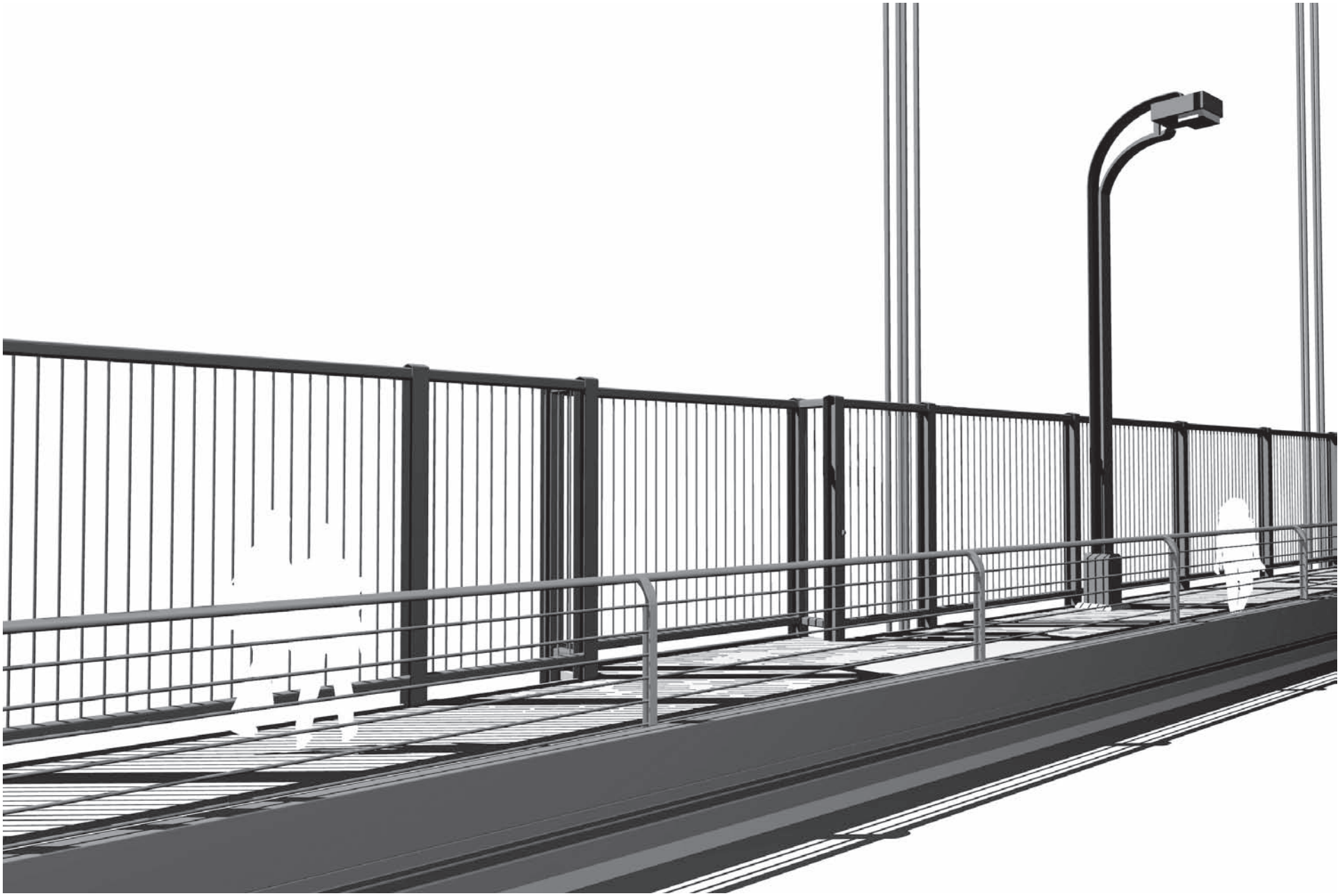

FIGURE 2.2a - EXAMPLE OF CONCEPT 2 (EXAMPLE SHOWN WITH HEIGHT OF 10’-0”, NO VISIBLE WINGLET ; 50” UNDER DECK WINGLET ON EAST SIDE AND 48” CATWALK ON WEST SIDE, VERTICAL ROD MEMBERS SPACED AT 6”, SOLID RATIO OF 18%)
VIEW FROM ROADWAY

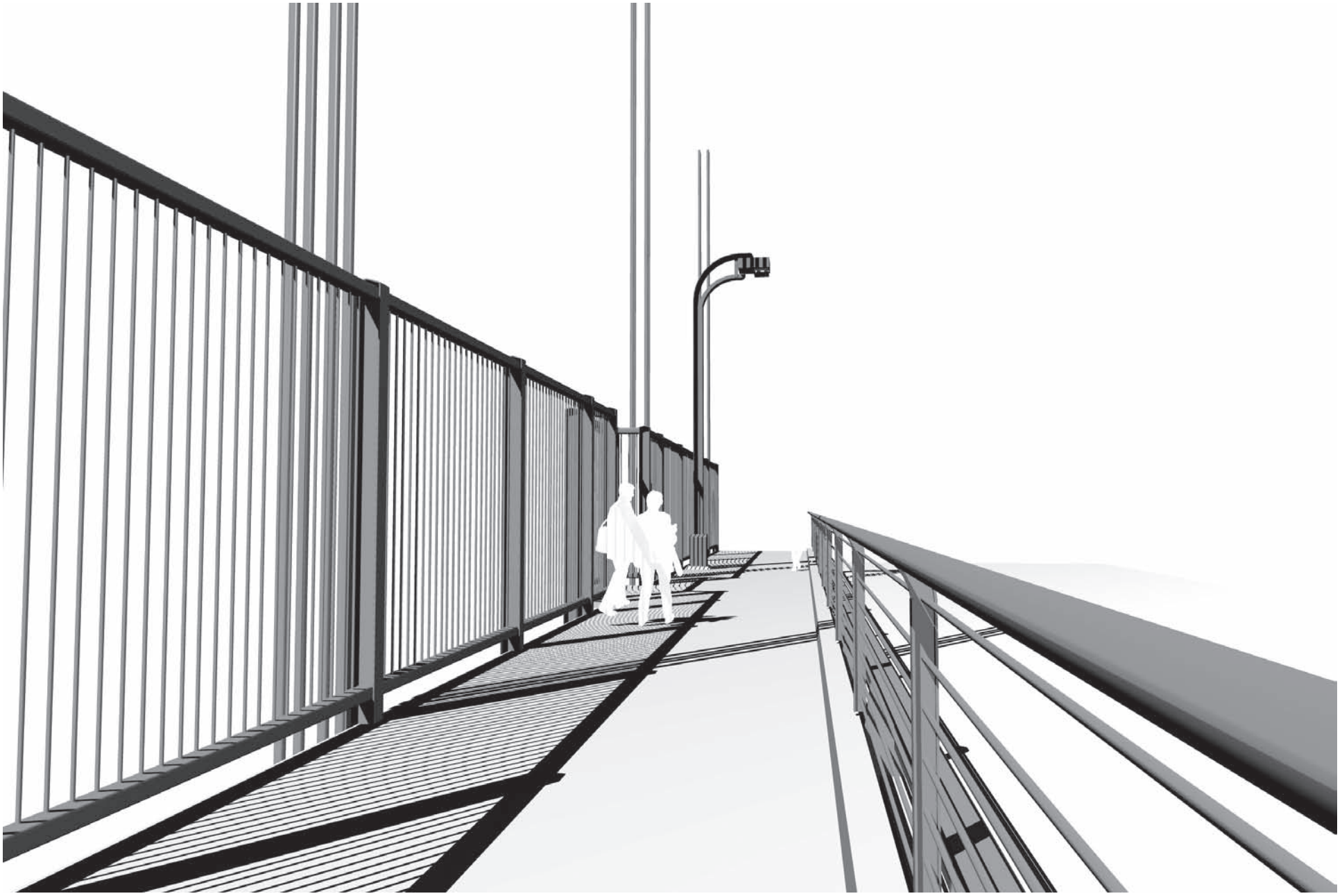

FIGURE 2.2b - EXAMPLE OF CONCEPT 2 (EXAMPLE SHOWN WITH HEIGHT OF 10’-0”, NO VISIBLE WINGLET; 50” UNDER DECK WINGLET ON EAST SIDE AND 48” CATWALK ON WEST SIDE, VERTICAL ROD MEMBERS SPACED AT 6”, SOLID RATIO OF 18%)
VIEW FROM SIDEWALK

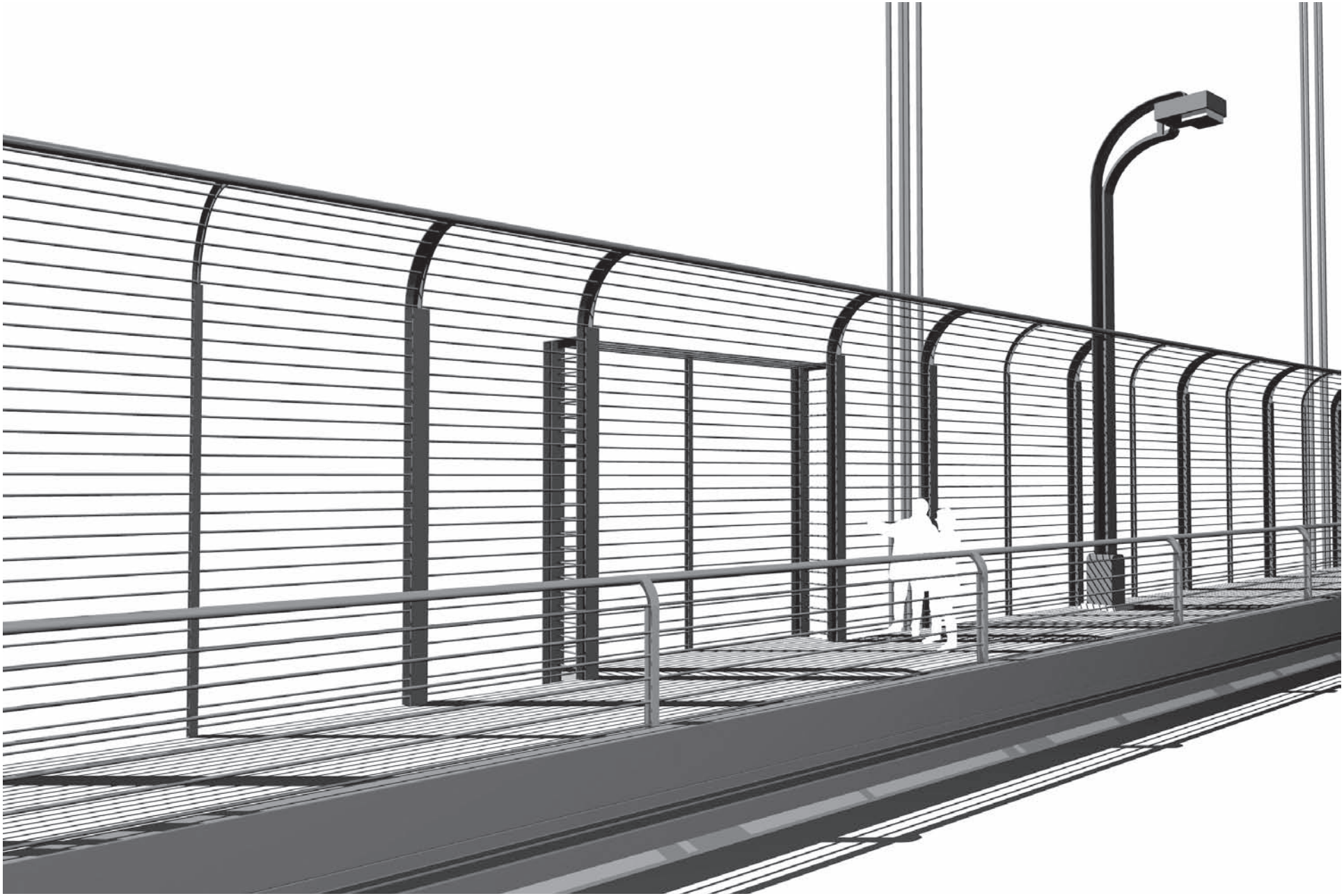

FIGURE 2.3a - EXAMPLE OF CONCEPT 2 (EXAMPLE SHOWN WITH HEIGHT OF 14’-0”, NO VISIBLE WINGLET; 50” UNDER DECK WINGLET ON EAST SIDE AND 48” CATWALK ON WEST SIDE, CURVED TOP, HORIZONTAL CABLE MEMBERS SPACED AT 6”, SOLID RATIO OF 16%) *VIEW FROM ROADWAY*

FIGURE 2.3b - EXAMPLE OF CONCEPT 2 (EXAMPLE SHOWN WITH HEIGHT OF 14’-0”, NO VISIBLE WINGLET; 50” UNDER DECK WINGLET ON EAST SIDE AND 48” CATWALK ON WEST SIDE, CURVED TOP, HORIZONTAL CABLE MEMBERS SPACED AT 6”, SOLID RATIO OF 16%) *VIEW FROM SIDEWALK*

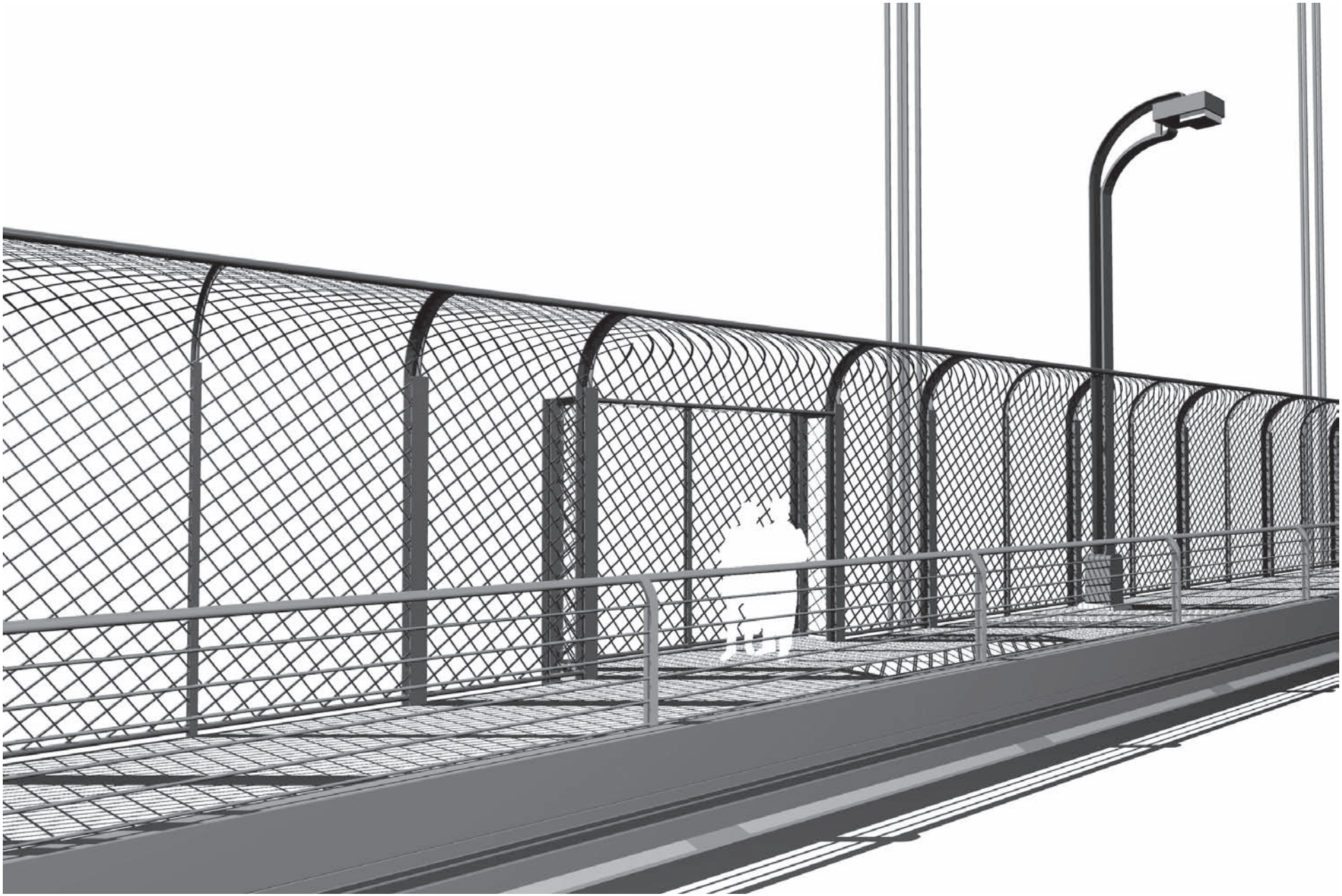

FIGURE 2.4a - EXAMPLE OF CONCEPT 2 (EXAMPLE SHOWN WITH HEIGHT OF 12’-0”, NO VISIBLE WINGLET; 50” UNDER DECK WINGLET ON EAST SIDE AND 48” CATWALK ON WEST SIDE, DIAGONAL WIRE MESH OF 6”, SOLID RATIO OF 16%)
VIEW FROM ROADWAY

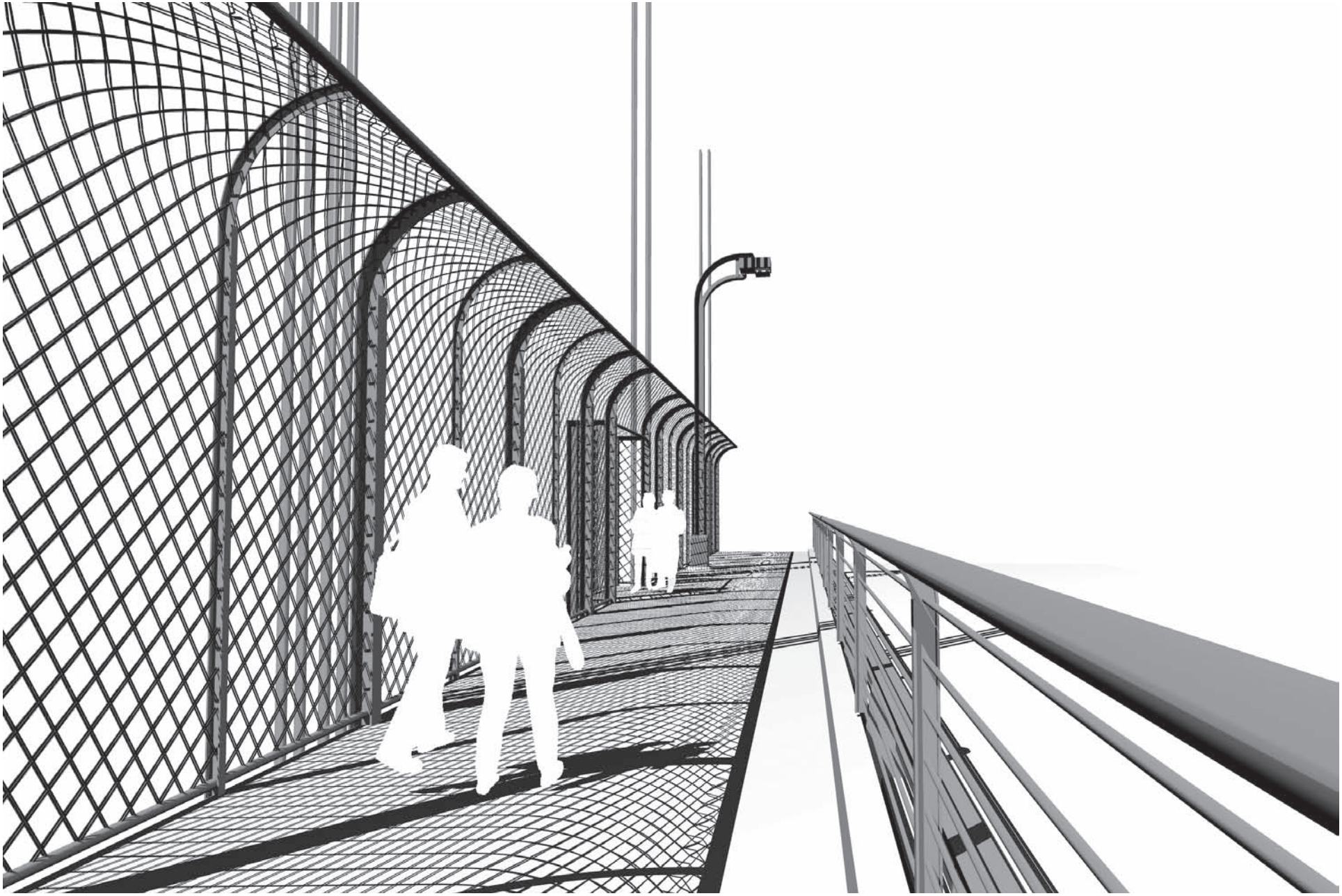

FIGURE 2.4b - EXAMPLE OF CONCEPT 2 (EXAMPLE SHOWN WITH HEIGHT OF 12’-0”, NO VISIBLE WINGLET; 50” UNDER DECK WINGLET ON EAST SIDE AND 48” CATWALK ON WEST SIDE, DIAGONAL WIRE MESH OF 6”, SOLID RATIO OF 16%)
VIEW FROM SIDEWALK

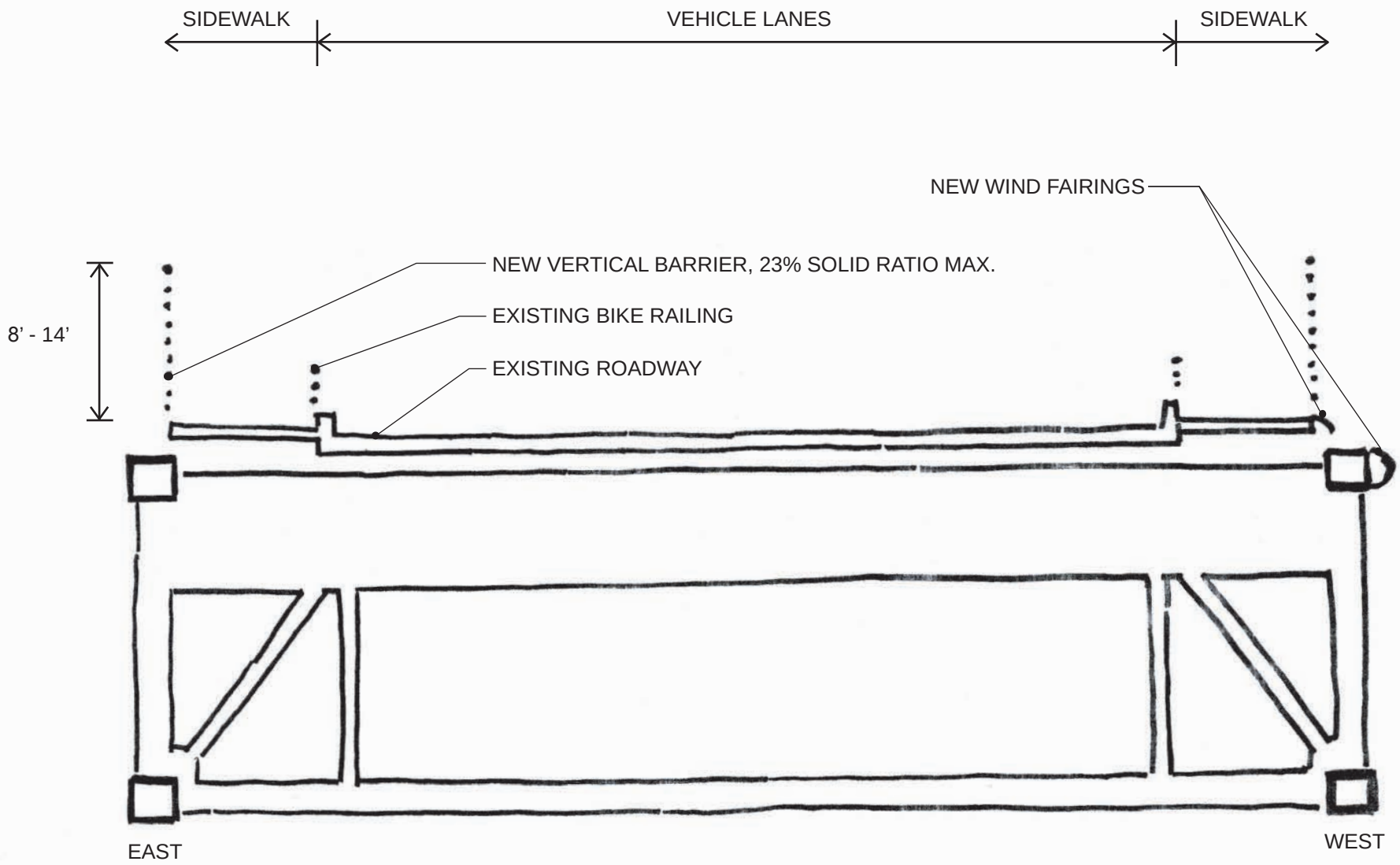

FIGURE 2.5 - CONCEPT 2 : REPLACING THE EXISTING RAILING; WIND FAIRINGS ON TRUSS
SCALE : NOT TO SCALE

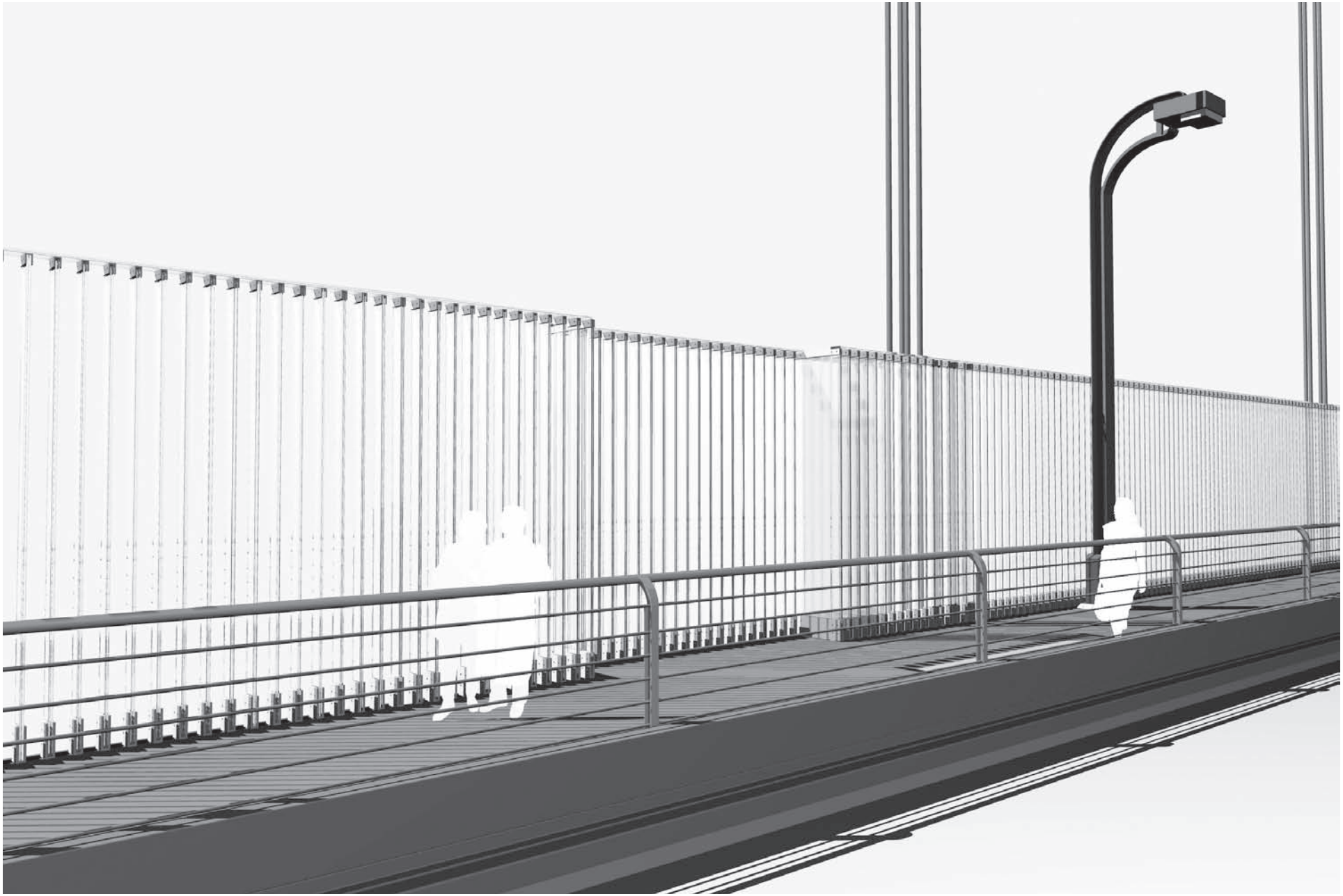

FIGURE 2.6a - EXAMPLE OF CONCEPT 2 (EXAMPLE SHOWN WITH HEIGHT OF 12’-0”, NO WINGLET; WIND FAIRINGS ON TRUSS AND SIDEWALK, VERTICAL GLASS PICKETS SPACED AT 7”, SOLID RATIO OF 23%) *VIEW FROM ROADWAY*

FIGURE 2.6b - EXAMPLE OF CONCEPT 2 (EXAMPLE SHOWN WITH HEIGHT OF 12’-0”, NO WINGLET; WIND FAIRINGS ON TRUSS AND SIDEWALK, VERTICAL GLASS PICKETS SPACED AT 7”, SOLID RATIO OF 23%) *VIEW FROM OUTBOARD*

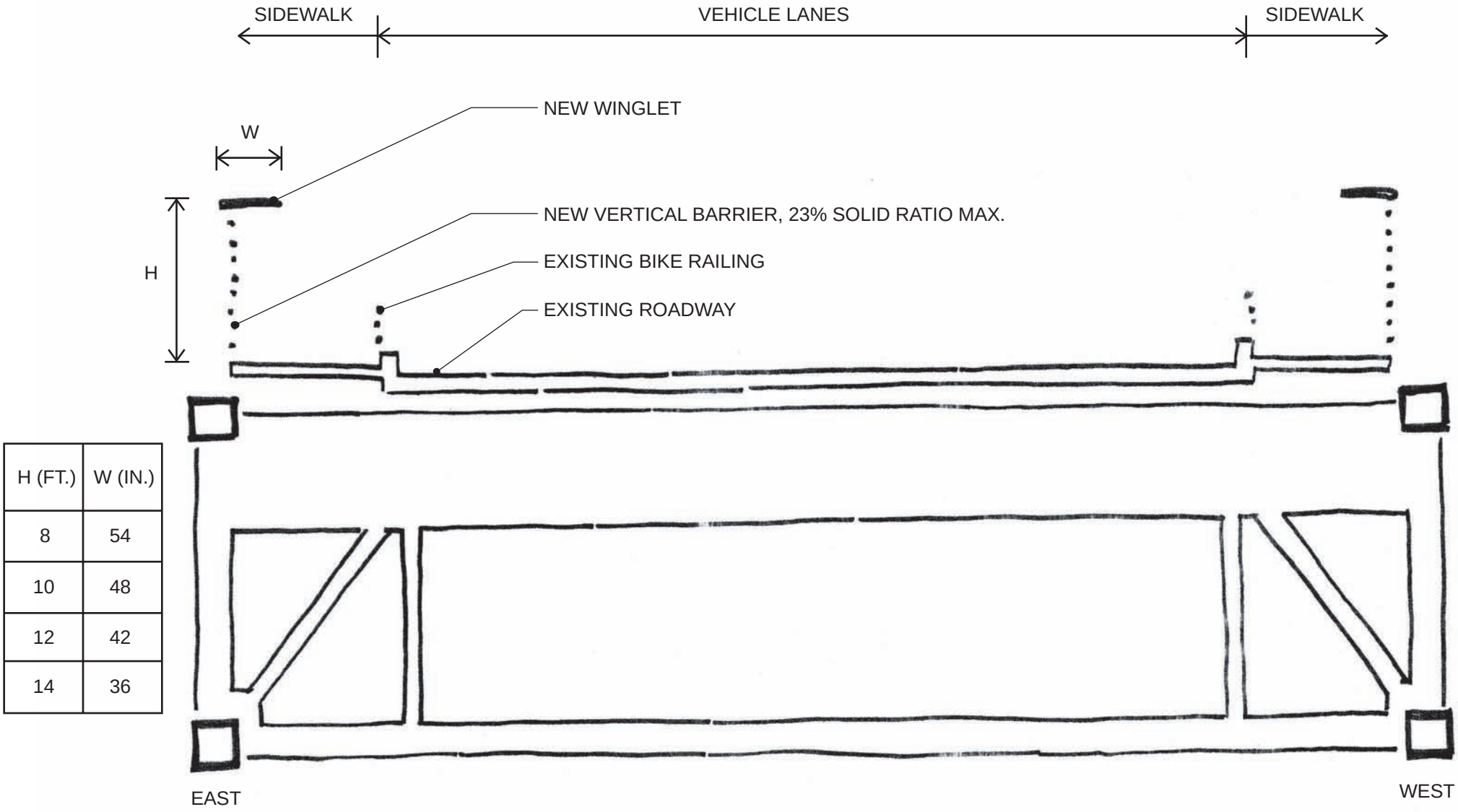

H (FT.)	W (IN.)
8	54
10	48
12	42
14	36

FIGURE 2.7 - CONCEPT 2 : REPLACING THE EXISTING RAILING ; WINGLETS MOUNTED OVER BARRIER

SCALE : NOT TO SCALE

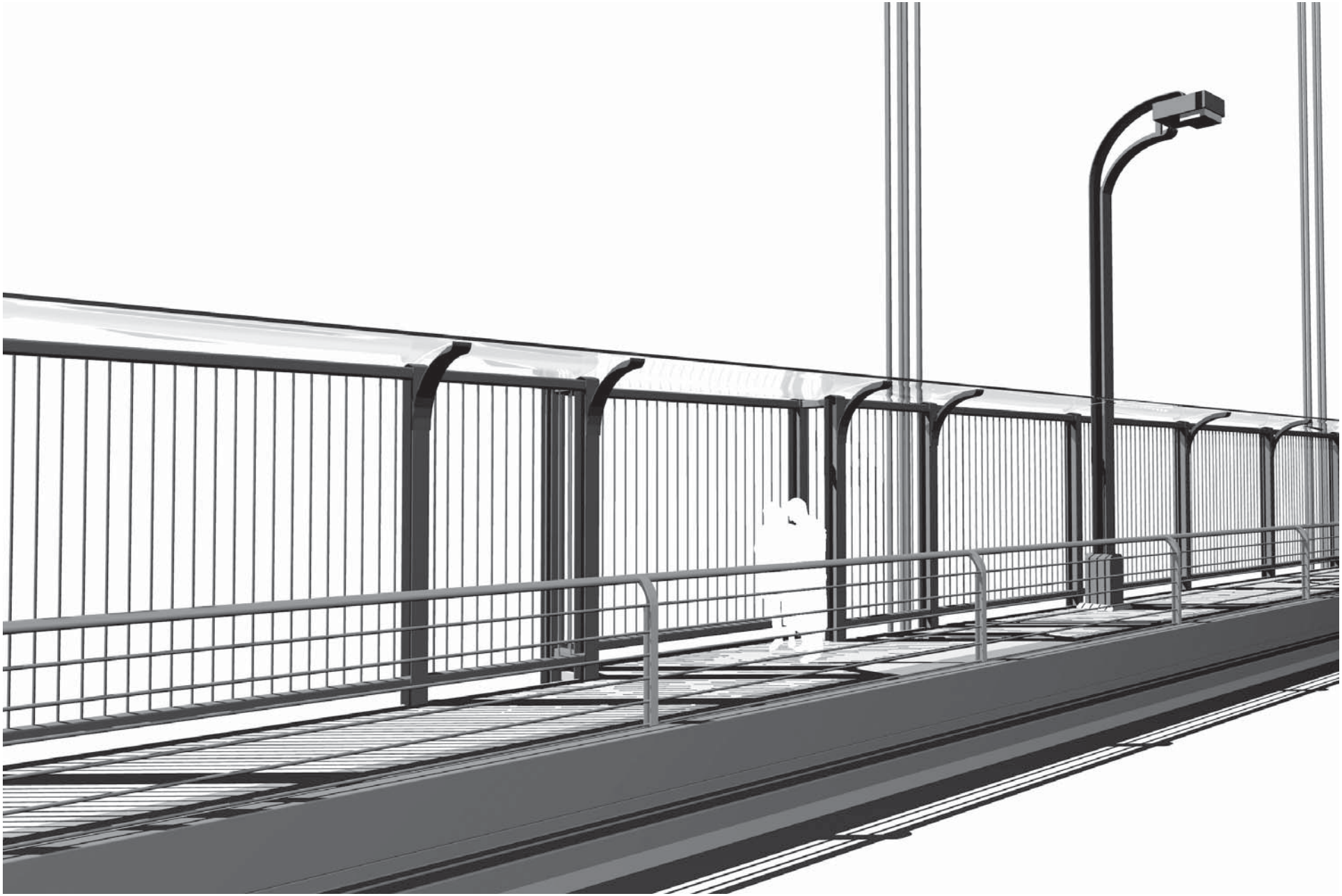

FIGURE 2.8a - EXAMPLE OF CONCEPT 2 (EXAMPLE SHOWN WITH HEIGHT OF 10’-0”, 48” TRANSPARENT WINGLET, VERTICAL MEMBERS SPACED AT 6”, SOLID RATIO OF 18%) *VIEW FROM ROADWAY*

FIGURE 2.8b - EXAMPLE OF CONCEPT 2 (EXAMPLE SHOWN WITH HEIGHT OF 10’-0”, 48” TRANSPARENT WINGLET, VERTICAL MEMBERS SPACED AT 6”, SOLID RATIO OF 18%) *VIEW FROM SIDEWALK*

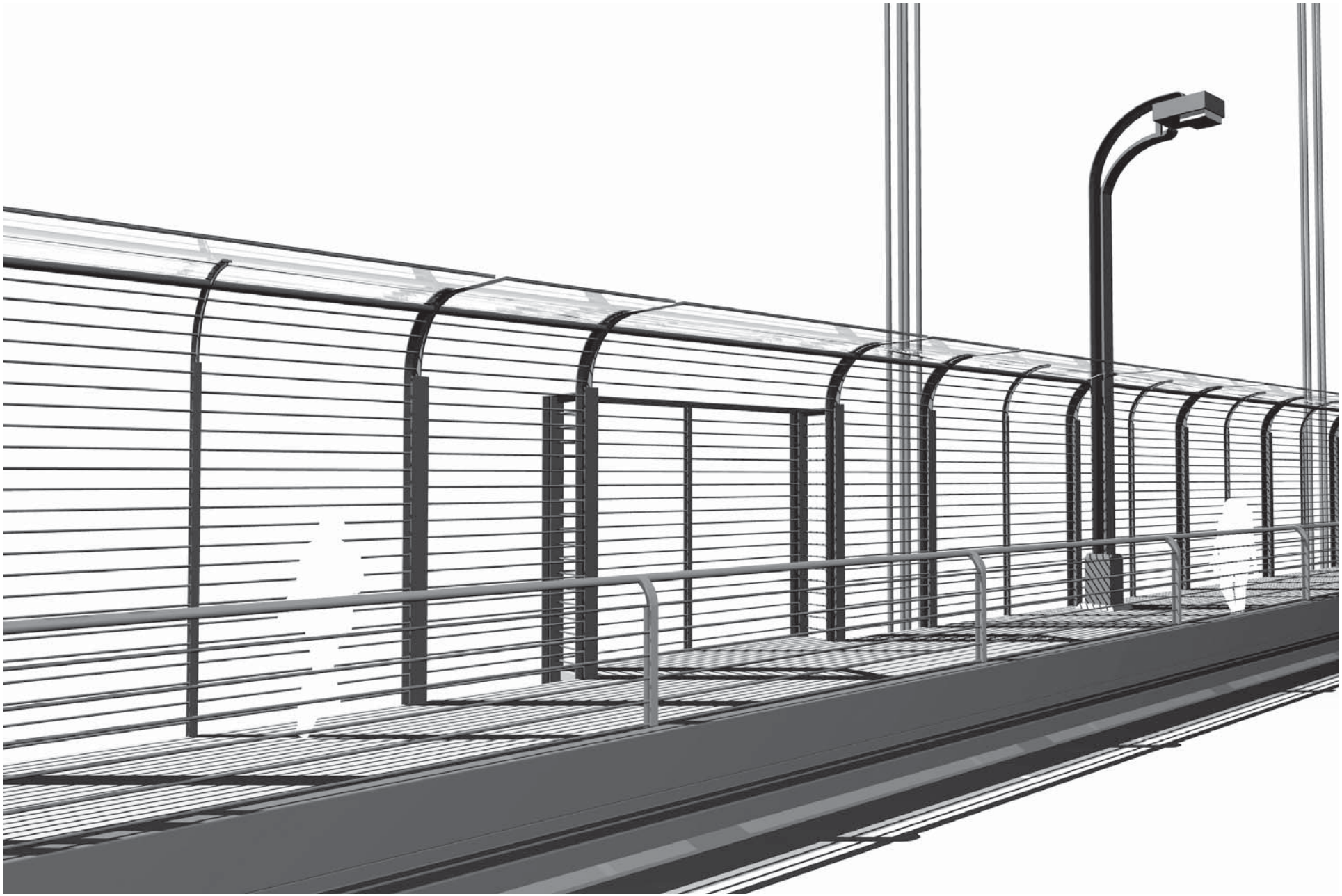

FIGURE 2.9a - EXAMPLE OF CONCEPT 2 (EXAMPLE SHOWN WITH HEIGHT OF 12’-0”, 42” TRANSPARENT WINGLET, HORIZONTAL MEMBERS SPACED AT 6”, SOLID RATIO OF 17%) *VIEW FROM ROADWAY*

FIGURE 2.9b - EXAMPLE OF CONCEPT 2 (EXAMPLE SHOWN WITH HEIGHT OF 12’-0”, 42” TRANSPARENT WINGLET, HORIZONTAL MEMBERS SPACED AT 6”, SOLID RATIO OF 17%) *VIEW FROM SIDEWALK*

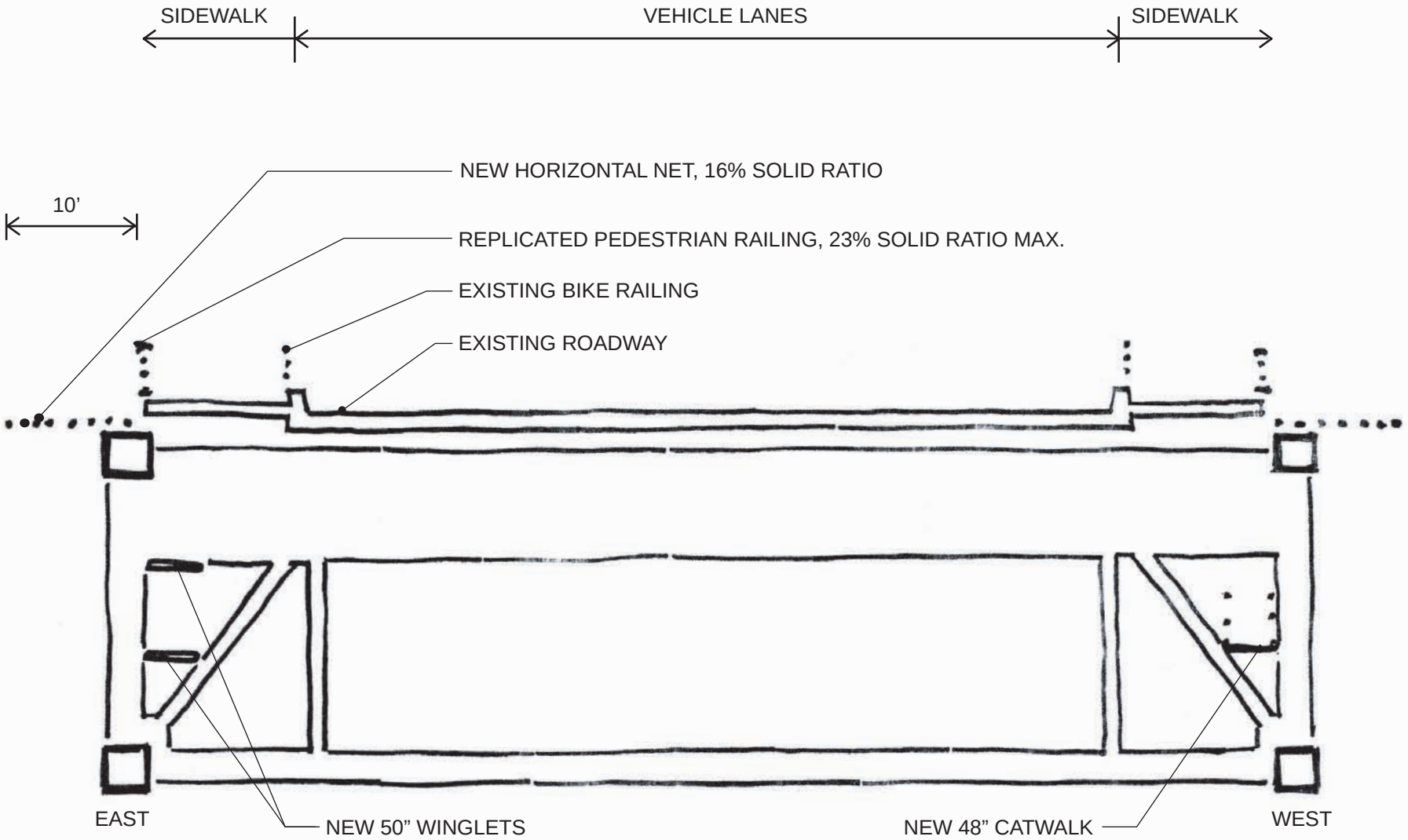

FIGURE 3.1 - CONCEPT 3 : UTILIZING NETS THAT CANTILEVER OUT HORIZONTALLY W/ REPLICATED PEDESTRIAN RAILING
SCALE : NOT TO SCALE

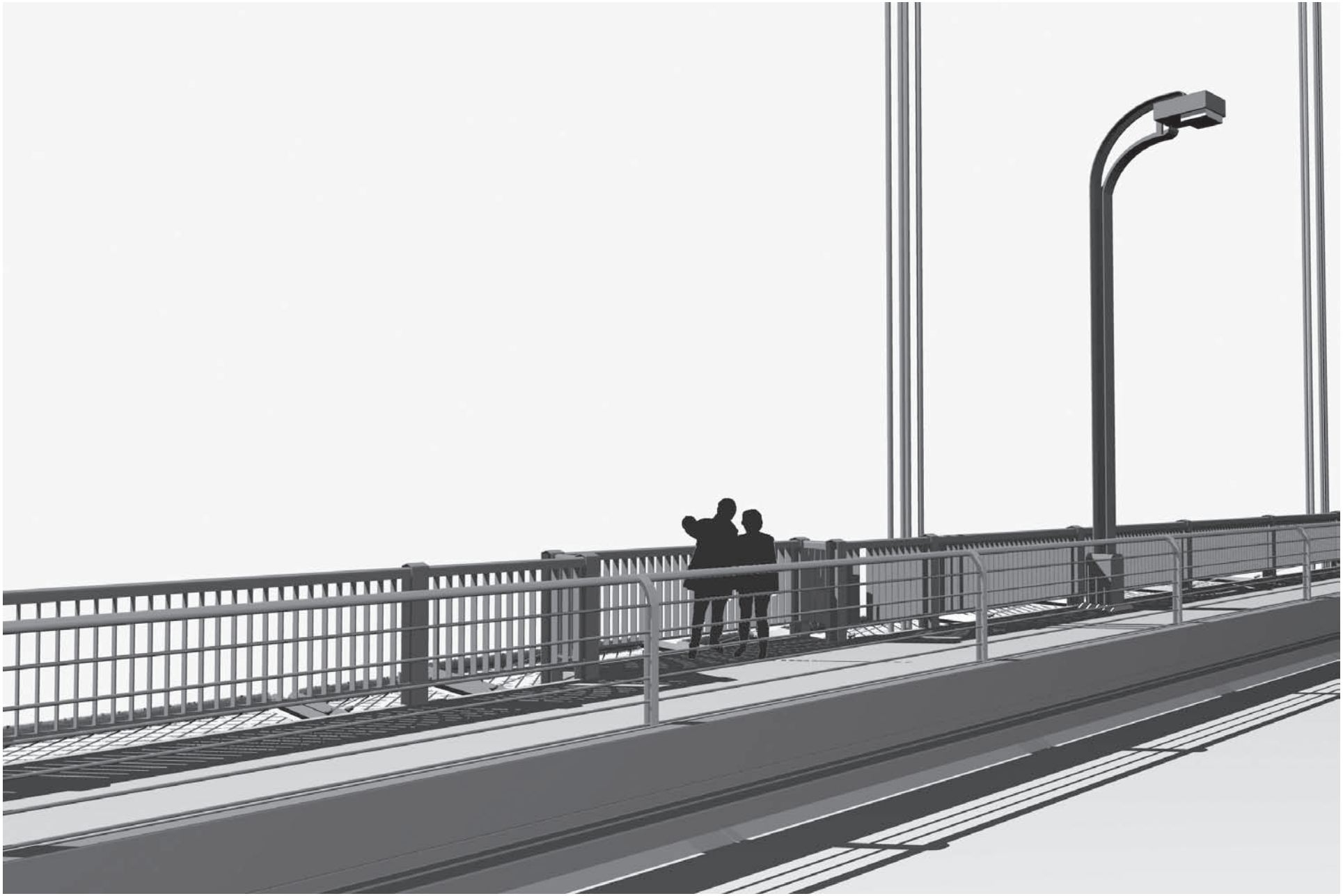

FIGURE 3.2a - EXAMPLE OF CONCEPT 3 (EXAMPLE SHOWN WITH A NET PROJECTING 10’ AT LEVEL OF REPLICATED PEDESTRIAN RAILING, SOLID RATIO OF 23%, NET SOLID RATIO OF 16%) *VIEW FROM ROADWAY*

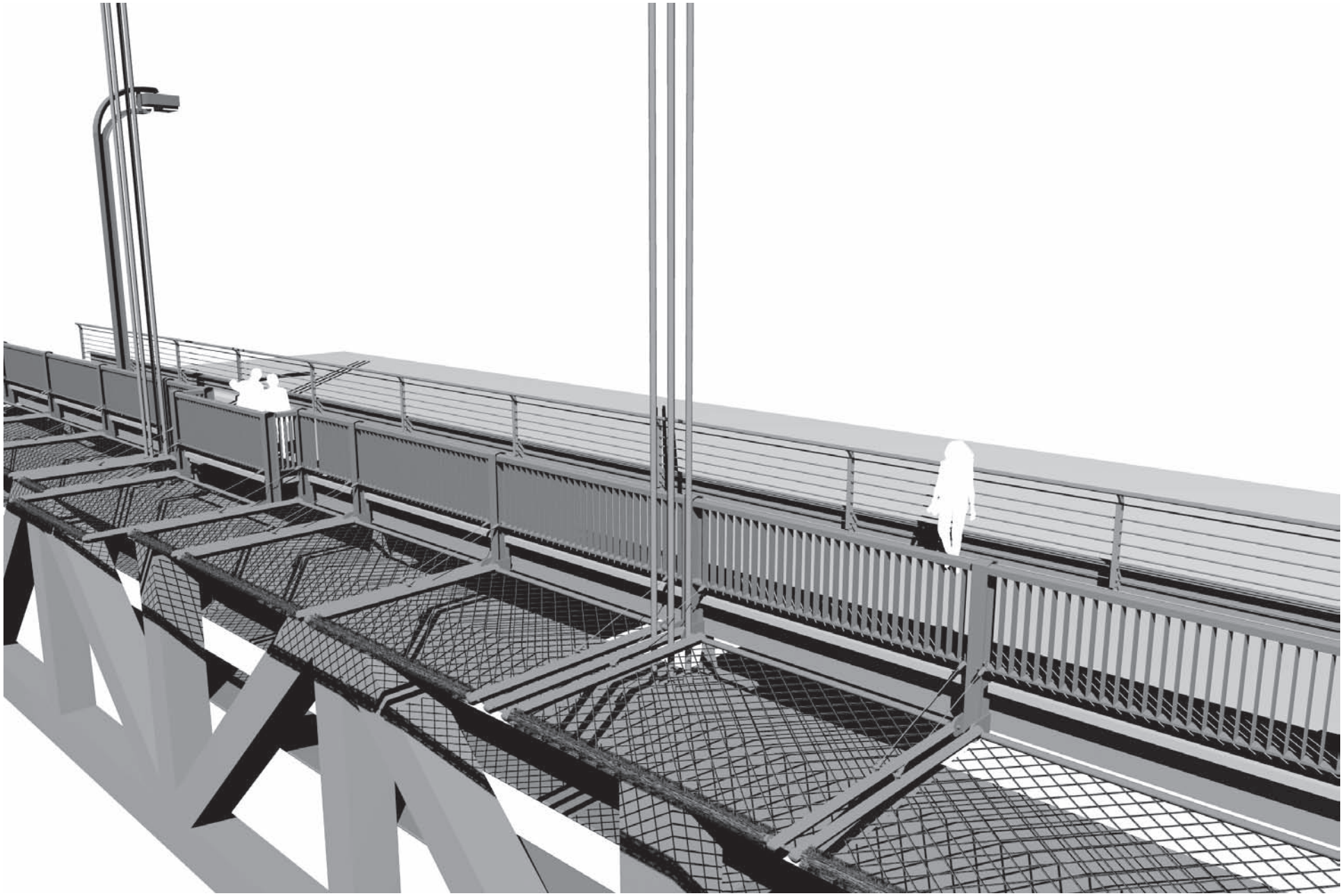

FIGURE 3.2b - EXAMPLE OF CONCEPT 3 (EXAMPLE SHOWN WITH A NET PROJECTING 10’ AT LEVEL OF REPLICATED PEDESTRIAN RAILING, SOLID RATIO OF 23%, NET SOLID RATIO OF 16%) *BIRDS EYE VIEW FROM OUTBOARD*

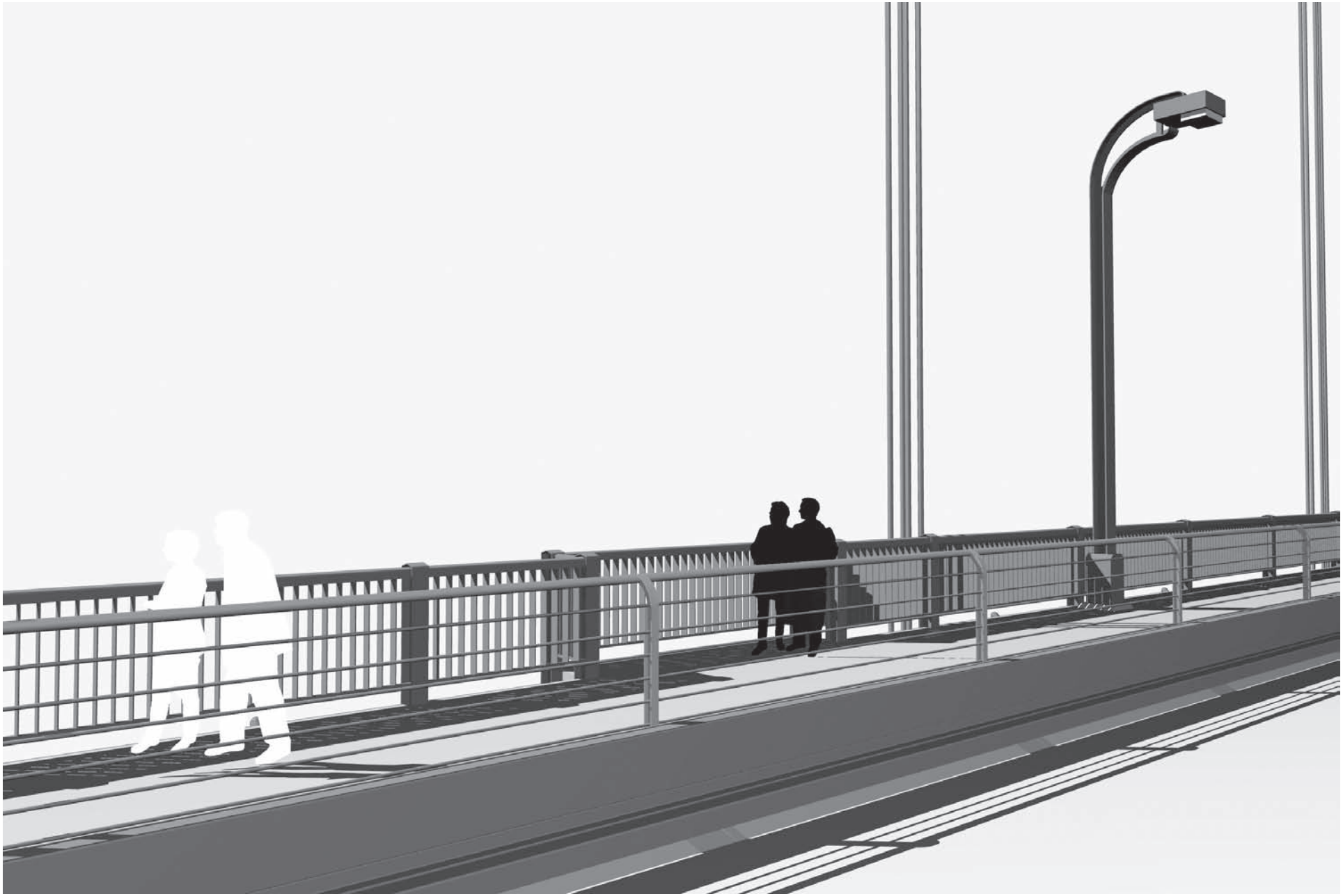

FIGURE 3.3a - EXAMPLE OF CONCEPT 3 (EXAMPLE SHOWN WITH A NET PROJECTING 10’ MOUNTED BELOW REPLICATED PEDESTRIAN RAILING, SOLID RATIO OF 23%, NET SOLID RATIO OF 16%) *VIEW FROM ROADWAY*

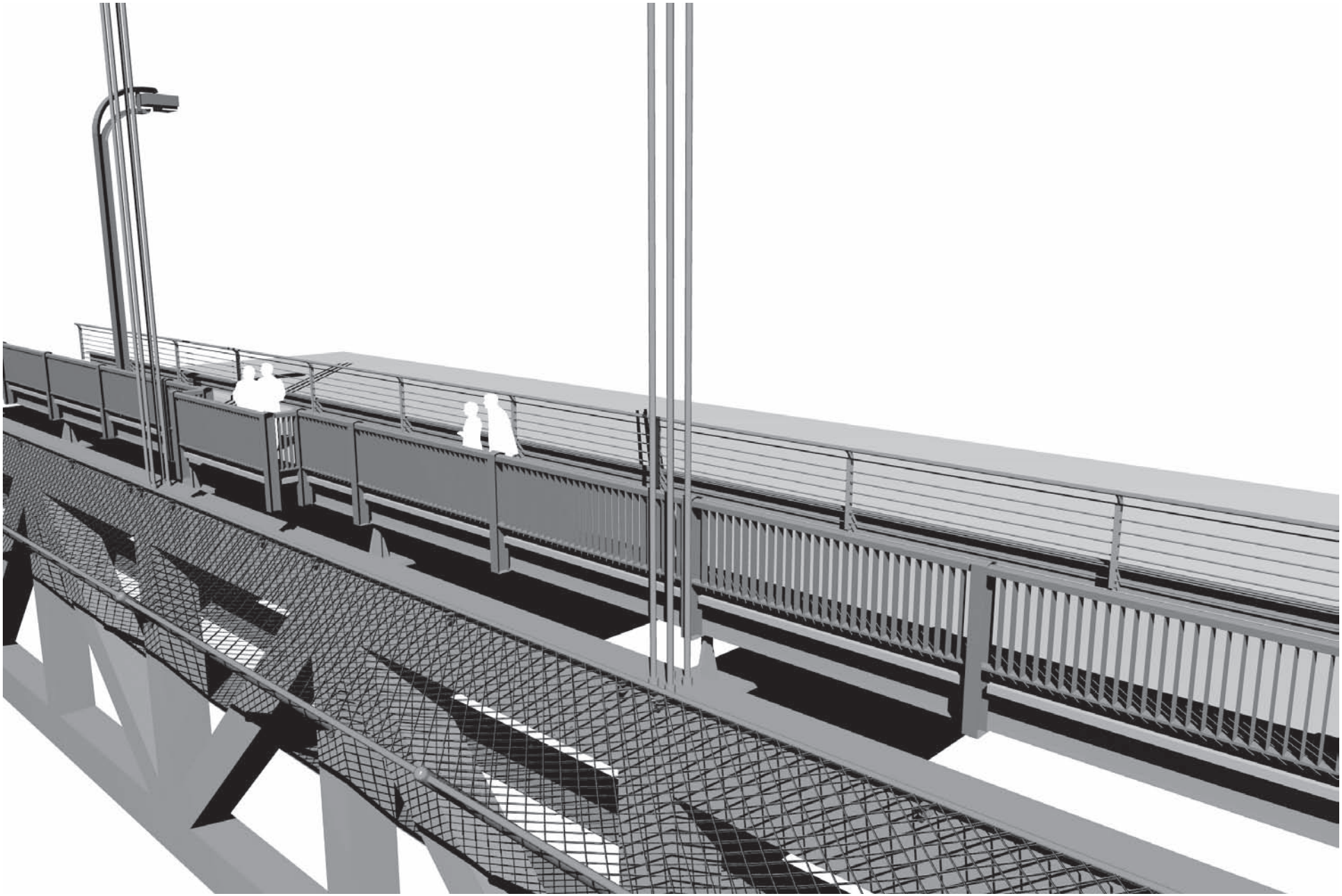

FIGURE 3.3b - EXAMPLE OF CONCEPT 3 (EXAMPLE SHOWN WITH A NET PROJECTING 10’ MOUNTED BELOW REPLICATED PEDESTRIAN RAILING, SOLID RATIO OF 23%, NET SOLID RATIO OF 16%) *BIRDS EYE VIEW FROM OUTBOARD*

SECTION A
INTRODUCTION AND OBJECTIVES

The objective of the Phase 1 wind study is to determine the performance of the Golden Gate Bridge in strong winds with a variety of possible suicide deterrent systems added to the existing bridge deck and to evaluate the performance of the bridge with the addition of wind performance enhancement elements. Because the bridge is sensitive to strong winds, the Golden Gate Bridge, Highway and Transportation District specified that any proposed modifications to the bridge should provide for the stability of the bridge in a 100 mph wind, a wind speed with a recurrence interval of approximately 10,000 years.

For new bridges, a typical design criterion is that a flutter instability should not occur for a wind speed with a recurrence interval any less than 10,000 years. For the Golden Gate Bridge, a ten-minute averaged, 10,000 year wind speed at the bridge deck level is 100 mph for winds from the west and approximately 66 mph for winds from the east (Ref 5). See Appendix 1.

The existing railings on the bridge are very solid - with a large horizontal member top and bottom with 4 inch wide H-beam pickets on a spacing of approximately 8 inches. This railing is virtually solid aerodynamically and is one contributing component of the aerodynamic sensitivity of the bridge. Removal of the existing railing increases the critical flutter wind speed by 40%. In the previous study (Ref 2), the wind retrofit system designed for the west side opened up the railing (with new plate pickets parallel to the wind) and added fairings to direct winds smoothly up over the sidewalk and deck. This scheme will increase the critical flutter wind speed to well over 100 mph.

Another scheme that has been proposed (Ref 7) is to add a pair of winglets (one on each side of the bridge) that act as aerodynamic dampers to dampen any torsional (and vertical) disturbance, and not allow it to grow without bound (which is the definition of a flutter instability). The fairing system proposed, and winglet pairs, were considered in this study as reasonable aerodynamic enhancements that can improve the performance of the bridge in strong winds to meet the project criteria.

Three general types of suicide deterrent systems were considered:

Concept 1) Adding to the existing railing to increase its height;
Concept 2) An all new vertical barrier/railing system; and
Concept 3) Nets that cantilever out horizontally.

This wind study resulted in a number of technically feasible suicide deterrent systems from a wind perspective. From an aerodynamic point of view, a technically feasible system must meet the wind speed criteria (in its various forms) for horizontal winds, for winds from -3 degrees, for winds from +3 degrees, and for the suicide deterrent system in combination with a possible moveable traffic barrier in one of seven positions (any possible lane position from one side of the bridge to the other).

In order to meet the specified objective, the wind study was divided into two parts.

Part I - Preliminary Study

In this part of the study the following tasks were performed:

1) Determine base-line aerodynamic characteristics for the existing bridge;

2) Determine the sensitivity of the critical flutter wind speeds to the placement of the moveable traffic barrier in its various positions;

3) Determine the critical flutter wind speeds for the bridge with various generic barrier types (of the three types specified) having different heights and solid ratios (the ratio of the projected area of solid material to the total gross area); and

4) Determine whether or not additional treatment is needed for the proposed suicide deterrent system to meet the specified aerodynamic criteria (critical flutter wind speed greater than 100 mph).

Wind induced motions are produced primarily by the aerodynamic loads on the bridge deck. It is the policy of the West Wind Laboratory to obtain aerodynamic characteristics of the bridge deck using large scale (1:50) model of a section of the bridge deck 267 ft long. At that scale, details in the deck section can be modeled with accuracy.

Aerodynamic characteristics of the bridge deck (static and dynamic) are then used with an analytical model of the turbulent wind field, and an analytical model of the structure, to compute the response of the bridge in a strong wind using a time domain procedure. The wind field is generated using a procedure defined in Ref 3. The time domain analytical procedure is similar to that defined in Ref 4 and is described in greater detail in Appendix 3. If the motions are greater at the end of the numerical simulation than they are at the beginning, then the bridge is unstable (otherwise it is stable). At a design level wind, a static equivalent model response is defined as a mean plus 2.5 standard deviation response. Response statistics are obtained from the numerical simulations for a full-scale period of 10-minutes (See Appendix 3).

A detailed analysis of the existing bridge was performed to determine its baseline critical flutter wind speed. It was noted, in that analysis that 1) the instability observed was a single degree of freedom torsional flutter instability, 2) vertical motions were highly damped, and 3) there was no coupled (vertical and torsional) instability observed amongst any pair of modes of vibration (See Appendix 6). Therefore, it was concluded that in the preliminary studies, critical flutter instabilities could be identified by observing single-degree-of-freedom torsional motion only. A critical flutter wind speed for torsional motion alone was determined as outlined in Appendix 6. This is the maximum critical

flutter wind speed possible assuming that the configuration tested is representative of that over the entire bridge.

In this preliminary study, generic barrier types were studied (i.e., barriers of various solid ratios and barriers of various heights). As this iterative process evolved, aerodynamic enhancements were added. Both evolved simultaneously with the current configuration being tested dependent upon the performance of the previous configuration. In this way, 6 configurations (each with multiple traffic barrier options) were identified, out of 72, that met the flutter wind speed criterion. Results of the preliminary study are presented in Section B.

Part II - Detailed Study

In this part of the study, the six aerodynamically independent configurations identified in Part 1 that met the critical flutter wind speed criterion were analyzed. The performance of the Golden Gate Bridge in strong winds, was analyzed with those six configurations, with various moveable traffic barrier locations, at mean angles of incidence of -3, 0, and 3 degrees, for winds from the west, and for winds from the east.

For each possible configuration (for horizontal winds from the west) the maximum possible critical flutter wind speed was identified from torsional motions. For the most critical traffic barrier placement, detailed stability and buffeting analyses were performed for the entire bridge as outlined in Appendix 3. The flutter and buffeting analyses were performed based on measured flutter derivatives, static aerodynamic coefficients and bridge geometric and dynamic modal data. The bridge is modeled using ADINA structural analysis software. A description of the ADINA modeling is provided in Appendix 6.

The aerodynamic enhancements were reduced in spread over the length of the bridge until the stability wind speed criterion was just met. For this configuration, with a reduced spread of the aerodynamic enhancements, a buffeting analysis was performed at the 100 year, design wind speed.

The wind study was based upon aerodynamic coefficients (static and dynamic) on the bridge deck that were obtained experimentally using a large scale (1:50) model of a section of the bridge deck. The section model was based upon the design record drawings from the original construction and from the various modifications to the Bridge (e.g. deck replacement, bottom laterals, public safety railing, etc.)

Results of the detailed study are presented in Section C.

SECTION B
PRELIMINARY STUDIES

Preliminary studies were performed to determine critical flutter wind speeds for the bridge with various suicide deterrent systems. Complete full-bridge analyses were not performed, but simplified analyses were performed, using a large-scale section model (1:50) that allowed torsional motion only (for these studies, vertical motions were constrained). The large-scale section model was used to obtain the aeroelastic flutter derivatives A2 and A3. The stability of the Golden Gate Bridge could then be computed analytically by evaluating the stability of the fundamental torsional mode of vibration (Mode 7 - see Appendix 6). For this bridge, this is a very good approximation to the full-bridge behavior at the critical flutter wind speed, assuming that the configuration being evaluated was representative of that over the entire length of the bridge.

Seventy-two bridge deck configurations were evaluated preliminarily GGB1 through GGB72. Those configurations are described in Tables B.1 and B.2 along with the critical flutter wind speed determined for each. Some results follow:

1) The critical flutter wind speed for the existing Golden Gate Bridge was preliminarily determined and compared to previous studies.

2) The critical flutter wind speed was not sensitive to the existence of, and placement of, a moveable traffic barrier. This is not entirely surprising because a moveable traffic barrier is approximately as high as the existing curb between the roadway and the sidewalk. This insensitivity was identified for the existing configuration as well as a modified configuration (with a critical flutter wind speed in excess of 100 mph).

3) None of the possible suicide deterrent configurations alone (new barrier on top of the existing railing, all new vertical railing and barrier, or horizontal netting scheme) met the critical flutter wind speed criterion of 100 mph. All required some aerodynamic enhancement to meet that criterion.

4) Possible aerodynamic enhancements that were added to meet the criterion were 1) a winglet pair installed above the bridge deck level at the top of a new vertical barrier, 2) winglets and smooth catwalks that behave like winglets below decks in the truss space, and 3) fairings on the west side, over the top chord and along the sidewalk edge. Those fairings had been tested before and are documented in Ref 2.

Only six distinctly different configurations (aerodynamically different) were identified that met the stability criterion (not including all the possible moveable traffic barrier locations). A barrier conforming to Concept 1 or Concept 2 that had vertical, rounded edged glass plates, or vertical rods/cables, or horizontal rods/cables, all with the same solid ratio (ratio of projected area of solid members to total, projected barrier area), are considered

to be aerodynamically similar. Those six configurations were advanced to the next study phase as technically feasible solutions. They are identified in Section C.

TABLE B.1 – Critical flutter wind speed (U_{CRIT}) for each bridge deck configuration

CASE	RETRO	*TRAFFIC BARRIER	SUICIDE DETER SYSTEM	U_{CRIT} (mph)	*2-4 DENOTES 2 LANES TO WINDWARD; 4 LANES TO LEE *UNLESS OTHERWISE NOTED ALL TESTS AT 0^{O}
GGB12	WIND	NONE	NONE	>130.69	
GGB13	WIND	0-6	NONE	>127.72	
GGB14	WIND	1-5	NONE	123.48	
GGB15	WIND	2-4	NONE	>130.23	
GGB16	WIND	3-3	NONE	>126.79	
GGB17	WIND	4-2	NONE	>131.17	
GGB18	WIND	5-1	NONE	>130.63	
GGB19	WIND	6-0	NONE	>132.79	
GGB20	FAIRINGS ONLY TO WIND	NONE	SDS2	>129	
GGB21	FAIRINGS ONLY TO WIND	NONE	SDS3	104.7	
GGB22	FAIRINGS TO LEE	NONE	SDS3	77.8	
GGB23	FAIRINGS TO LEE	2-4	SDS3	84.0	

TABLE B.1 (Cont)

CASE	RETRO	*TRAFFIC BARRIER	SUICIDE DETER SYSTEM	U_{CRIT} (mph)
GGB24	FAIRINGS TO LEE	4-2	SDS3	101.6
GGB25	NO	NONE	SDS4	51.5
GGB26	NO	NONE	SDS5	57.1
GGB27	NO	NONE	SDS6	55,6
GGB28	WIND	NONE	SDS6	61.6
GGB29	WIND	NONE	SDS4	77.3
GGB30	NO	NONE	SDS7	>115.9
GGB31	NO	0-6	SDS7	113.9
GGB32	NO	1-5	SDS7	113.6
GGB33	NO	2-4	SDS7	>115.5
GGB34	NO	3-3	SDS7	>115.2
GGB35	NO	4-2	SDS7	>116.2
GGB36	NO	5-1	SDS7	>115.5
GGB37	NO	6-0	SDS7	>115.6
GGB38	NO	NONE	SDS8	55.4
GGB39	NO	NONE	SDS9	57.3
GGB40	NO	NONE	SDS10	73.3
GGB41	NO	NONE	SDS11	52.5
GGB42	NO	NONE	SDS12	77
GGB43	NO	NONE	SDS13	106
GGB44	NO	NONE	SDS14	91
GGB45	NO	NONE	SDS15	>114
GGB46	NO	NONE	SDS16	82
GGB47	NO	NONE	SDS17	93
GGB48	NO	NONE	SDS18	89
GGB49	NO	NONE	SDS19	95
GGB50	NO	NONE	SDS20	101
GGB51	NO	NONE	SDS21	99
GGB52	NO	NONE	SDS22	84
GGB53	NO	NONE	SDS23	99
GGB54	NO	NONE	SDS24	119
GGB55	NO	NONE	SDS25	72
GGB56	NO	NONE	SDS26	57

TABLE B.1 (Cont)

CASE	RETRO	*TRAFFIC BARRIER	SUICIDE DETER SYSTEM	U_{CRIT} (mph)
GGB57	NO	NONE	SDS27	68
GGB58	NO	NONE	SDS28	63
GGB59	NO	NONE	SDS29	105
GGB60	NO	NONE	SDS30	72
GGB61	NO	NONE	SDS31	78
GGB62	NO	NONE	SDS32	77
GGB63	YES	NONE	SDS33	79
GGB64	NO	NONE	SDS34	87
GGB65	NO	NONE	SDS35	108
GGB66	NO	NONE	SDS36	91
GGB67	NO	NONE	SDS37	83.2
GGB68	NO	NONE	SDS38	91.6
GGB69	NO	NONE	SDS39	67.9
GGB70	NO	NONE	SDS40	70.3
GGB71	NO	NONE	SDS41	81.8
GGB72	NO	NONE	SDS42	110.7

TABLE B.2 – Designation and description of the suicide deterrent systems tested

DESIGNATION	SUICIDE DETERRENT SYSTEM
SDS1	10 ft high solid (glass) barriers
SDS2	New full height (to 10 feet) suicide barriers of round members with a solid ratio of 10.4%, both sides
SDS3	New full height (to 10 feet) suicide barriers of round members with a solid ratio of 20.8%, both sides
SDS4	Horizontal netting extending 10 feet out from the edge of the sidewalk, both sides, with a solid ratio of 15.6%
SDS5	The same as SDS4 but with 50 inch wide winglets with the outboard edge 17.92 feet out from the sidewalk
SDS6	Horizontal netting extending 10 feet out from the edge of the sidewalk, both sides, with a solid ratio of 56.9%
SDS7	New, uniform, 10 foot high suicide barriers, with a 50 inch wide winglet at the 10 foot elevation, both sides 20.8% solid
SDS8	Existing railings with suicide barrier on top to 10 feet with a 10.4% solid ratio
SDS9	Existing railings with suicide barrier on top to 10 feet with a 20.8% solid ratio
SDS10	Existing railings, suicide barrier on top to 10 feet with 20.8% solid ratio, with 50 inch wide winglets at the 10 foot level
SDS11	Existing railings with a solid barrier on top up to 10 feet
SDS12	14 foot high barrier/railings both sides with 23% solid ratio
SDS13	Same as SDS12 with 50" winglet and 14' on windward side only
SDS14	Same as SDS12 with 50" winglet at 14' on leeward side only
SDS15	Same as SDS12 with 50" winglets at 14' on both sides
SDS16	SDS12 plus catwalk (50" wide above bottom chord) to windward
SDS17	SDS12 plus catwalks on both sides
SDS18	SDS12 plus enlarged catwalk to lee
SDS19	SDS12 plus enlarged catwalk to wind
SDS20	SDS12 plus catwalks both sides with underside winglet (50" wide at underside of crossbeams) to lee
SDS21	SDS12 plus catwalk and underside winglet to lee only
SDS22	SDS12 plus catwalk and underside winglet to wind only
SDS23	SDS12 plus catwalks both sides and underside winglet to wind

TABLE B.2 (Cont)

DESIGNATION	SUICIDE DETERRENT SYSTEM
SDS24	Existing unmodified railings with 75" wide winglets at 14' both sides, with no new barriers
SDS25	Existing railings with 75" wide catwalk and 75" wide underside winglet to lee only.
SDS26	Existing, plus 10' horizontal net, 21% solid ratio
SDS27	SDS26 with 50" winglet at mid truss height lee side only
SDS28	SDS26 with 50" winglet at edge of net lee side only
SDS29	SDS26 with 75" winglet pair at 14' height
SDS30	New railing and barrier to 14' with 23% solid ratio, tilted inboard 20 degrees
SDS31	SDS30 vertical
SDS32	SDS30 tilted outboard 20 degrees
SDS33	Fairing with new railing and barrier to 14' on west side; existing railing with new barrier above to 14' (23% solid ratio on all new railings and barriers)
SDS34	New railing and barriers to 14' both sides with 23% solid ratio; with 36" winglet at 14' windward side only
SDS35	SDS34 with 36" winglets at 14' both sides
SDS36	SDS34 with 36" winglet at 14' lee side only
SDS37	New barriers 14' high with a 23% solid ratio, and highy curved winglets at 14' that are 36 inches wide (curve on outside with 2.1 feet radius) both sides
SDS38	Same as SDS37 but with 50 inch wide, highly curved winglets
SDS39	Horizontal netting extending 10 feet (16% solid ratio) with new 54 inch high railings with 25% solid ratio
SDS40	SDS39 with sidewalk fairings only to windward
SDS41	SDS39 with a catwalk 50 inch winglet (below deck) to lee
SDS42	SDS39 with a catwalk 50 inch winglet, (below deck) and a second 50 inch winglet on underside of crossbeam, to lee

SECTION C
DETAILED STUDIES

A detailed study was performed to determine the performance of the Golden Gate Bridge with six distinctly different (aerodynamically different) suicide deterrent systems. These configurations were identified from the preliminary studies. The six configurations, plus W1 (alternate), are defined in Figures C.1 through C.7, and are designated W1, W1 (alternate), W2, W3, W4, W5, and W6. The existing bridge configuration is defined as W0.

W0 Existing bridge
W1 12' tall vertical barrier with solid ratio of 23% and under deck winglets and/or catwalk. An alternate to W1 is the use of wind fairings in lieu of winglets
W2 12' tall vertical barrier with solid ratio of 23% and winglets mounted over the new barrier
W3 A new vertical barrier mounted over the existing railing with a maximum solid ratio of 12% and with winglets mounted over the new barrier
W4 Similar to W1 except a new barrier height of 10' instead of 12'
W5 Similar to W2 except with a new barrier height of approximately 10' and with a winglet mounted at 10'-6"
W6 A horizontally projecting net. Net projection of 10' with a maximum solid ratio of 16%. Modify existing railing to have a maximum solid ratio of 23%. Below deck winglets and catwalk required

The objectives of this portion of the study were the following:

1) determine the maximum possible critical flutter wind speeds for each configuration, with and without moveable traffic barriers in any of 7 possible locations, for winds with vertical angles of incidence of -3, 0, and 3 degrees;

2) determine the minimum length (spread) of aerodynamic enhancements (fairings or winglets) required for each configuration to just meet the critical flutter wind speed threshold of 100 mph; and

3) for each configuration with minimal spread aerodynamic enhancements, determine the buffeting response of the bridge to a turbulent wind field with a mean hourly wind speed of 76 mph.

It is instructive first to determine the performance, precisely, of the existing bridge. The dynamic response characteristics of the bridge, and its inertial properties, are presented in Appendix 6. A detailed stability analysis was performed as described in Appendix 3. Results of that stability analysis, including 10 modes of vibration simultaneously, are presented in Table C.1. All modes of vibration were given an initial unit disturbance. If the last-to-first ratio of modal responses (after 5 minutes of exposure to the specified

wind speed) is greater than 1.00, then that mode of vibration (and the entire bridge) is unstable.

Note that the vertical modes of vibration (Modes 2, 4, 5, 6, and 9) are highly damped at all wind speeds. Shown in Table C.2 are the frequencies at which each mode of vibration is vibrating. Note that for all strong wind speeds, almost all modes are coupling aerodynamically (by definition of a normal mode of vibration, they are decoupled mechanically) to the first asymmetric torsional mode (Mode 7), or the first symmetric torsional mode (Mode 8). This is identified because the modal frequencies are all matched to the torsional modes. These are not coupled instabilities, but are responses of those non-torsional modes from the coupling aeroelastic flutter derivatives, notably A1 and H3, that are driving the vertical response. The torsional motions are driving the vertical modes of vibration aerodynamically. Table C.3 shows the mean magnitude of the modal response at the end of the simulation. All numbers are small relative to unity, so static divergence did not occur (except the Mode 1 response which is just an expected, mean sway).

This analysis of the existing bridge is instructive for the following reasons:

1) The only possible instability is a torsional instability;

2) Vertical motions are highly damped;

3) No coupled instability occurs (although other modes are driven by the torsional motions); and

4) The critical flutter wind speed obtained in this study is very close to that obtained for the existing bridge considering torsional motion alone for Case GGB1 in the preliminary studies.

These conclusions are used to guide the detailed analyses of the bridge with the suicide deterrent systems that have been advanced to this phase.

For the options considered, to do detailed stability and buffeting analyses, a full set of aeroelastic flutter derivatives, and static aerodynamic coefficients are required. That was not done explicitly, but done implicitly using the conclusions from the analyses of the existing bridge. A torsional aeroelastic instability is governed by the aeroelastic flutter derivatives A2 and A3. Those were measured explicitly for each option. Since the vertical motions of the bridge were highly damped, the precise measurement of the H1 and H4 aeroelastic terms was not required. It is a fact, however, that at high wind speeds (and large values of U/nB where U is the mean wind speed, n is the frequency of vibration, and B is the bridge chord - 27.432m) the aeroelastic flutter derivatives approach asymptotically values well defined from the static coefficients alone. For

$$K = 2\pi n \frac{B}{U}$$

H1 approaches $$-\left(\frac{1}{K}\right)\frac{dC_L}{d\alpha}$$

H3 approaches $$\left(\frac{1}{K^2}\right)\frac{dC_L}{d\alpha}$$

A1 approaches $$-\left(\frac{1}{K}\right)\frac{dC_M}{d\alpha}$$

for all values of *U/nB* (Ref 1). The static coefficients (C_D, C_L, C_M) for all options were measured and are presented in Appendix 7. The rate of change of C_L and C_M with angle of incidence, α, could then be computed. In this way H1, H3, and A1 were computed from the static aerodynamic coefficients.

The remaining aeroelastic flutter derivatives (H2, H4, and A4) play a very minor role in computing the aeroelastic stability of this bridge because no coupled flutter is expected. The values for the existing bridge were used as being representative of the various options.

Torsional flutter instabilities were computed first for the various options from torsional motions alone assuming that the specified option was representative of the crossection of the bridge for its full length. Critical flutter wind speeds were computed as described in Appendix 6 using the single torsional mode of vibration, Mode 7. For each option measurements were made for the following cases:

1) Angle of incidence equal to 0 degrees, traffic barriers in the 0, 1, 2, 3, 4, 5, 6, and 7 positions (0 - up against the windward curb; 6 - up against the leeward curb; 7 - no traffic barrier at all);

2) Angle of incidence equal to -3 degrees (downward angle), traffic barriers in the 1, 3, 5, and 7 positions; and

3) Angle of incidence equal to 3 degrees, traffic barriers in the 1,3,5, and 7 positions.

For the non-zero angles of incidence, for the traffic barrier positions not tested specifically, critical flutter wind speeds were interpolated from those wind speeds that were measured.

For the options W1, W2, W3, W5, and W6 the values of A2 andA3 were obtained and a critical flutter wind speed was computed. In those tables the following designations are used

Wabcd

where

a	option number;
b	wind angle (1 = -3 degrees, 2 = 0 degrees, 3 = +3 degrees);
c	traffic barrier position;
d	wind direction (1 - west wind; 2 - east wind).

A summary of the critical flutter wind speeds obtained is presented in Tables C.4 through C.8. Option W4 is similar to W1, but less critical, and so was not tested specifically. Option W1 (alternate) is not critical compared to W1, and was not tested over the full range relative to W1. The values of A2 and A3 were measured specifically for W1 (alternate) at a zero angle of incidence, without traffic barriers, for west winds. Those result are presented in Appendix 6 as W1271A.

It should be noted that for all cases, for zero angles of incidence, the critical flutter wind speeds are all equal to or greater than 100 mph, except W1201 which is 99.7 mph. For many of the non-zero angles of incidence this criterion is not met. If, under an extreme wind, the bridge deforms excessively in torsion, this criterion should be met at that particularly non-zero angle of incidence. This does not occur for the Golden Gate Bridge in any of its options (see the mean response of Modes 7 and 8 in the buffeting analyses). Steady, strong, mean winds at non-zero angles of incidence would be extremely rare (except for winds on the north side span, from the west, over the Marin Headlands). It is therefore typical in the profession to reduce the critical flutter wind speed threshold (the criterion) as a function of vertical angle of incidence. Typical reduction scale factors are 0.8 at angles of incidence of plus or minus 2.5 degrees; and 0.5, at angles of incidence of plus or minus 5.0 degrees. Linearly interpolating, this converts to a reduction scale factor of 0.733 at plus or minus 3 degrees. That would define a critical flutter wind speed threshold of 73.3 mph at those non-zero angles of incidence. This reduction in critical flutter wind speed threshold has been accepted for many bridge designs throughout the world, specifically the Lantau Crossing bridges in Hong Kong, and the new Cooper River Bridge in Charleston, South Carolina. This reduction schedule has been in use since the 1950's. All of the non-zero results for all of the options considered in this study do meet this criterion.

For several options, for horizontal winds from the west, the critical flutter wind speed greatly exceeded the criterion of 100 mph. For those cases, the aerodynamic enhancements are not required to extend for the full length of the bridge. Mode 7 torsional motions on the sidespans are minimal. Aerodynamic enhancements (winglets and fairings) contribute nothing to the stabilization of Mode 7 if placed on the sidespans. Mode 8 torsional motions are small on the sidespans. The effectiveness of the aerodynamic enhancements on the sidespans to Mode 8 is real, but minor.

Detailed stability analyses were therefore performed for each optional crossection (W1 - W6) with the aerodynamic enhancements (winglets or fairings) distributed over differing portions of the bridge. Aerodynamic enhancements are most effective if placed where torsional modal displacements are greatest (the one-quarter span lengths at the quarter points of the main span for Mode 7, and the middle half-span of the main span for Mode 8). Therefore, the possible distributions of aerodynamic enhancements considered are those shown on Figures C.8, C.9 and C.10. For the regions where there are no aerodynamic enhancements proposed, aeroelastic flutter derivatives for those cases shown in the following table were used.

OPTION	CASE WITHOUT AERODYNAMIC ENHANCEMENTS
W1	GGB42
W1 (alt)	GGB42
W2	GGB42
W3	GGB1
W5	GGB42
W6	GGB69

The flutter derivatives were used for the various options (W1 - W6) for zero angle of incidence, for a barrier placed that produced the lowest critical flutter wind speed. Those specific cases used were as follows:

OPTION	CRITICAL CASE USED
W1	W1201
W1 (alt)	W1271A
W2	W2201
W3	W3231
W5	W5201
W6	W6201

It should be noted that many of the critical cases had the barrier on the windward curb. Extreme winds come from the west, so stow the traffic barrier on the east curb, not the west. For these detailed analyses, winds were horizontal and from the west. For the cases without the aerodynamic enhancements, no barriers were in place. These are areas of little aerodynamic importance (hence no enhancements are needed there), and critical flutter wind speeds are generally insensitive to barrier placement, so only minor second order errors are expected with the use of these preliminary study values, in these non-critical locations.

The results of these analyses indicated that aerodynamic enhancements are required, for the various options, only over those portions identified in Figures C.11 through C.13. For each of those cases, results of the stability analyses are presented in Tables C.9 through C.14. Note that for case W1201 (Option W1 with a traffic barrier at position 0) the critical flutter wind speed is only 98 mph. For all other traffic barrier placements, or

no traffic barrier, the critical flutter wind sped exceeds 100 mph, i.e., do not store the traffic barrier to the west.

For all of these studies, the extreme wind was assumed to come from the west. From Ref 5 (see Appendix 1) the percentage of time that 100 year wind speeds (or greater) come from the east (at the San Francisco International Airport, and similarly at the Golden Gate Bridge) are three orders of magnitude lower than the percentage of time those winds come from the south or west. Probabilities are proportional to these percentages, and return periods are proportional to the inverse of those probabilities. Therefore a 100 year, one hour averaged wind speed of 76 mph from the west corresponds to 100,000 year, one hour averaged wind speed from the east. The options W1, W1 (alternate), and W6 are unsymmetric. The preliminary cases that correspond to the W1 - W6 options for wind from the east, and their critical flutter wind speeds are as follows (all cases without traffic barriers):

OPTION FOR WEST WIND	CASE FOR EAST WIND	U_{CRIT} (mph) FOR EAST WIND
W1	GGB53	99
W1 (alt)	GGB42	77
W2	-	>118
W3	-	119
W5	-	>118
W6	GGB41	82

For all cases the critical flutter wind speeds for each winds exceed the 100,000 year wind speed from the east of 76 mph.

For Cases 0W1201, 4W2201, 2W3231, 4W5201, 4W6201, and 4W1271A (where the first number indicates the lateral spread of aerodynamic enhancements required to meet the stability criterion - see Figures C.8, C.9, and C.10) buffeting analyses were performed (using the numerical simulation procedure defined in Appendix 3). With the peak nodal displacements, member actions and stresses throughout the bridge for each mode of vibration can then be determined. A stress at any point can then be computed as the square-root-of-the-sum-of-the-square (SRSS) combination of those modal stresses (or some other reasonable combination procedure).

It should be noted that a buffeting analysis, at the 100 year design level wind speed, could not be computed (at 34 m/s) for the existing bridge. However, buffeting analyses can be compared to the existing state through their static aerodynamic coefficients. Static aerodynamic coefficients for various options are shown below:

CASE	C_D	$dC_L/d\alpha$	$dC_M/d\alpha$
W0	.357	3.203	-.002
W1	.371	2.989	.377

W2	.371	2.964	.346
W3	.394	2.627	.404
W6	.356	2.455	.273

The drag coefficients with the suicide deterrent and aerodynamic enhancement systems are generally higher than the drag coefficient for the existing case, by as much as 10% for W3, but generally by as much as 4% for options W1, W2, and W6. The vertical buffeting response is proportional to the slope of the lift curve ($\frac{dC_L}{d\alpha}$). In all cases, with the suicide deterrent and aerodynamic systems, the slope of the lift curve is less than what it is for the existing state. In all cases too, the slope of the moment coefficient is significantly greater than it is for the existing case, and torsional motions are proportional to the slope of the moment coefficient. However, the absolute values (typically are less than 0.4) are small compared to the maximum possible of 1.5708 for an airfoil.

TABLE C.1

EXISTING CONDITION 4/2/7

RATIO OF FINAL MODAL STANDARD DEVIATION RESPONSES TO INITIAL MODAL STANDARD DEVIATION RESPONSES

LENGTH OF RECORD (SEC) 300

WWL MODE	DMJM MODE	U(M/S) - TEN MINUTE AVERAGED WIND SPEED AT DECK 20.0	22.0	24.0	26.0	28.0	30.0	32.0
1	1	0.234	0.213	0.193	0.175	0.159	0.145	0.131
2	2	0.024	0.017	0.016	0.034	0.097	0.255	0.717
3	3	0.104	0.093	0.083	0.074	0.066	0.059	0.056
4	4	0.010	0.013	0.023	0.046	0.093	0.214	0.574
5	5	0.062	0.052	0.039	0.043	0.091	0.214	0.635
6	6	0.008	0.006	0.009	0.017	0.038	0.088	0.234
7	7	0.135	0.196	0.307	0.557	1.093	2.341	5.515
8	8	0.086	0.115	0.153	0.216	0.352	0.645	1.310
9	9	0.011	0.008	0.004	0.005	0.012	0.028	0.093
10	10	0.043	0.044	0.058	0.065	0.103	0.197	0.461

TABLE C.2

EXISTING CONDITION 4/2/7

FINAL MODAL FREQUENCIES

LENGTH OF RECORD (SEC) 300

WWL MODE	DMJM MODE	U(M/S) - TEN MINUTE AVERAGED WIND SPEED AT DECK 20.0	22.0	24.0	26.0	28.0	30.0	32.0
1	1	0.050	0.050	0.050	0.050	0.050	0.050	0.050
2	2	0.087	0.140	0.177	0.177	0.180	0.180	0.180
3	3	0.110	0.110	0.110	0.110	0.110	0.110	0.109
4	4	0.129	0.193	0.192	0.192	0.192	0.192	0.191
5	5	0.134	0.133	0.131	0.188	0.183	0.181	0.180
6	6	0.159	0.206	0.198	0.193	0.194	0.194	0.194
7	7	0.182	0.182	0.181	0.181	0.180	0.180	0.180
8	8	0.195	0.194	0.195	0.194	0.194	0.194	0.194
9	9	0.198	0.201	0.213	0.180	0.180	0.180	0.182
10	10	0.203	0.202	0.201	0.192	0.191	0.192	0.193

TABLE C.3

EXISTING CONDITION 4/2/7

CHECK FOR STATIC DIVERGENCE
FINAL AVERAGE MODAL RESPONSES

LENGTH OF RECORD (SEC) 300

WWL MODE	DMJM MODE	U(M/S) - TEN MINUTE AVERAGED WIND SPEED AT DECK 20.0	22.0	24.0	26.0	28.0	30.0	32.0
1	1	-0.940	-1.140	-1.359	-1.597	-1.854	-2.130	-2.425
2	2	-0.004	-0.003	-0.002	0.000	0.003	0.040	0.126
3	3	-0.007	-0.006	-0.006	-0.005	-0.004	-0.003	-0.001
4	4	-0.025	-0.029	-0.035	-0.040	-0.047	-0.057	-0.075
5	5	-0.001	-0.000	-0.000	-0.000	-0.000	-0.013	-0.042
6	6	-0.009	-0.011	-0.013	-0.015	-0.018	-0.021	-0.026
7	7	0.008	0.012	0.014	0.016	0.034	-0.069	-0.241
8	8	-0.022	-0.027	-0.030	-0.042	-0.053	-0.073	-0.107
9	9	0.000	0.000	0.000	0.000	0.000	-0.001	-0.005
10	10	0.018	0.022	0.028	0.030	0.034	0.035	0.033

TABLE C.4
CRITICAL FLUTTER WIND SPEED (mph)
CASE W1

ANGLE OF INCIDENCE (DEGREES)	TRAFFIC BARRIER	U_{CRIT} (mph)
0	NONE	105.4
0	0	99.7
0	1	107.1
0	2	112.3
0	3	>118.0
0	4	>119.0
0	5	118.4
0	6	109.0
-3	NONE	107.7
-3	0	103.9
-3	1	103.9
-3	2	110.8
-3	3	>117.6
-3	4	116.0
-3	5	114.4
-3	6	107.7
3	NONE	85.6
3	0	85.6
3	1	92.4
3	2	96.5
3	3	100.6
3	4	97.4
3	5	94.1
3	6	85.6

TABLE C.5
CRITICAL FLUTTER WIND SPEED (mph)
CASE W2

ANGLE OF INCIDENCE (DEGREES)	TRAFFIC BARRIER	U_{CRIT} (mph)
0	NONE	>117.8
0	0	116.8
0	1	>117.9
0	2	>119.2
0	3	>119.6
0	4	>119.3
0	5	>119.6
0	6	116.9
-3	NONE	92.0
-3	0	92.0
-3	1	91.6
-3	2	91.3
-3	3	91.1
-3	4	95.6
-3	5	100.2
-3	6	92.0
3	NONE	>120.6
3	0	>120.6
3	1	>117.6
3	2	>117.6
3	3	>118.8
3	4	>118.8
3	5	>121.2
3	6	>120.6

TABLE C.6
CRITICAL FLUTTER WIND SPEED (mph)
CASE W3

ANGLE OF INCIDENCE (DEGREES)	TRAFFIC BARRIER	U_{CRIT} (mph)
0	NONE	118.8
0	0	121.5
0	1	119.1
0	2	118.3
0	3	113.9
0	4	116.3
0	5	118.5
0	6	110.1
-3	NONE	83.9
-3	0	83.9
-3	1	80.3
-3	2	87.2
-3	3	94.5
-3	4	90.3
-3	5	86.1
-3	6	83.9
3	NONE	91.5
3	0	91.5
3	1	89.9
3	2	88.0
3	3	86.0
3	4	86.2
3	5	86.3
3	6	91.5

TABLE C.7
CRITICAL FLUTTER WIND SPEED (mph)
CASE W5

ANGLE OF INCIDENCE (DEGREES)	TRAFFIC BARRIER	U_{CRIT} (mph)
0	NONE	112.3
0	0	100.3
0	1	116.2
0	2	>120.9
0	3	>116.9
0	4	>119.2
0	5	>121.2
0	6	>119.3
-3	NONE	90.7
-3	0	90.7
-3	1	83.1
-3	2	88.0
-3	3	92.9
-3	4	92.6
-3	5	92.3
-3	6	90.7
3	NONE	102.7
3	0	102.7
3	1	>118.9
3	2	>118.5
3	3	>118.5
3	4	116.15
3	5	113.8
3	6	102.7

TABLE C.8
CRITICAL FLUTTER WIND SPEED (mph)
CASE W6

ANGLE OF INCIDENCE (DEGREES)	TRAFFIC BARRIER	U_{CRIT} (mph)
0	NONE	>113.5
0	0	104.8
0	1	105.6
0	2	>114.2
0	3	>115.5
0	4	>112.9
0	5	>112.7
0	6	>119.3
-3	NONE	104.0
-3	0	104.0
-3	1	95.3
-3	2	98.2
-3	3	101.0
-3	4	105.0
-3	5	109.0
-3	6	104.0
3	NONE	>114.5
3	0	>114.5
3	1	114.2
3	2	109.7
3	3	>109.7
3	4	109.8
3	5	109.9
3	6	>114.5

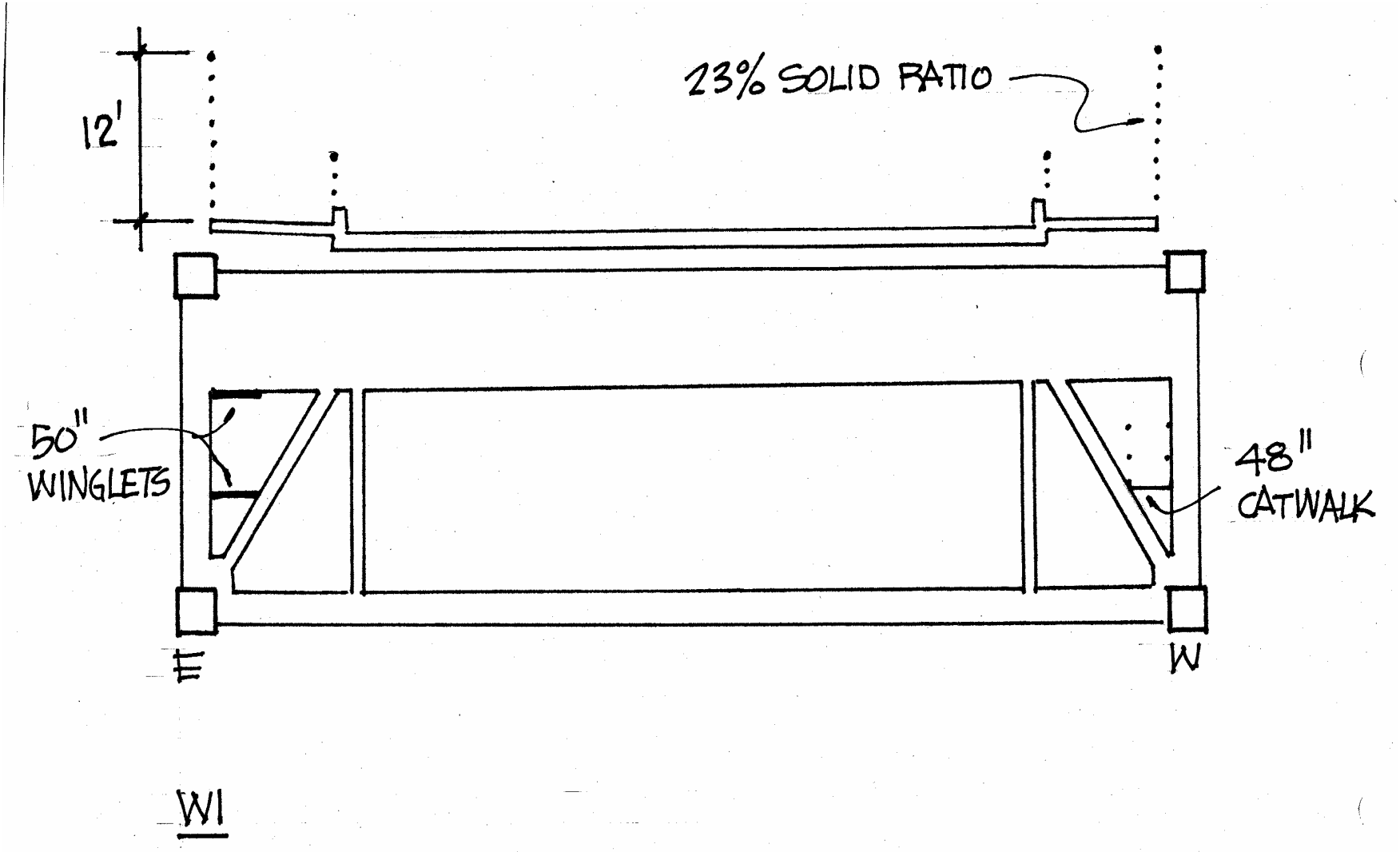

FIGURE C.1 - 12’ tall vertical barrier with solid ratio of 23% and under deck winglets and/or catwalk

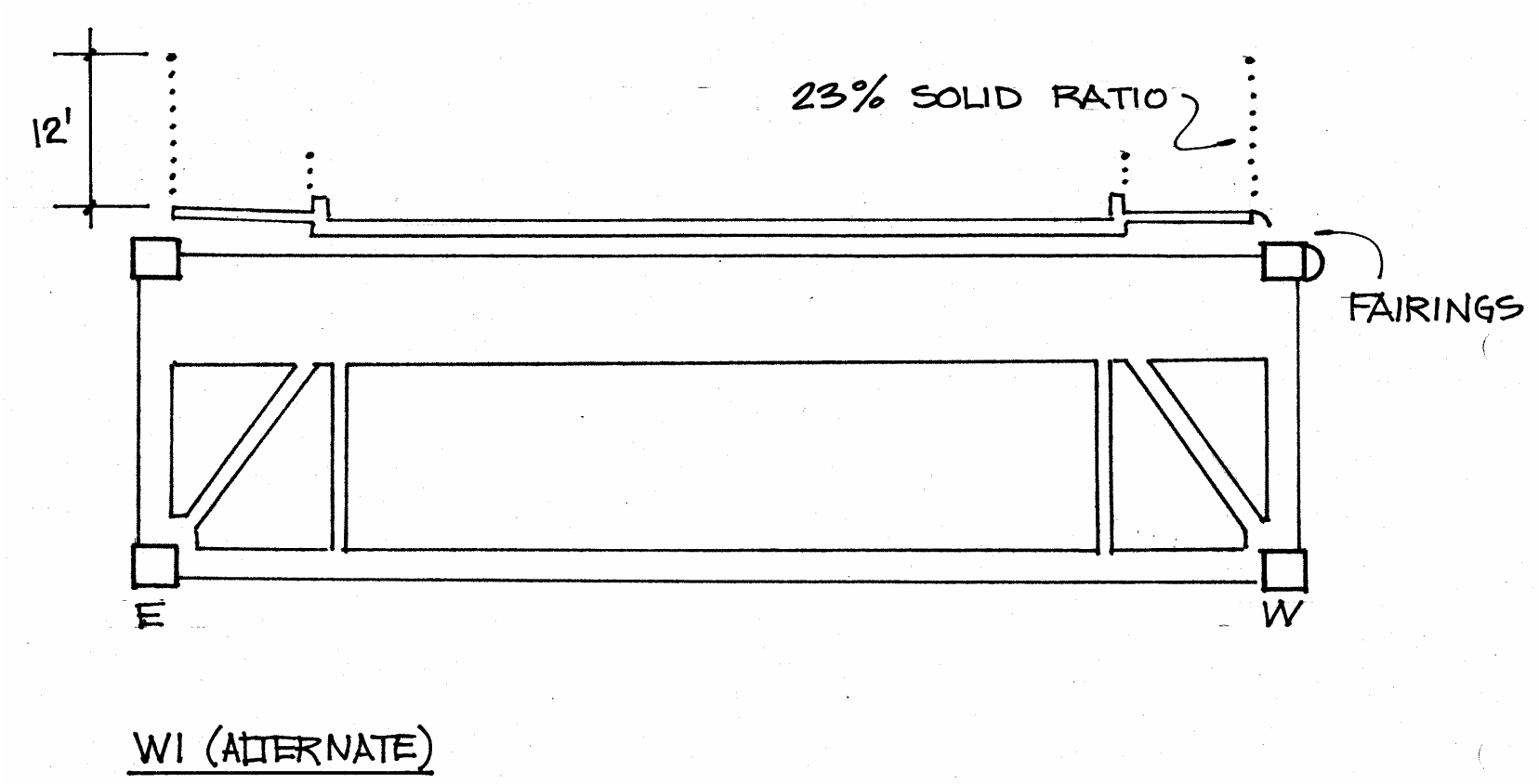

FIGURE C.2 - 12' tall vertical barrier with solid ratio of 23% and use of wind fairings in lieu of winglets

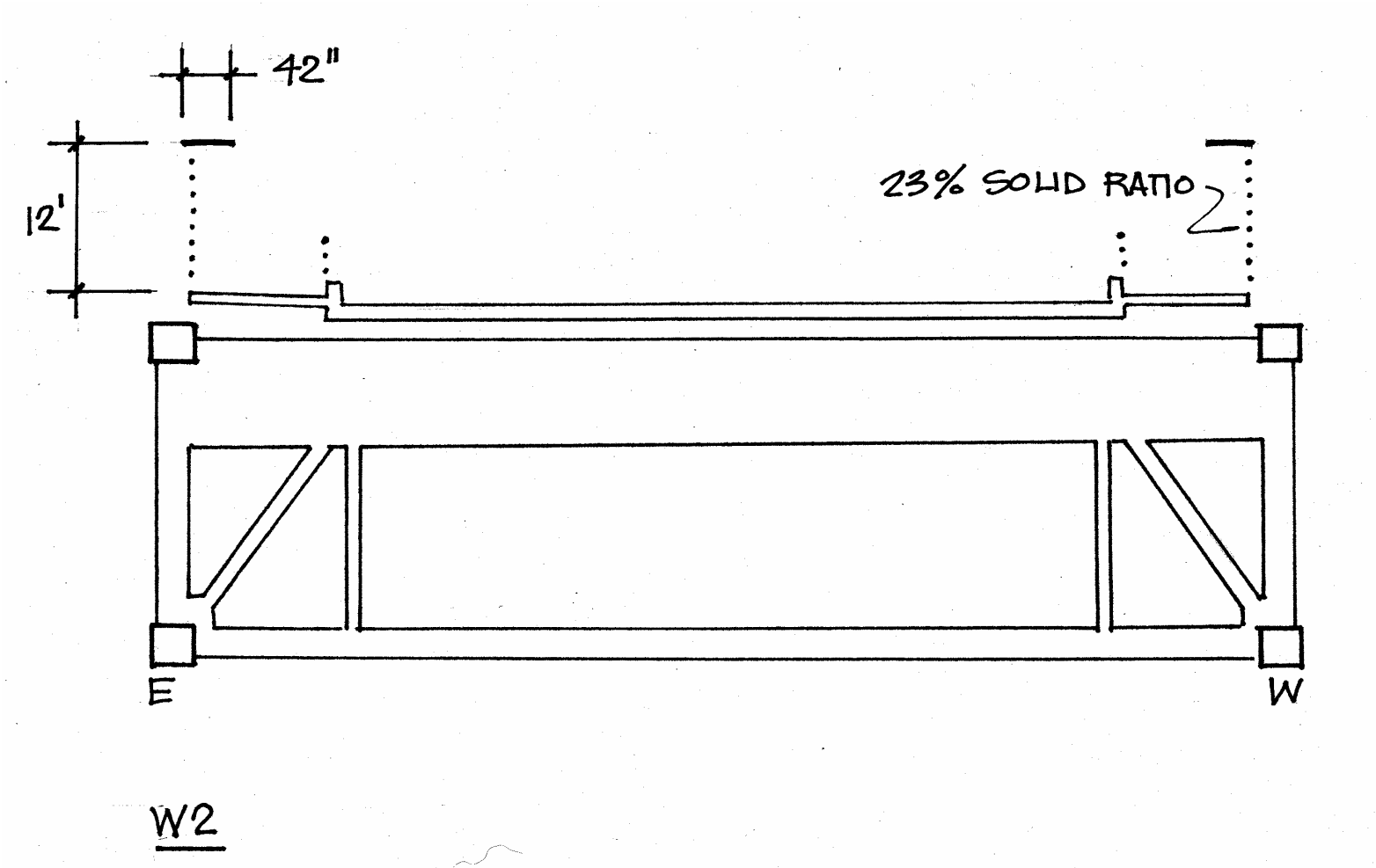

FIGURE C.3 - 12’ tall vertical barrier with solid ratio of 23% and winglets mounted over the new barrier

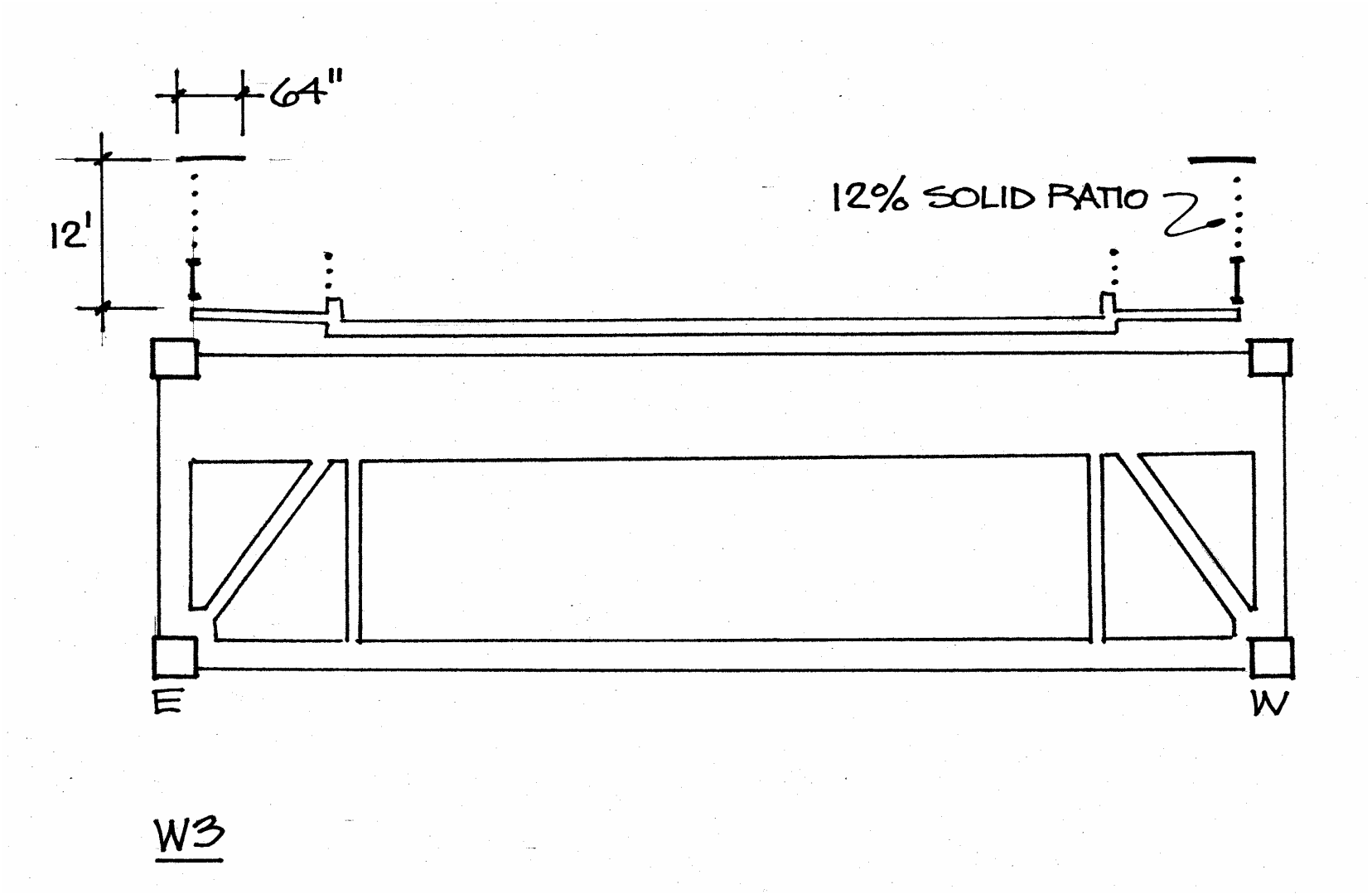

FIGURE C.4 - A new vertical barrier mounted over the existing railing with a maximum solid ratio of 12% and with winglets mounted over the new barrier

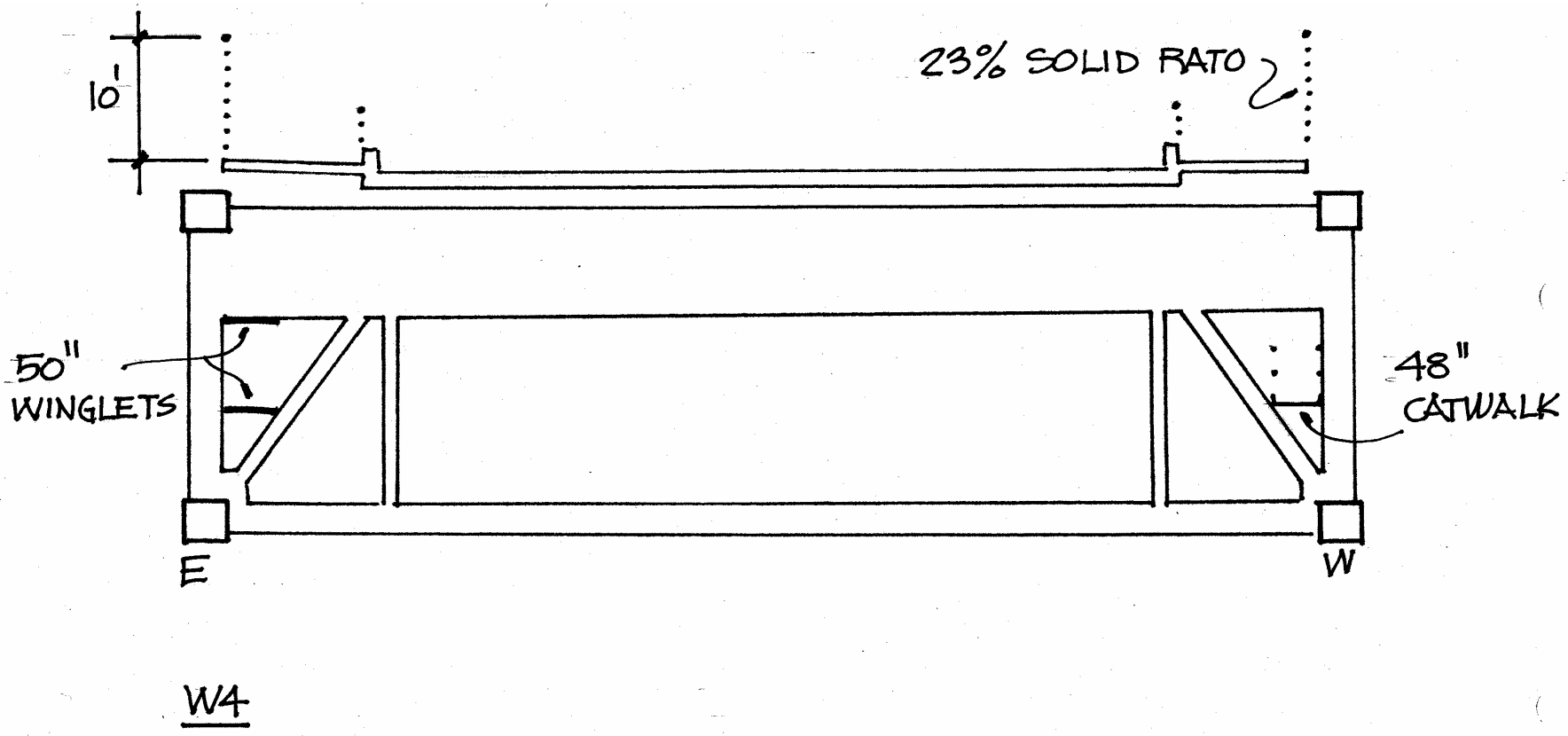

FIGURE C.5 - Similar to W1 except a new barrier height of 10’ instead of 12’

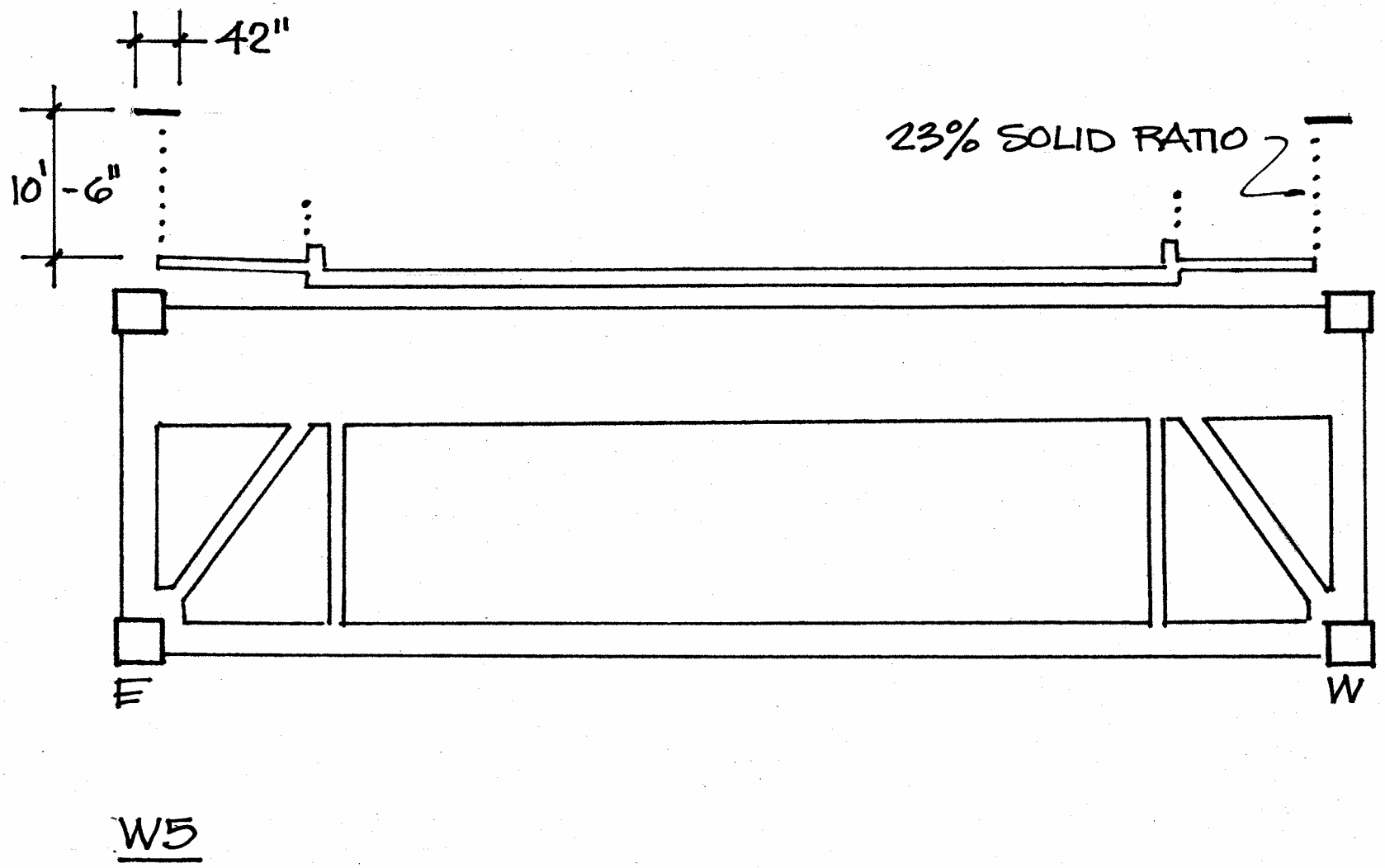

FIGURE C.6 - Similar to W2 except with a new barrier height of approximately 10’ and with a winglet mounted at 10’-6”

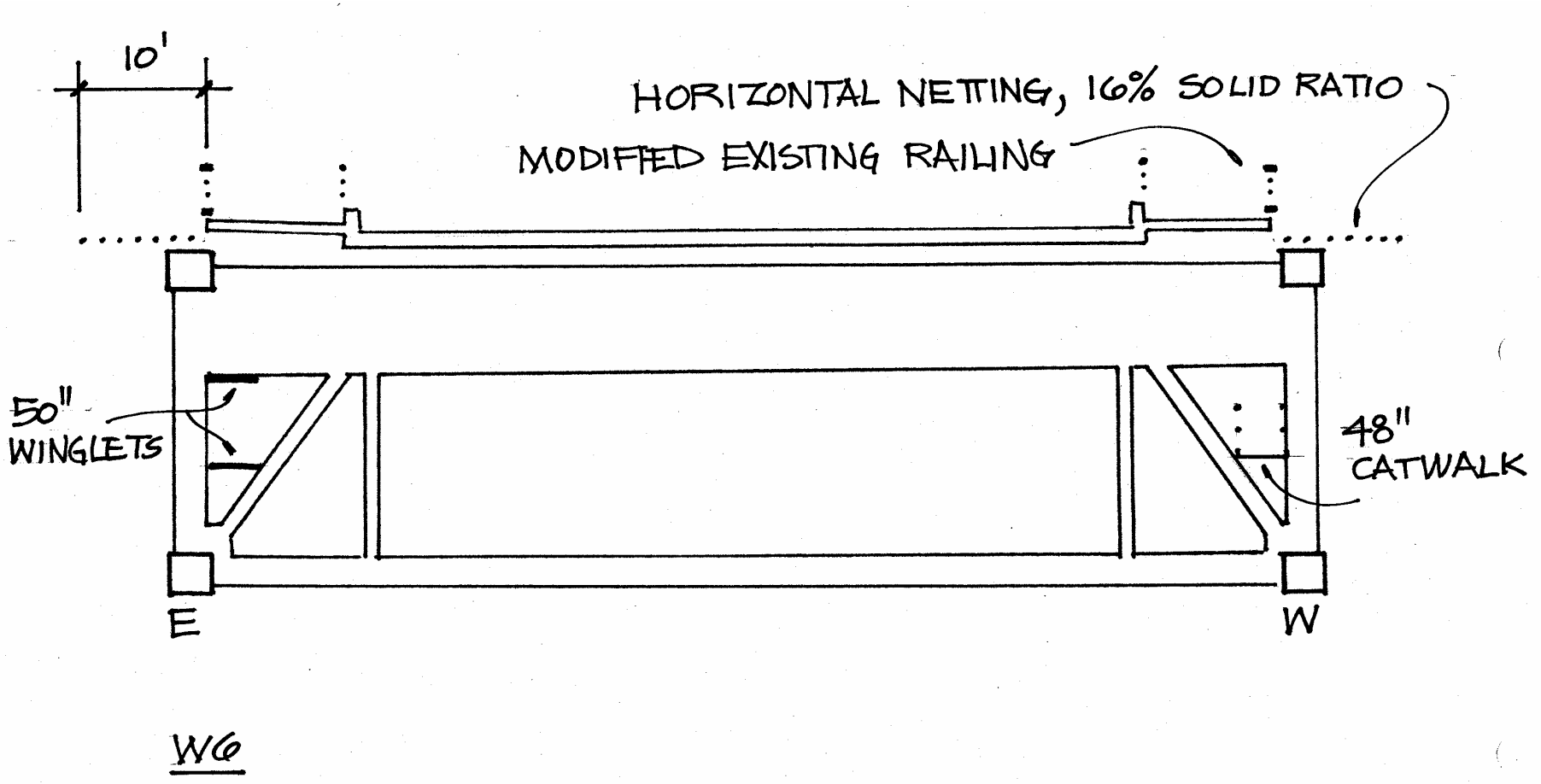

FIGURE C.7 - A horizontally projecting net. Net projection of 10' with a maximum solid ratio of 16%. Modify existing railing to have a maximum solid ratio of 23%. Below deck winglets and catwalk required

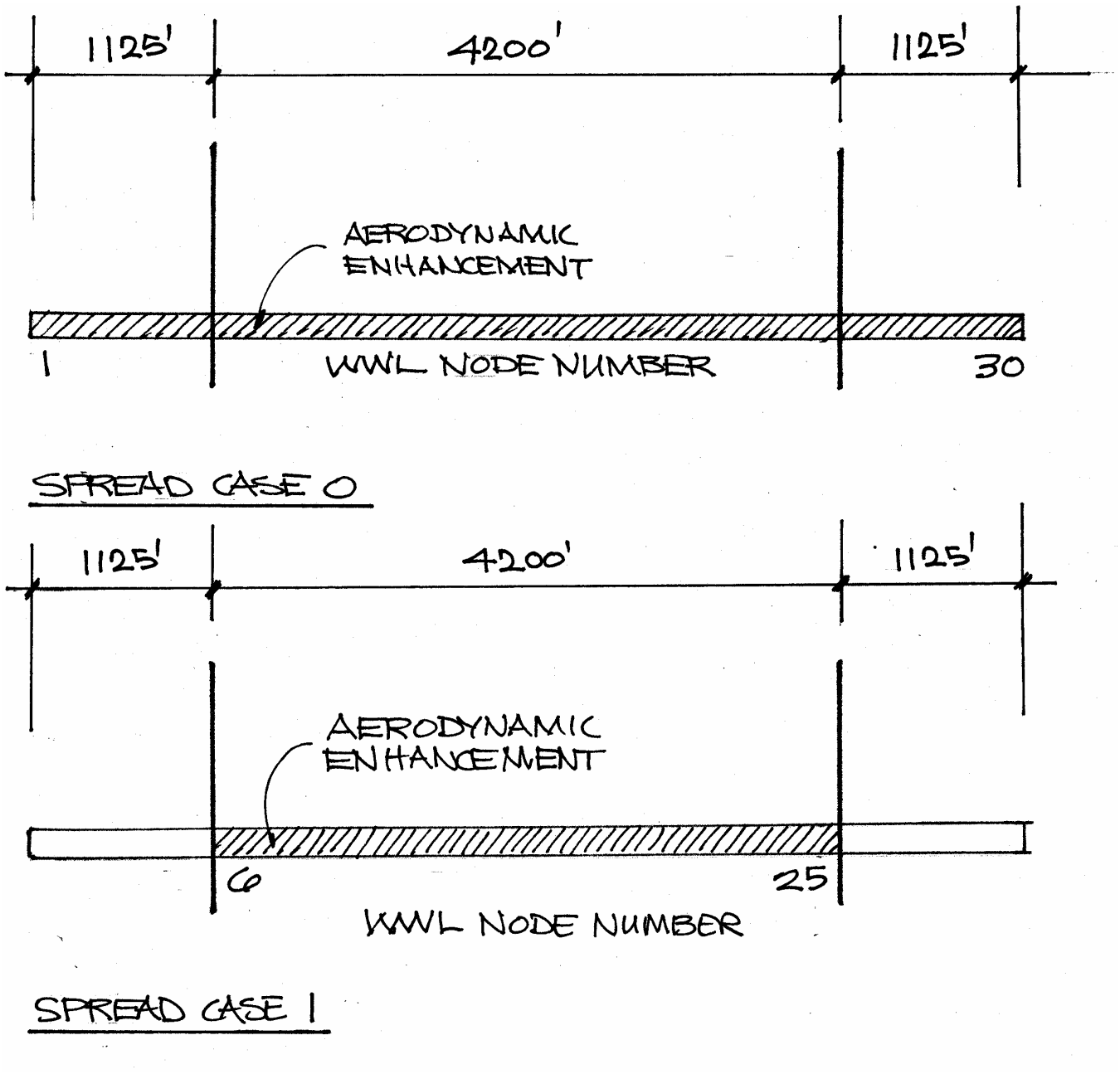
1125'
4200'
1125'
AERODYNAMIC ENHANCEMENT
1
WWL NODE NUMBER
30
SPREAD CASE 0
1125'
4200'
1125'
AERODYNAMIC ENHANCEMENT
6
25
WWL NODE NUMBER
SPREAD CASE 1

FIGURE C.8

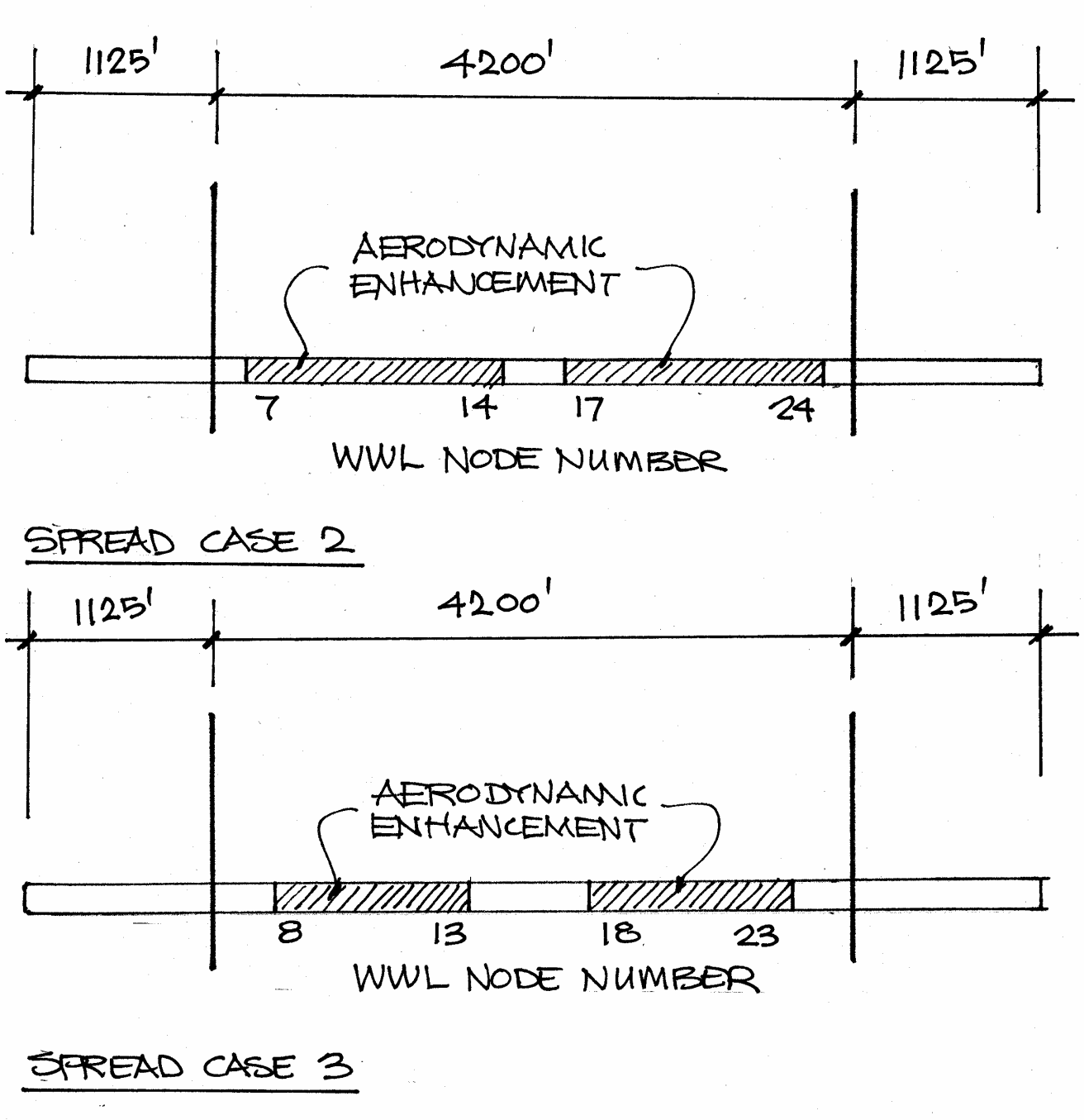
1125'
4200'
1125'
AERODYNAMIC ENHANCEMENT
7
14
17
24
WWL NODE NUMBER
SPREAD CASE 2
1125'
4200'
1125'
AERODYNAMIC ENHANCEMENT
8
13
18
23
WWL NODE NUMBER
SPREAD CASE 3

FIGURE C.9

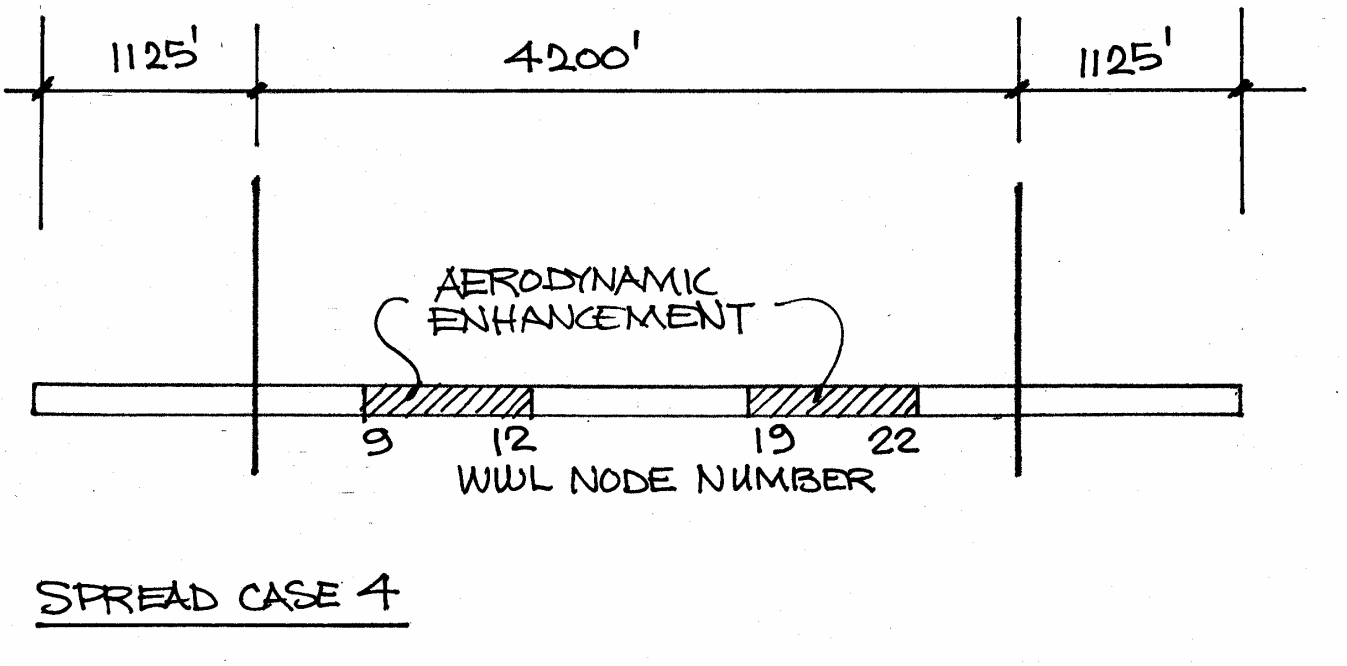
1125'
4200'
1125'
AERODYNAMIC
ENHANCEMENT
9
12
19
22
WWL NODE NUMBER
SPREAD CASE 4

FIGURE C.10

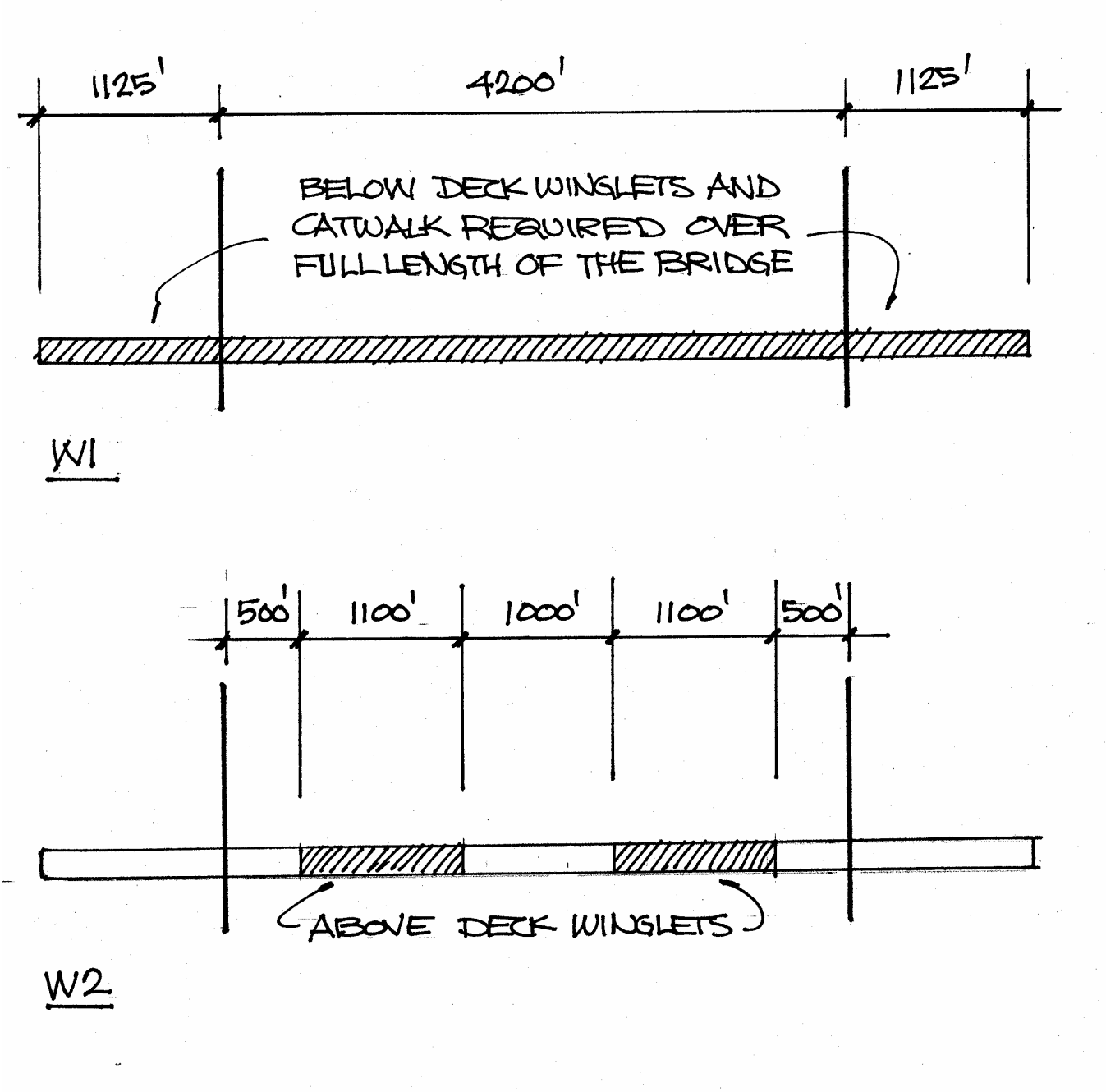
1125'
4200'
1125'
BELOW DECK WINGLETS AND CATWALK REQUIRED OVER FULL LENGTH OF THE BRIDGE
W1
500'
1100'
1000'
1100'
500'
ABOVE DECK WINGLETS
W2

FIGURE C.11

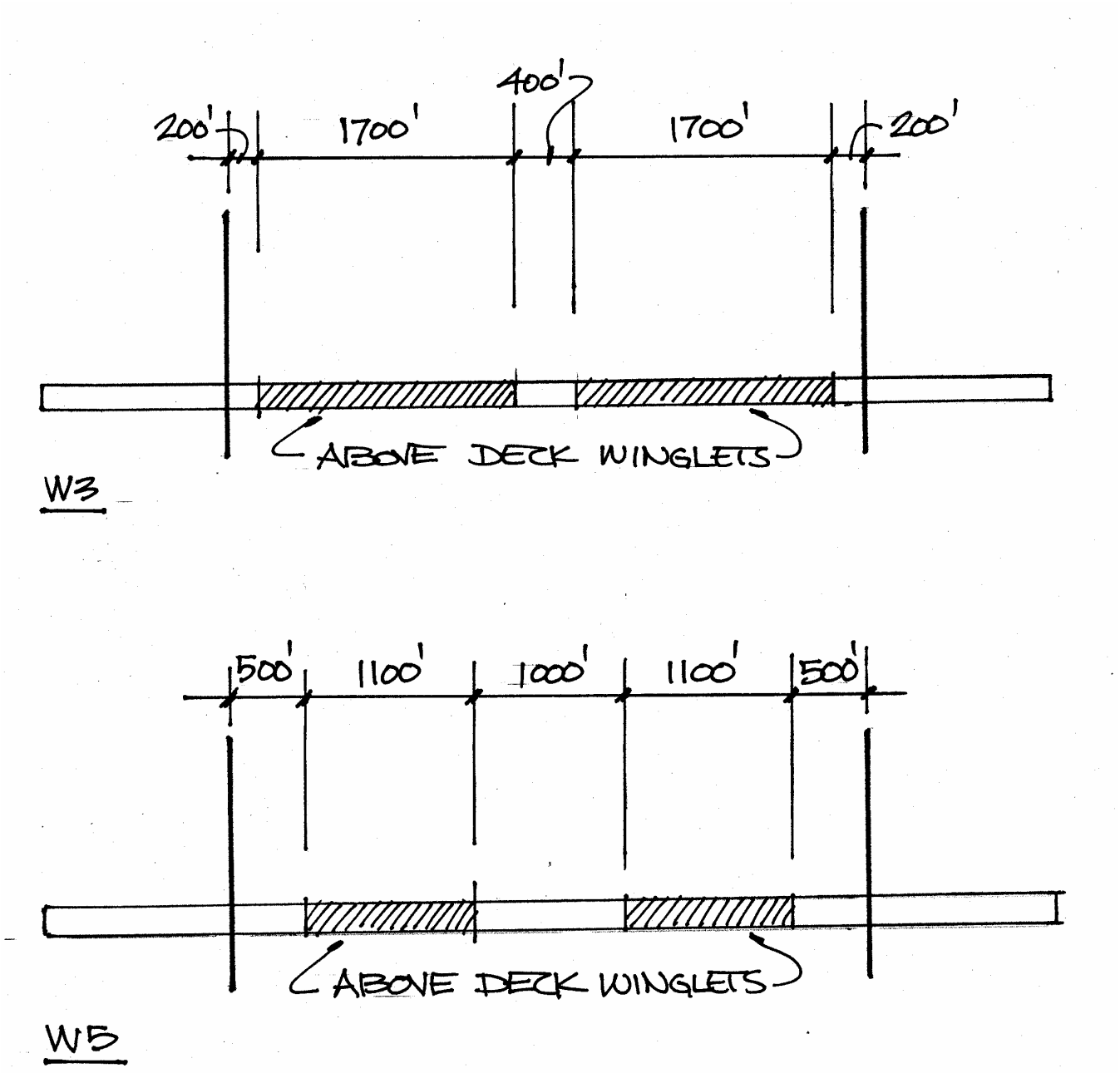
200'
1700'
400'
1700'
200'
ABOVE DECK WINGLETS
W3
500'
1100'
1000'
1100'
500'
ABOVE DECK WINGLETS
W5

FIGURE C.12

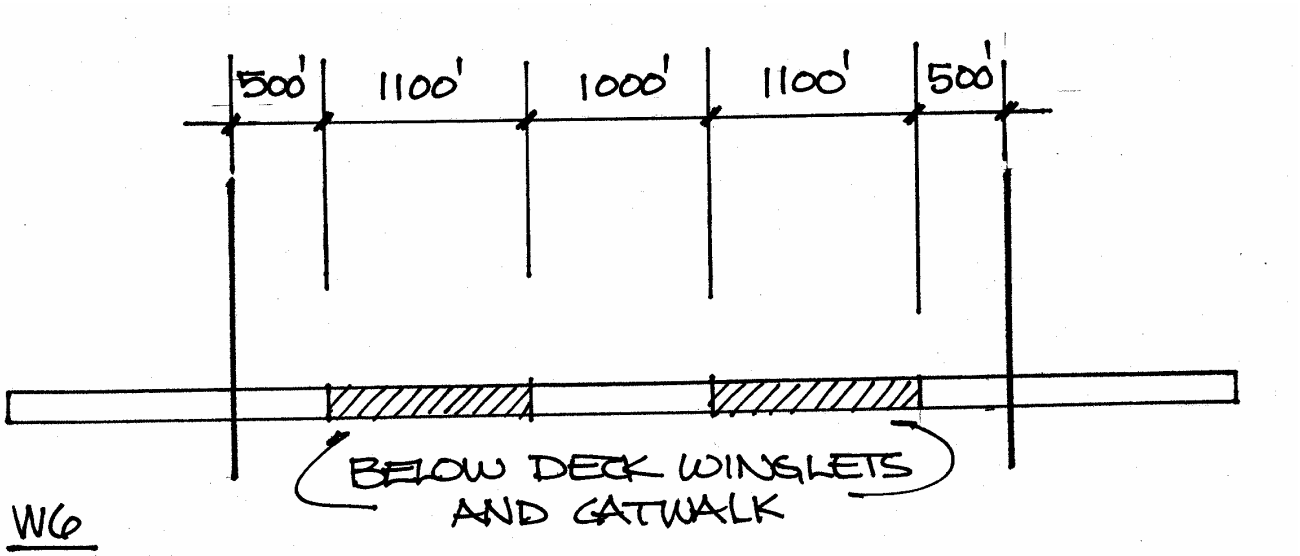
500'
1100'
1000'
1100'
500'
BELOW DECK WINGLETS
AND CATWALK
W6

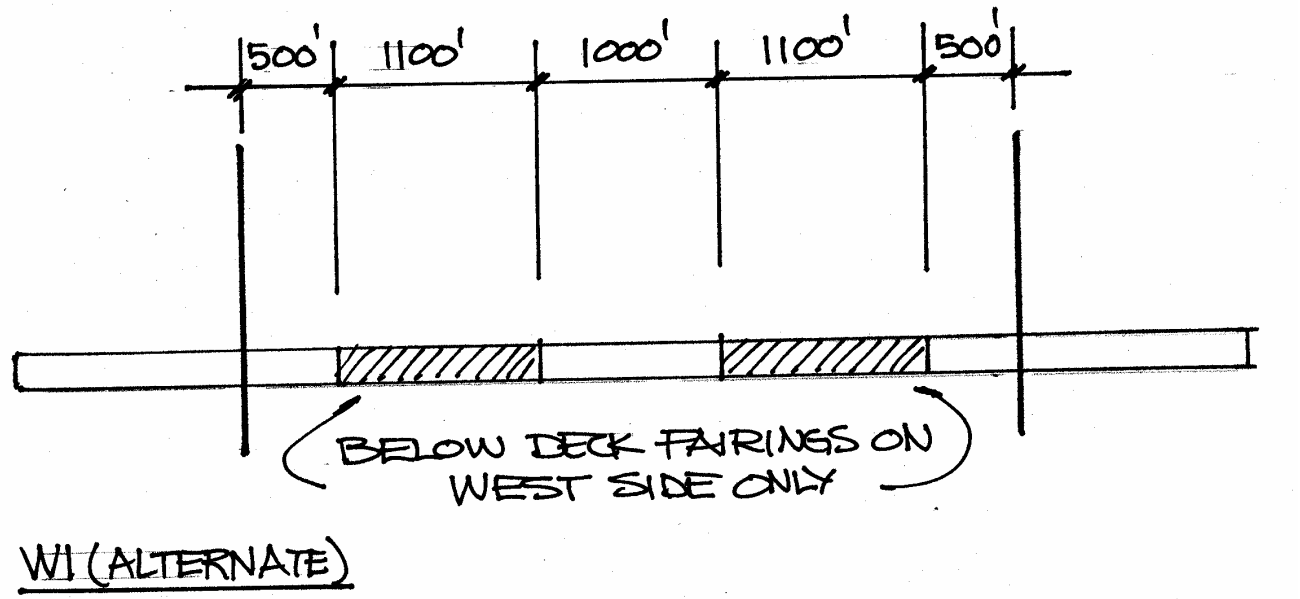
500'
1100'
1000'
1100'
500'
BELOW DECK FAIRINGS ON
WEST SIDE ONLY
W1 (ALTERNATE)

FIGURE C.13

APPENDICES

APPENDIX 1
WIND ENVIRONMENT AT THE SITE

A detailed analysis of historical winds was not made for this study, but the results of a previous study, made specifically for the Golden Gate Bridge, Highway and Transportation District were used (Ref 5).

For a bridge that is a vital transportation link in a major disaster, it is appropriate that the design wind speed be a wind speed with a return period of at least 100 years. An omnidirectional, one hour averaged wind speed, at the bridge deck elevation, with a return period of 100 years, was found to be 76 mph (Ref 5).

An aeroelastic flutter instability can be catastrophic (as it was for the Tacoma Narrows Bridge). Consequently, it is appropriate to specify that an aeroelastic flutter instability should not occur for a wind speed with a return period less than 10,000 to 100,000 years. From the referenced historical wind speed analysis (Ref 5), such an appropriate critical flutter wind speed criterion was determined to be 100 mph. This is a 10-minute averaged wind speed at the bridge deck elevation (70.87 m).

Strong winds are most likely to come from the south and the west. See Figure 1.1, taken from Ref 5. Also note that, at the site, the percentage of time that strong winds (with a return period of 100 years or more) come from the east is three orders of magnitude lower than the percentage of time that strong winds come from the west. Probabilities are proportional to the percentages, and return periods are proportional to the inverse of the probabilities. Therefore, the return period for equal wind speeds from the east will have a return period approximately 1,000 times longer than the return period for a comparable wind speed from the west. Winds from the west are critical.

An omnidirectional 100 year wind (essentially equal to a 100 year wind from the south or the west) of 34 m/s (76 mph) was determined. It is reasonable to assume, therefore, from Figure 1.1 in Ref 5 that this wind speed, 34 m/s (76 mph, would have a return period of 100,000 years for winds from the east. Assuming that the distribution of annual extremes at the site, for winds from the east, are similar to those from the west, it can be computed that for winds from the east, an hour averaged wind speed of 20.6 m/s (46 mph) would have a return period of 100 years, and a 10-minute averaged wind speed of 29.5 m/s (66 mph) would have return period of 10,000 years. These are approximate values, but are suitable for the analyses for these non-critical directions.

Note that winds from the south may also be likely. However, winds that are essentially perpendicular to the axis of the bridge (the axis of the bridge is north-south) are critical from a stability and buffeting point of view.

FIGURE 1.1

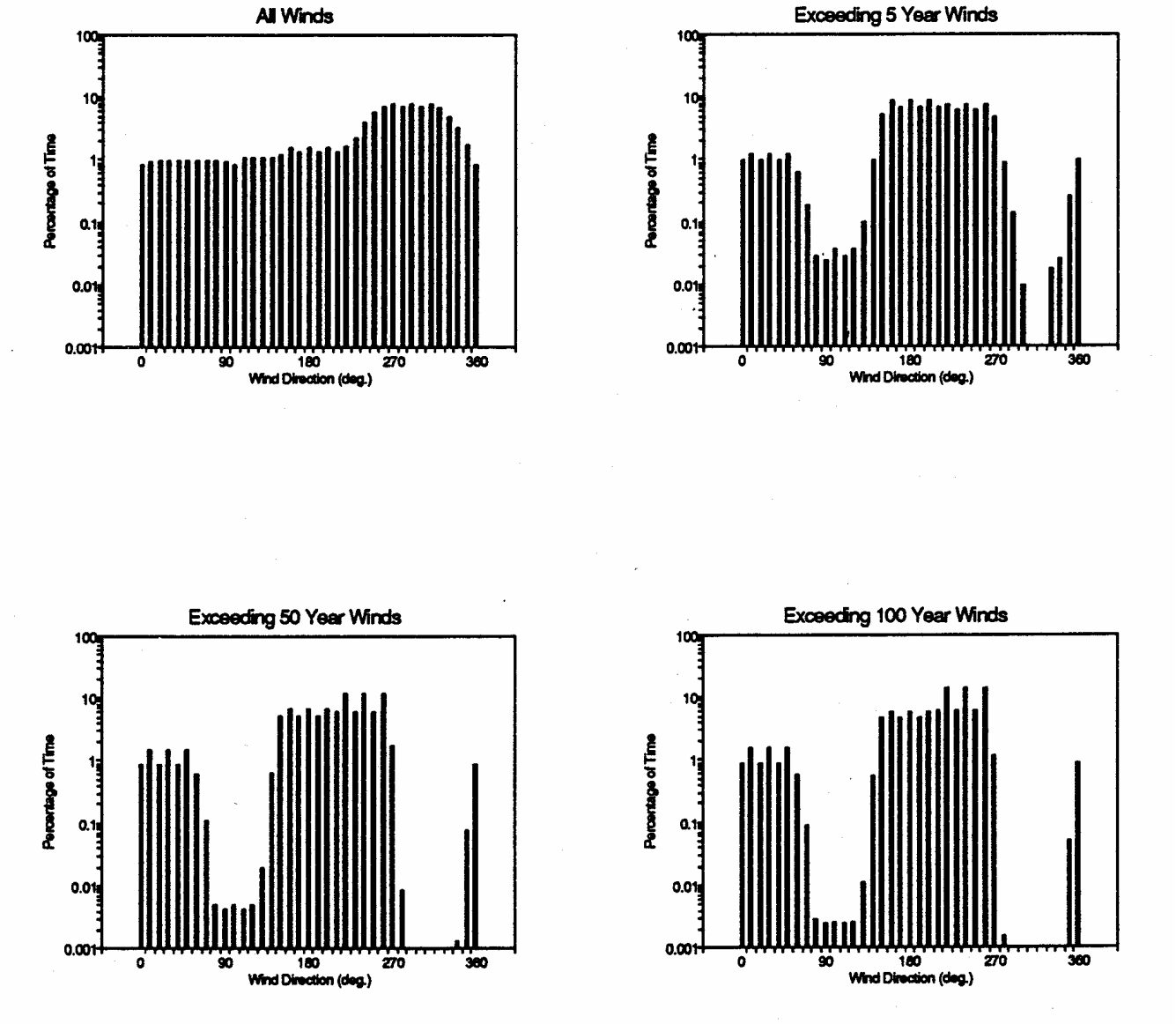
All Winds
Exceeding 5 Year Winds
Exceeding 50 Year Winds
Exceeding 100 Year Winds
Percentage of Time
100
10
1
0.1
0.01
0.001
0
90
180
270
360
Wind Direction (deg.)

APPENDIX 2
TEST FACILITIES

Wind tunnel tests were performed in the 1 x 4 m open return type atmospheric boundary layer wind tunnel, designed specifically for bridge section model and full-bridge model testing, owned and operated by the West Wind Laboratory, Inc. Drawings of the wind tunnel are shown on Figure 2.1. Wind speed profiles upstream and downstream from the section model test section are shown in Figures 2.2 and 2.3. Shown in Figure 2.4 is the boundary layer at one end plate. Wind speeds are continuously variable from 0 to 6.1 m/s.

The test section is open without walls or a ceiling. Ambient pressures within the test chamber therefore are essentially constant. Furthermore, winds can flow around and over the models without constriction (as in the full-scale environment). Therefore, blockage effects are minimal, i.e., wind speed will not be artificially accelerated around the model because there are no walls to constrict and accelerate the flow.

The wind tunnel extends 6.1 m upstream from the test section without flair or constriction. Atmospheric boundary layers can be generated in this space with the use of spires and blocks on the wind tunnel floor.

Model displacements, and force transducer displacements are measured with Macro Sensors PRH-812-050 LVDT Transducers and Macro Sensors LPC-2000 Signal Conditioners. Mean wind speeds are measured with a Sierra Instruments Model 618 Air Velocity Meter. Mean and fluctuating wind speeds are measured with a total head tube and Setra System, Inc. 239 Pressure Transducer.

Analog signals from the transducers are digitized on a ComputerBoards PCM-DAS08 Analog to Digital Converter.

FIGURE 2.1
1 X 4 m ATMOSPHERIC BOUNDARY LAYER WIND TUNNEL

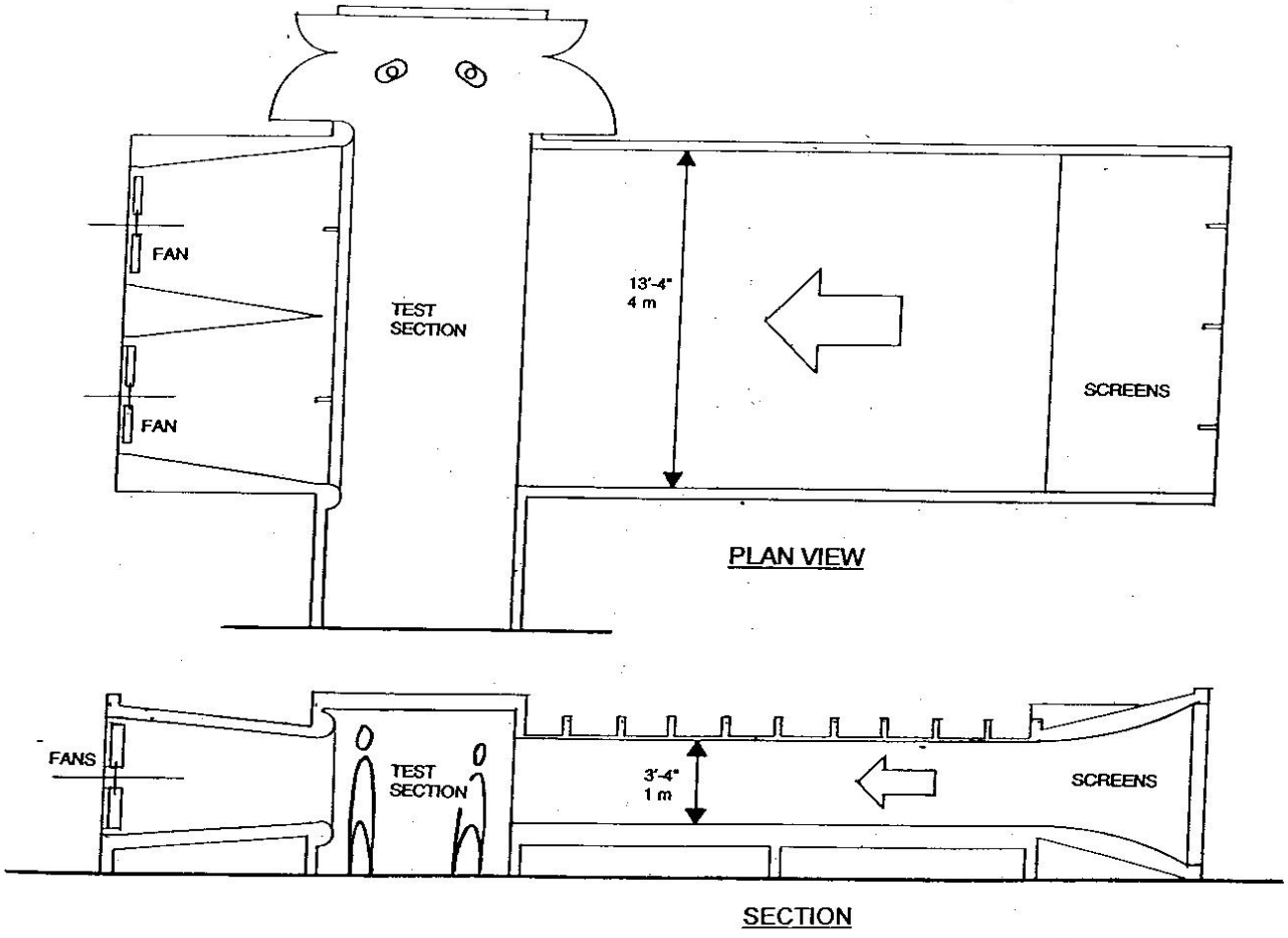

FIGURE 2.2

MEAN VELOCITY PROFILE
0.5 METER UPSTREAM

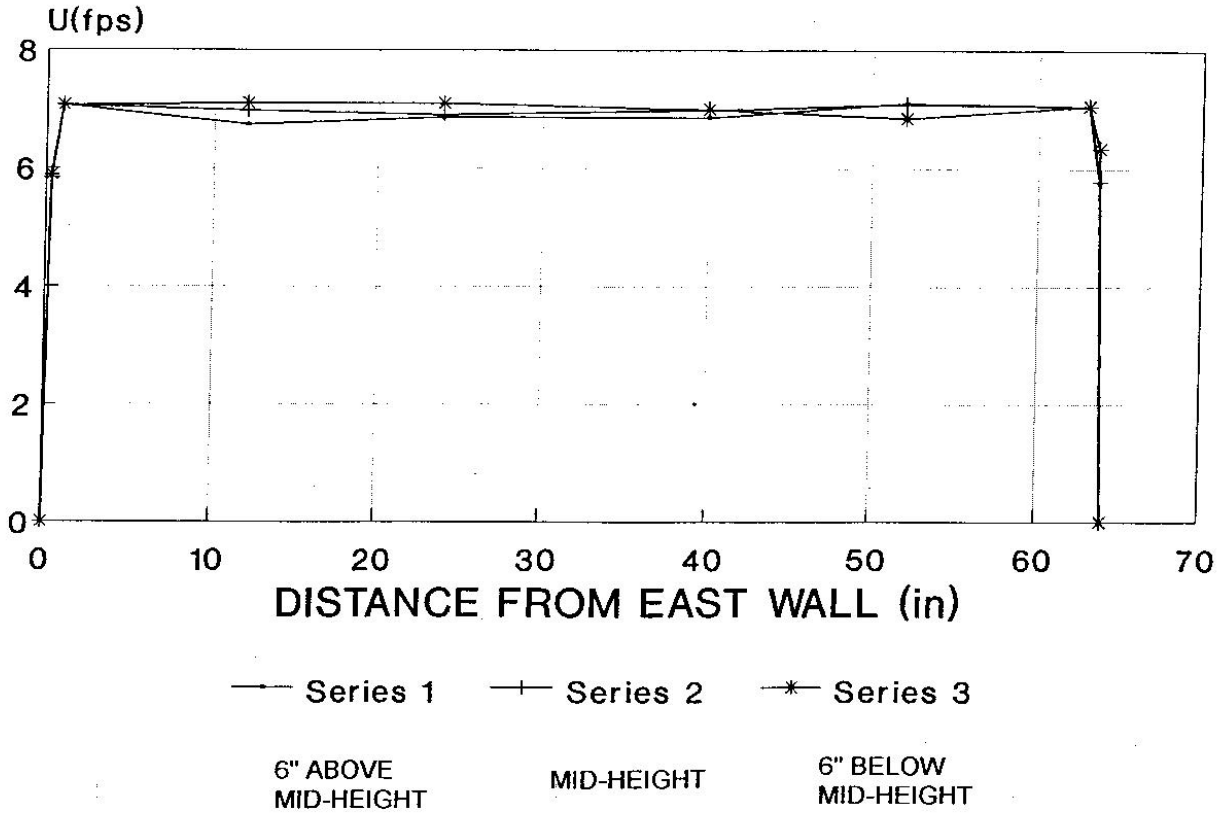

FIGURE 2.3

MEAN VELOCITY PROFILE
0.5 METER DOWNSTREAM

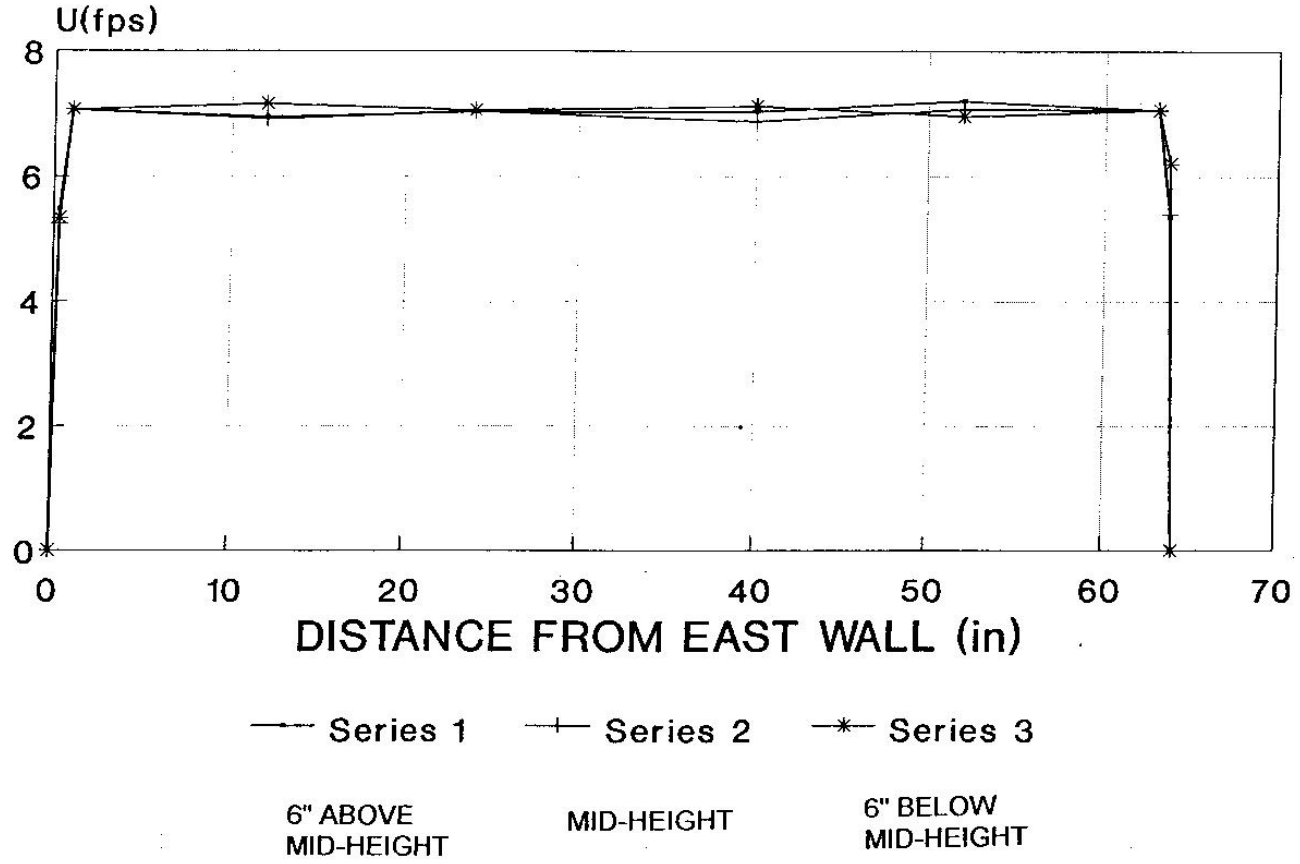

FIGURE 2.4

MEAN VELOCITY PROFILE
SIDE BOUNDARY LAYER

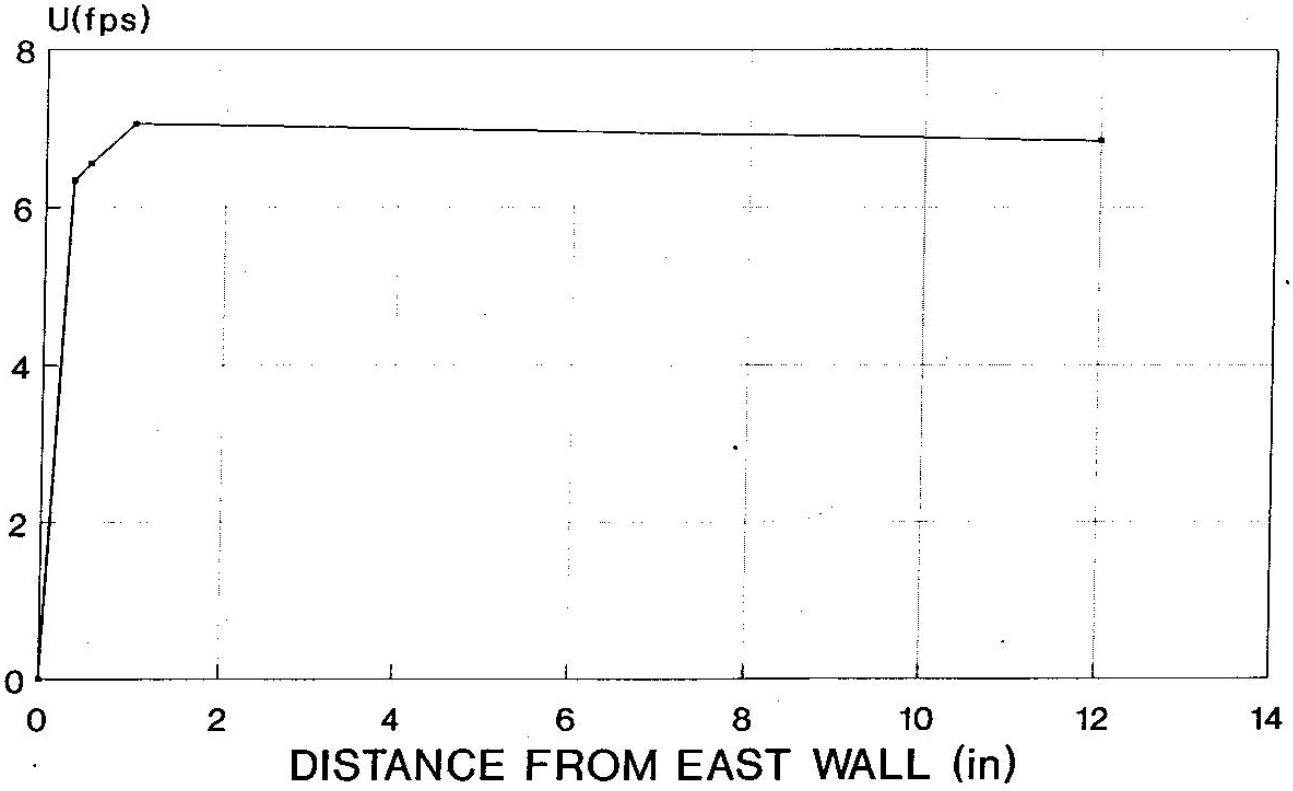

MID-HEIGHT

APPENDIX 3
PROCEDURE TO PREDICT FULL BRIDGE MOTIONS IN STRONG TURBULENT WINDS

The procedure described here differs from that presented in Ref 4 only in the description of the aerodynamic loads on the bridge deck. Otherwise, they are the same. Specifically, the bridge deck is divided into finite sized elements. On each, the aerodynamic load is computed including motion dependent terms and buffeting terms. Generalized actions are computed for each mode. The response of each mode is computed for the next time step using these generalized actions, the total physical bridge motions are then computed, new aerodynamic loads are computed on each element using these elemental physical motions, and the process is once again repeated for the next step in time. The three dimensional flow field was generated analytically as described in Ref 3.

Chen, Matsumoto, and Kareem describe in Ref 4 the motion dependent aerodynamic loads, in the time domain, for arbitrary motions, in terms of impulse functions. While not as elegant mathematically, the motion dependent aerodynamic loads can also be described directly in terms of the aeroelastic flutter derivatives. This description is computationally more efficient and it eliminates numerical uncertainties associated with one additional series of transformations (to obtain impulse functions from flutter derivatives).

Central to this description is the assumption that the motion dependent aerodynamic loads can be described as the superposition of modal, motion dependent, aerodynamic loads. This has been demonstrated to be valid for years. See Appendix 4.

Motion dependent aerodynamic lift, L_{ij} , and moment, M_{ij} , on the ith deck element, due to the jth mode of vibration can be given by Simiu and Scanlan (Ref 1)

$$L_{ij} = 1/2\rho U^2 B(KH_{1ij}^*((dhij / dt) / U) + KH_{2ij}^*(B(d\alpha ij / dt) / U) + K^2H_{3ij}^*\alpha_{ij} + K^2H_{4ij}^*(h_{ij}/B)) \qquad (3.1)$$

$$M_{ij} = 1/2\rho U^2 B^2(KA_{1ij}^*(dhij / dt) / U) + KA_{2ij}^*(B(d\alpha ij / dt) / U) + K^2A_{ij}^*\alpha_{ij} + K^2A_{4ij}^*(h_{ij}/B)) \qquad (3.2)$$

where ρ = air density, $K = \omega B/U$ and $\omega = 2\pi n$, and A_{1ij}^*, A_{2ij}^*, A_{3ij}^*, A_{4ij}^*, H_{1ij}^*, H_{2ij}^*, H_{3ij}^*, and H_{4ij}^* aeroelastic flutter derivatives. See Figure 3.1 for positive coordinate directions, and positive action directions. The aeroelastic flutter derivatives can be interpreted as frequency dependent aerodynamic stiffness and damping terms, valid for steady, decaying, or diverging harmonic motions. The flutter derivatives typically are obtained as those damping and stiffness terms that must have existed to produce the observed, superimposed torsional and vertical motions of a section model, each with its own frequency of vibration.

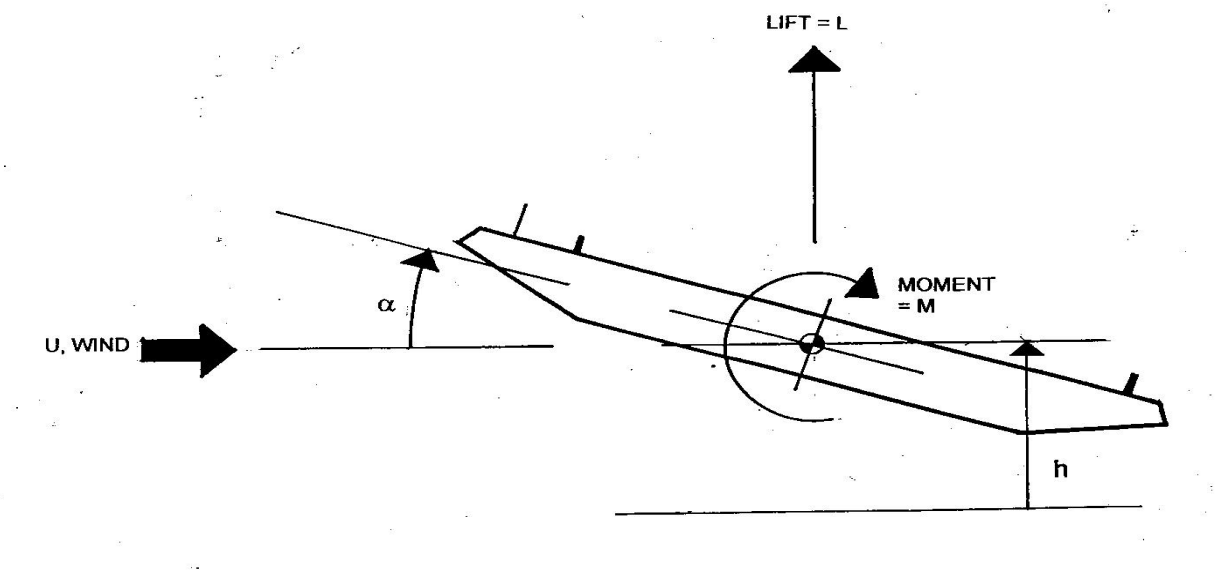

At the onset of each simulation, in smooth or turbulent flow, each mode is given a unit modal displacement. They are all released simultaneously. Although the bridge motion may look arbitrary and erratic, each mode of vibration typically is a slowly varying harmonic motion at a single frequency for which the flutter derivatives are valid. At the onset, each mode of vibration typically will vibrate near its aerodynamically stiffened (or softened) natural frequency. As the motion progresses, various modes will couple aerodynamically and gradually change their frequency to some other, but single, frequency of vibration.

The use of impulse functions, in convolution integrals, to describe the motion dependent aerodynamic loads on a bridge deck, is essentially equivalent to the use of continuously variable (with respect to frequency) flutter derivatives in (3.1) and (3.2). Because the products of K or K^2 and the flutter derivatives vary so slowly with frequency, the flutter derivatives can be varied at finite steps in time (as required), instead of being varied continuously, without loss of precision (certainly with respect to the experimental errors associated with the experimentally obtained flutter derivatives and associated impulse functions). In this procedure, at 20 second intervals (in a 10-minute simulation) all products of K or K^2 and the corresponding flutter derivatives are re-evaluated, for each element, for each mode of vibration, based upon the average frequency of vibration for the preceding 20-second time segment, for the mode in question and based upon the average wind speed for that 20-second time segment. The average 20-second wind speeds, and fluctuating wind speeds about that average, are used to compute the aerodynamic loads.

In this simulation procedure, a simplified, quasi-steady form of the buffeting forces (Ref 1) is also used. This is a conservative assumption, but it is not assumed to be too conservative. For normal values of U/nB at design wind speeds, the products (KH_{1ij}^*) and ($K^2H_{3ij}^*$) are very nearly frequency independent and are approximated well with quasi-steady lift in this flat, frequency independent range.

The step size in all simulations is 0.04 seconds. Bridge motions are simulated for a duration of 10 minutes (15,000 total steps in the simulation)

APPENDIX 4
IDENTIFICATION PROCEDURE FOR FLUTTER DERIVATIVES FROM SECTION MODEL TESTS

A linear description of the motion of this section model, for small motions, is

$$m(d^2h / dt^2) + c_h(dh / dt) + k_h h = LI \qquad (4.1)$$

$$I(d^2\alpha / dt^2) + c_\alpha(d\alpha / dt) + k_\alpha \alpha = MI \qquad (4.2)$$

where

m	mass of section model;
I	rotational inertia of section model;
c_h	damping coefficient for vertical motion
c_α	damping coefficient for torsional motion
k_h	vertical stiffness;
k_α	torsional stiffness; and
l	model length.

L and M, and positive coordinate and action directions are presented in Appendix 3.

It is assumed here that the bridge deck is symmetrical about its centerline, so there are no mechanical coupling terms. The linear description of the motion is valid because motions are constrained to be very small. Any motion that becomes large is of academic interest only, and is to be avoided at all costs by the bridge designer. If a large motion is expected over the life span of the bridge, the bridge deck geometry, structure, or energy dissipation capability is changed until that motion is again expected to be small. The linear description of small bridge structure motions is well established.

In this form, all of the aeroelastic flutter coefficients are dimensionless. For the description of the identification procedure here, consider the simplified description

$$(d^2h / dt^2) + 2\omega_h\zeta_h(dh / dt) + \omega_h{}^2 h = H_1(dh / dt) + H_2(d\alpha / dt) + H_3\alpha + H_4 h \qquad (4.3)$$

$$(d^2\alpha / dt^2) + 2\omega_\alpha\zeta_\alpha(d\alpha / dt) + \omega_\alpha{}^2\alpha = A_1(dh / dt) + A_2(d\alpha / dt) + A_3\alpha + A_h h \qquad (4.4)$$

where

$$\omega_h{}^2 = k_h \; m$$

$$\omega_\alpha^2 = k_\alpha \quad I$$

$$\zeta_h = c_h \quad 2\omega_h m$$

$$\zeta_\alpha = c_\alpha \quad 2\omega_\alpha I$$

and Hi and Ai are related to their respective Hi* and Ai* in an obvious manner. Again the Hi and Ai are not constants, but are functions of the wind speed U, or the reduced velocity U/nB, or a form of its inverse (the reduced frequency) K = ωB/U.

Let Equations 4.3 and 4.4 be rearranged one more time for convenience, to the following form:

$$(d^2h / dt^2) + (2\omega_h\zeta_h - H_1)(dh / dt) + (\omega_h^2 - H_4)h = H_2(d\alpha / dt) + H_3\alpha \qquad (4.5)$$

$$(d^2\alpha / dt^2) + (2\omega_\alpha\zeta_\alpha - A_2)(d\alpha / dt) + (\omega_\alpha^2 - A_3)\alpha = A_1(dh / dt) + A_4h \qquad (4.6)$$

Consider first, the single Equation 4.5. This is simply the equation of motion of a single-degree-of-freedom oscillator with dynamic response characteristics ω and ζ where

$$\omega^2 = \omega_h^2 - H_4 \qquad (4.7)$$

and

$$2\zeta\omega = 2\zeta_h\omega_h - H_1 \qquad (4.8)$$

subject to the forcing function $F(t) = H_2(d\alpha / dt) + H_3\alpha$

The frequency ω typically will be close to the circular frequency for vertical motion, ω_h. The general solution to this equation (4.5) for an interval of time from t_1 to t_2, can be described as a linear combination of four solutions:

$$h(t) = Y_1y_1(t) + Y_2y_2(t) + Y_3y_3(t) + Y_4y_4(t) \qquad (4.9)$$

where

$y_1(t)$ the response of the oscillator to a unit displacement at t_1;

$y_2(t)$ the response of the oscillator to a unit velocity at t_1;

$y_3(t)$ the response of the oscillator to the "forcing function", (dα / dt), with zero initial conditions at t_1; and

$y_4(t)$ the response of the oscillator to the "forcing function", α(t), with zero initial conditions at t_1; and

The coefficients Y_1, Y_2, Y_3, and Y_4 are assumed, in this linear representation of the motion, to be constants for a given ω, ζ, and reduced velocity U/nB for the particular test.

The four solutions are transient solutions. The solutions $y_1(t)$ and $y_2(t)$ are obviously exponentially varying (not necessarily decaying) harmonic functions with circular frequency, ω, and viscous damping coefficient, ζ (which is not necessarily positive). Since the torsional motions of the section model, $\alpha(t)$ and $\alpha(t)$, are also likely to be exponentially varying harmonic motions, the responses $y_3(t)$ and $y_4(t)$ are likely to be as well. These responses, $y_3(t)$ and $y_4(t)$, however will have a frequency equal to the circular frequency of the measured torsional motion, which in turn, typically is very close to the still-air torsional frequency, ω_α.

The objective for Equation 4.5 is again to identify, from recorded section model motions h(t) and $\alpha(t)$, and from the wind-off dynamic response characteristics ω_h, ω_α, ζ_h, and ζ_α, the four flutter coefficients H_1, H_2, H_3, and H_4. If ω_h and ζ_h are known (the observed dynamic response characteristics for the vertical motion with wind speed U), then H_1 and H_4 can be determined from Equations 4.7 and 4.8. If the observed response is decomposed in the form of Equation 4.9, then it follows that $H_2 = Y_3$ and $H_3 = Y_4$. A combined exhaustive search procedure (educated trial and error approach) and a linear-least-squares fitting procedure in the time domain is used to identify ω, ζ, Y_3, and Y_4.

In order for the response to be decomposed into the four transient responses as defined by Equation 4.9, the section model test set-up must be designed specifically to make that decomposition possible. All four transient responses, $y_1(t)$, $y_2(t)$, $y_3(t)$, and $y_4(t)$ are exponentially varying harmonic functions. If the vertical motion frequency and the torsional motion frequency are similar, there is no way that the response can be decomposed *uniquely* as shown in Equation 4.9. Whether or not the frequencies are separated, in reality, for the full-scale bridge, they must be separated in the section model test if this procedure is to be used. Since the objective from the section model test is to determine the flutter coefficients (not simulate the actual bridge behavior), the two section model frequencies can be separated as much as possible, by any amount that is convenient, in order to maximize the accuracy of the data to be collected. Once the flutter coefficients have been identified, they then can be used in an analytical model of the full bridge, including all modes of vibration, as outlined in Ref 1 to predict the critical flutter velocities, should they exist.

The precise identification procedure (for coefficients H_1, H_2, H_3, and H_4 from Equation 4.5) follows directly:

Define one more response

$$X(t) = Y_1y_1(t) + Y_2y_2(t) + Y_3y_3(t) + Y_4y_4(t) \qquad (4.10)$$

where the Y's and the y(t)'s are defined as before, for $t_1<t<t_2$. If the Y's, ω, and ζ will be found such that the squared error E

$$E = \int_{t_1}^{t_2} (X(t) - h(t))^2 dt \qquad (4.11)$$

is least.

First, for a given wind speed U, the model is perturbed such that significant, but still small, vertical and torsional motions are produced. A sample of the transient motions (either decaying motions or diverging motions) is recorded, i.e., h(t) and α(t) for $t_1<t_2$. It is assumed that the wind-off dynamic response characteristics have previously been recorded.

Second, values of ω and ζ are assumed. For this set of values, a linear-least-squares fitting procedure is used to determine the optimal values of Y_1, Y_2, Y_3, and Y_4, and the squared error E is computed using Equation 4.11. A modified version of a steepest descent procedure is used, with respect to the variables ω and ζ (and at each step the best-fit values of Y_1, Y_2, Y_3, and Y_4 are recalculated). In this manner an optimal set of ω, ζ, Y_1, Y_2, Y_3, and Y_4, are found from which the H_1, H_2, H_3, H_4, and in turn, the H_1^*, H_2^*, H_3^*, and H_4^* are found. It is assumed that these best-fit values of the flutter coefficients are in fact the best estimates of those true values for the section model.

The exact procedure is repeated using Equation 4.6 to determine the torsional flutter coefficients A_1^*, A_2^*, A_3^* and A_4^*.

There is no way to prove that this procedure will converge to the proper values of the flutter coefficients, but years of use seems to indicate that it will. Again, there is the possibility that a set of flutter coefficients is found that is locally optimal, but not globally optimal. The likelihood of that occurring is greatly reduced if small steps are made in incrementing the wind speed from one speed to another, and if the previous best-fit values of ω and ζ are used as initial estimates for the next wind speed (starting with wind-off values for the first step).

This identification procedure relies heavily upon the assumption that the mechanical vibrations of the model, and the unsteady aerodynamic loads are linear functions of the model motion. Shown on Figure 4.1, 4.2, and 4.3 are sets of two curves of A_2^* and H_1^* that were obtained for two different bridge sections. One A_2^* curve in a set was obtained from observed torsional motions with the vertical motion suppressed. The second A_2^* curve in the set was obtained using the procedure described in this paper from torsional motions that were superimposed upon vertical motions. Similarly, one H_1^* curve in a set was obtained from observed vertical motions with torsional motion suppressed. The second H_1^* curve in the set was obtained using the procedure described in this paper from vertical motions that were superimposed upon torsional motions. The good agreement between the two curves in each set verifies that validity of the assumption of linearity in the aerodynamic loads.

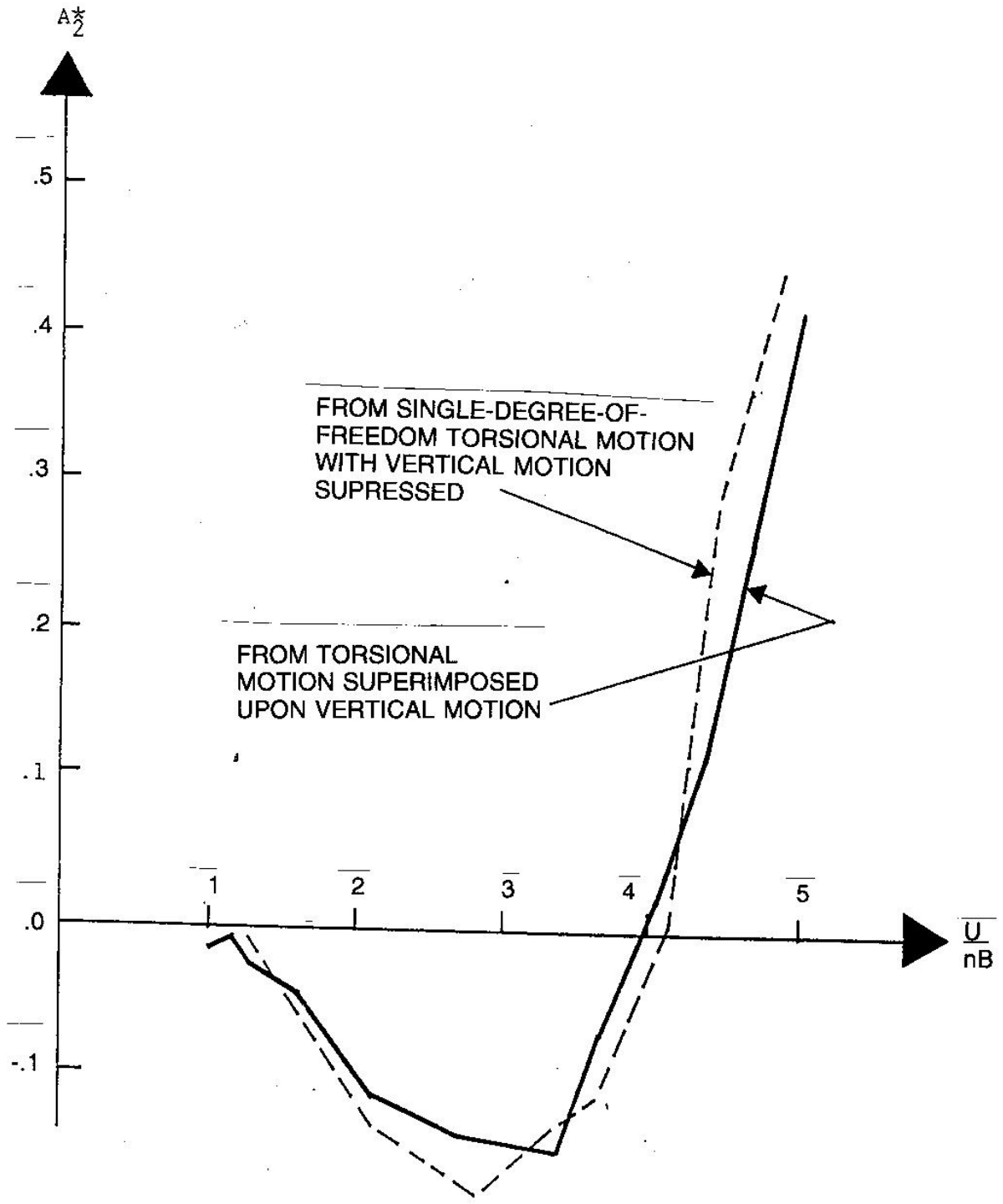
A*z
.5
.4
.3
.2
.1
.0
-.1
FROM SINGLE-DEGREE-OF-FREEDOM TORSIONAL MOTION WITH VERTICAL MOTION SUPRESSED
FROM TORSIONAL MOTION SUPERIMPOSED UPON VERTICAL MOTION
1
2
3
4
5
U/nB

FIGURE 4.01

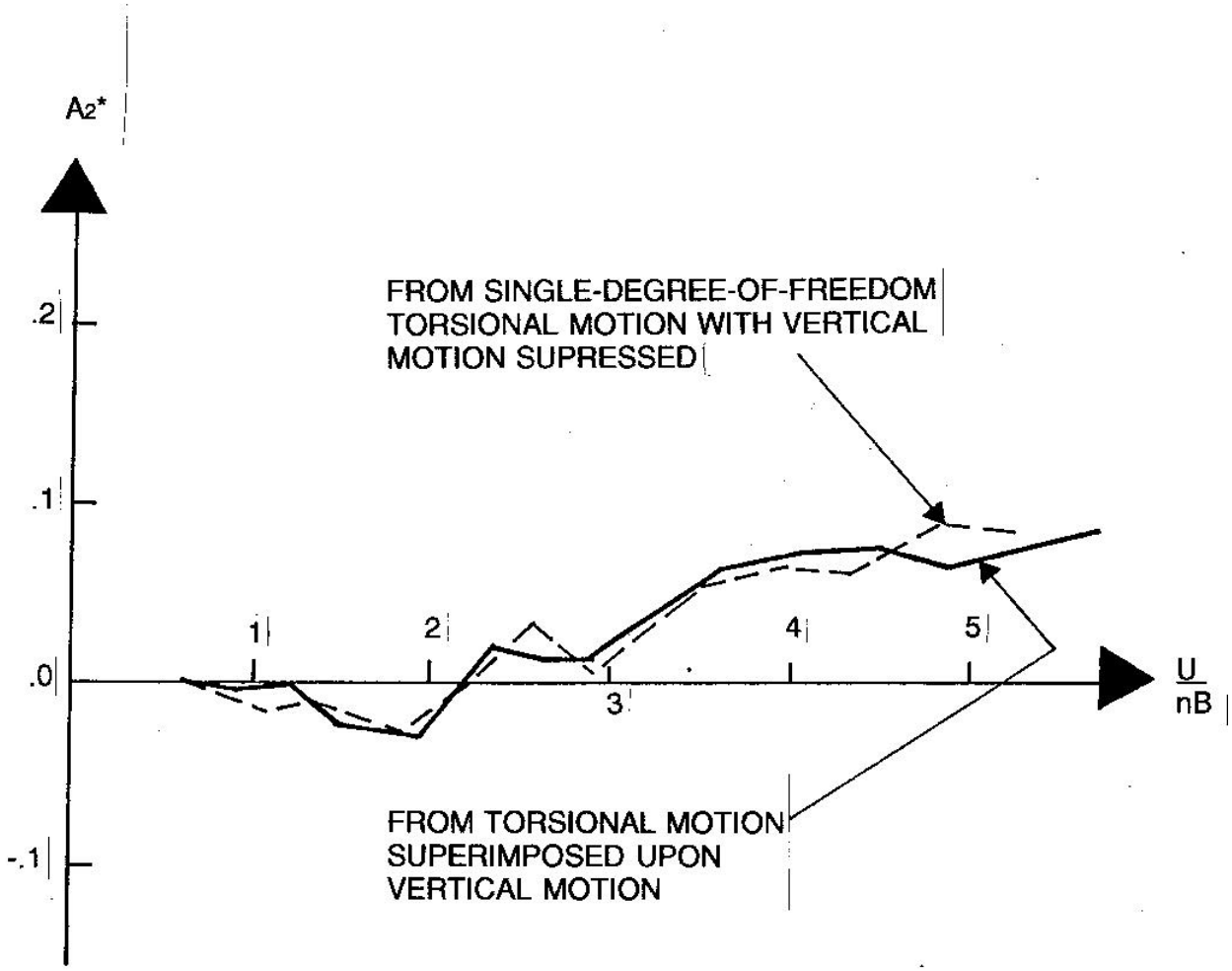
A2*
.2
.1
.0
-.1
1
2
3
4
5
U
nB
FROM SINGLE-DEGREE-OF-FREEDOM
TORSIONAL MOTION WITH VERTICAL
MOTION SUPRESSED
FROM TORSIONAL MOTION
SUPERIMPOSED UPON
VERTICAL MOTION

FIGURE 4.02

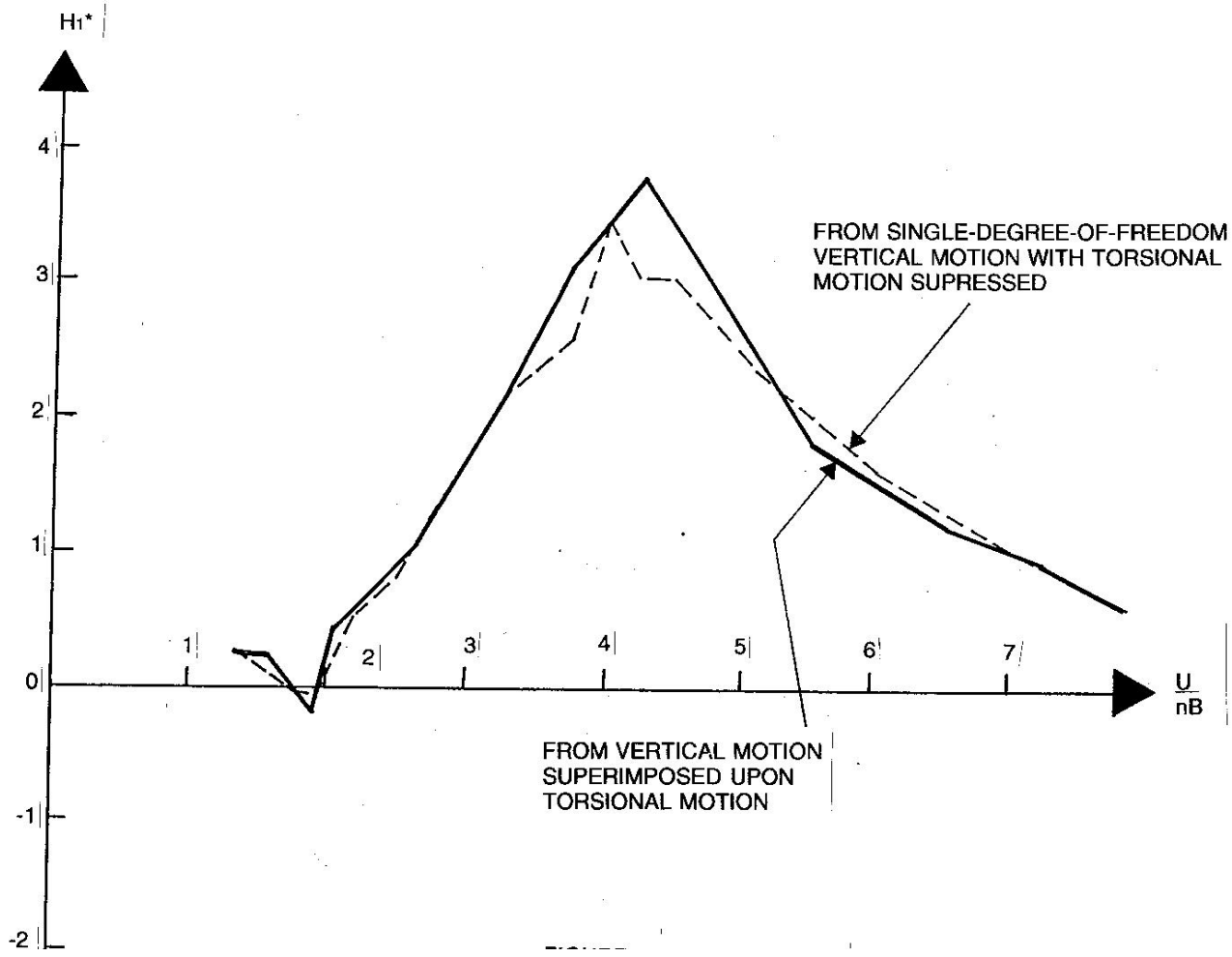
H1*
4
3
2
1
0
-1
-2
1
2
3
4
5
6
7
U
nB
FROM SINGLE-DEGREE-OF-FREEDOM
VERTICAL MOTION WITH TORSIONAL
MOTION SUPRESSED
FROM VERTICAL MOTION
SUPERIMPOSED UPON
TORSIONAL MOTION

FIGURE 4.03

APPENDIX 5
MODELS

For this study the 1:50 scale model used in the previous study (Ref 2) was used. The model was lengthened to fit the new wind tunnel (see Appendix 2 - Facilities). The model is 1.6256 m long, which models a portion of the full-scale bridge deck 81.28 m (266.67 feet) long.

The model was made of laser cut plastic. As described in Appendices 3 and 4, the model needed to be geometrically correct only. Inertial and elastic scaling was not required.

The model is shown in six configurations (the existing configuration and five suicide deterrent system configurations W0, W1, W1 (alternate), W2, W3, and W6) in the following photographs. Those configurations are defined in Section C.

Existing bridge (Test number W0)

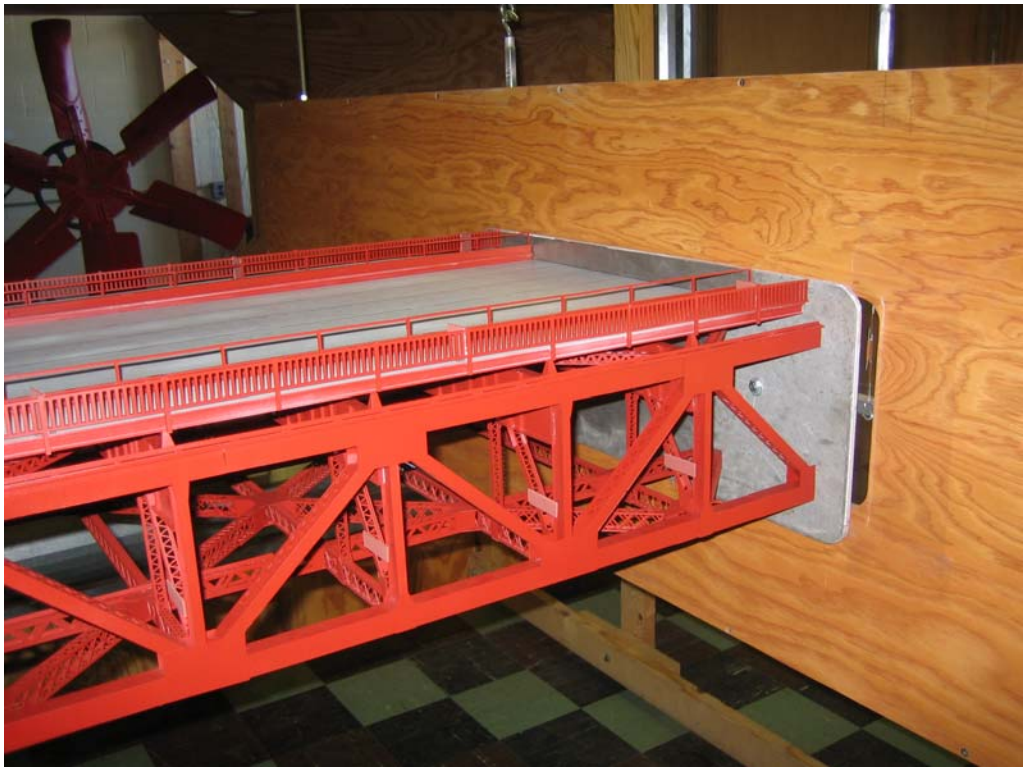

Existing bridge (Test number W0)

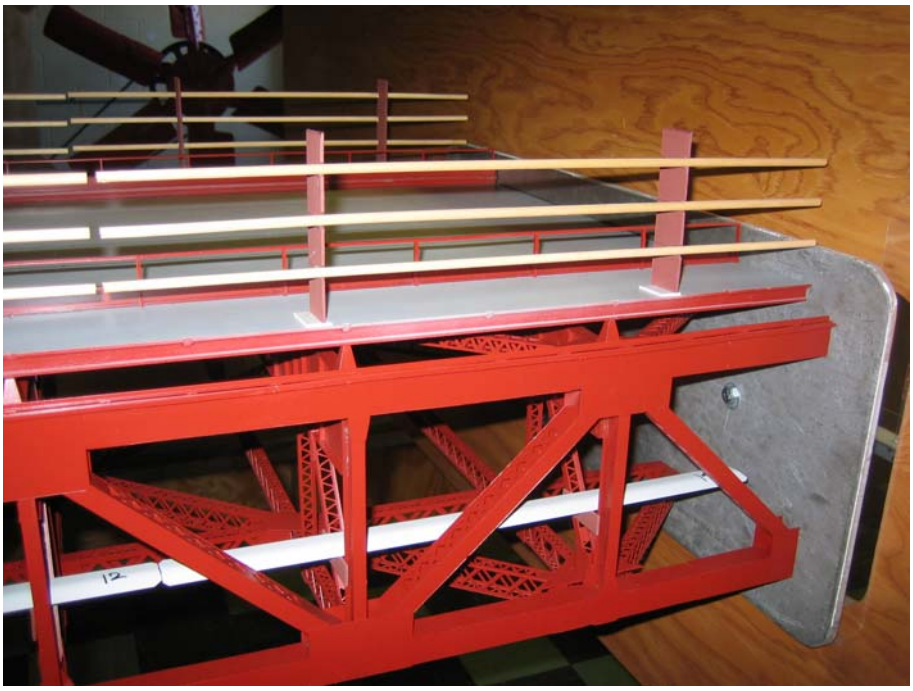

Vertical 12’ barrier with below deck winglets/catwalks (Test number W1)

Vertical 12’ barrier with wind fairings (Test number W1 Alt.)

Vertical 12’ barrier with above deck winglets (Test number W2)

Adding to the existing railing and with above deck winglets (Test number W3)

Vertical 10’ barrier with above deck winglets (Test number W5)

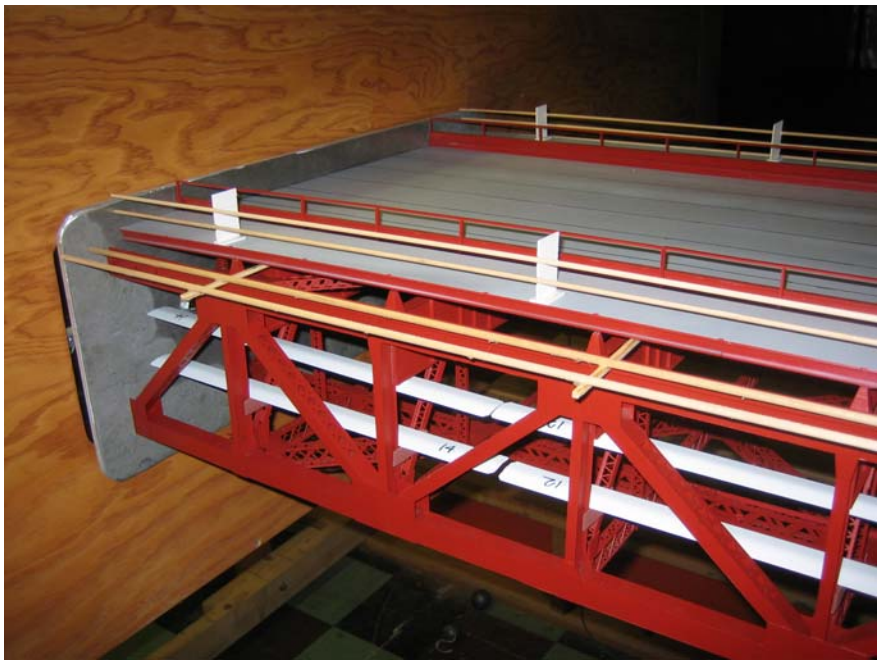

Horizontally projecting 10’ barrier with a modified pedestrian railing and with below deck winglets/catwalks (Test number W6)

APPENDIX 6
BRIDGE PROPERTIES

Properties of the bridge structure needed for the time domain numerical simulations are nodal coordinates, deck mass per unit length, deck mass moment of inertia about a longitudinal axis (at the center of mass), and the dynamic response characteristics (mode shapes and frequencies). The inertial properties were taken from Ref 5. The dynamic response characteristics were provided by DMJM Harris Inc. and a description of the ADINA modeling is provided below.

In a previous study on the Golden Gate Bridge, damping ratios were deduced from observed bridge motions (Ref 5). A suitable damping ratio of 0.006 was deduced. This is consistent with values of 0.004 for new steel bridges with welded and/or high strength bolted connections, and 0.005 for composite concrete and steel construction (Ref 6). Older, riveted steel truss bridges would be expected to have a higher damping value. The linear viscous damping ratio of 0.006 was therefore considered to be reasonable, and was used for all modes of vibration.

For the numerical simulations, wind speed time histories were generated at 30 locations along the span (approximately 60.96 m (200 feet) apart). Those nodal locations are defined in Table 6.1. The bridge properties used in this analysis are defined in Tables 6.2 through 6.13. The nodal locations are shown schematically in Figure 6.1. Positive coordinate directions (not standard) are shown in Figure 6.2.

ADINA Modeling

The ADINA model used for the wind stability assessment of the bridge was prepared and converted by International Civil Engineering Consultants, Inc. (ICEC) of Berkeley, California, for the Golden Gate Bridge, Highway and Transportation District (GGBHTD) of San Francisco, California, under a contract agreement by and between GGBHTD and ICEC.

The model includes the suspension bridge, the suspended main and side spans of the bridge from the North to the South anchor block. This model was developed for the modal conversion of the ABAQUS computer model for the suspended structure of the Golden Gate Bridge. It represents the structural configuration of the suspended main and side spans including with the proposed seismic retrofit of the structure.

The modeling of the suspended structure is shown in the following Figure; all major members were explicitly modeled with using linear elastic beam elements for the suspended stiffening trusses (the chords, verticals, diagonals) and the main tower (shafts, struts, verticals and diagonal braces), elastic truss elements for main cables and rocker-links, nonlinear truss elements for the suspenders, tie-downs and wind braces, nonlinear truss and member elements for the plinths (the bottom sections of the main towers), super-element (consisting of an equivalent lumped-mass matrix) for pylon, etc. Nonlinear dampers were also considered in the ADINA model.

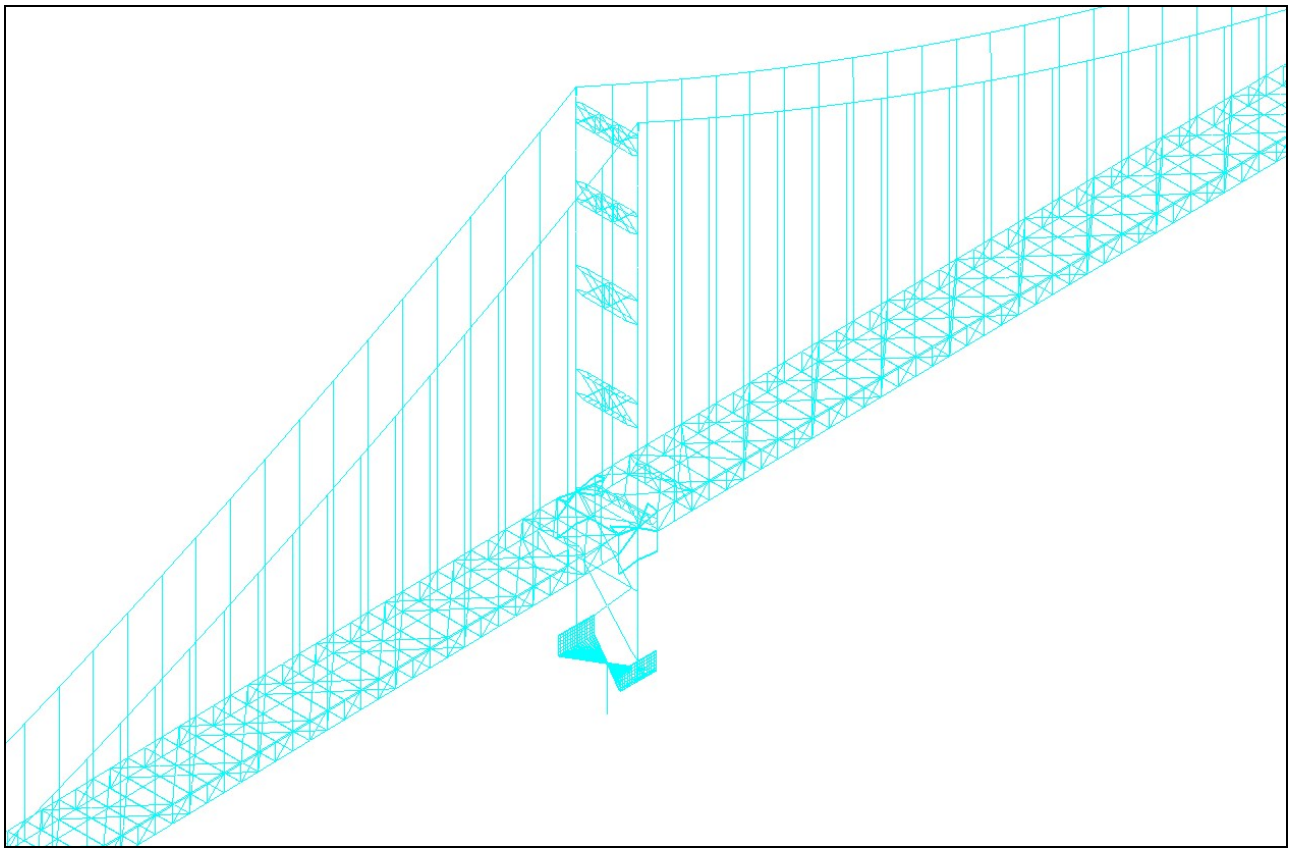

Computation of Frequencies and Mode Shapes

The modal analysis for determining the modal frequencies with the associated mode shapes was performed using the Version of 7.4 of the ADINA computer program.

The first-twenty modal frequencies as obtained from the ADINA modal analysis are summarized in the following table.

GGB Suicide Barrier Study
Frequencies per the Converted ADINA Computer Model

MODE NUMBER	FREQUENCY (Hz)	MODE SHAPE
1	0.048749	transverse, symmetric mode
2	0.086225	vertical, asymmetric mode
3	0.111783	transverse, asymmetric mode
4	0.128540	vertical, symmetric mode
5	0.133075	vertical, asymmetric mode
6	0.163712	vertical, symmetric mode
7	0.183531	torsional, asymmetric mode
8	0.195726	torsional-transverse, symmetric mode
9	0.198024	vertical, asymmetric mode
10	0.203344	cable transverse, symmetric mode
11	0.204704	torsional, symmetric mode
12	0.208492	cable transverse, asymmetric mode
13	0.211595	vertical, asymmetric mode
14	0.216478	cable transverse, asymmetric mode
15	0.224156	cable transverse, asymmetric mode
16	0.258650	vertical, symmetric mode
17	0.264104	transverse, asymmetric mode
18	0.265155	transverse, asymmetric mode
19	0.282724	vertical, symmetric mode
20	0.286409	torsional, symmetric mode

TABLE 6.1

WWL NODE	DMJM NODE
1	100580
2	101380
3	102180
4	102980
5	103780
6	105330
7	106130
8	106930
9	107730
10	108530
11	109330
12	110130
13	110930
14	111730
15	112530
16	212530
17	211730
18	210930
19	210130
20	209330
21	208530
22	207730
23	206930
24	206130
25	205330
26	203780
27	202980
28	202180
29	201380
30	200580

TABLE 6.2

B(M)= 27.432
NUMBER OF MODES= 10
NUMBER OF NODES= 30

NODE	DL(M)	M(KG/M)	MMI(KG*M^2/M)
1	60.96	29123	4.168E+06
2	60.96	29123	4.168E+06
3	60.96	29123	4.168E+06
4	60.96	29123	4.168E+06
5	60.96	29123	4.168E+06
6	60.96	29123	4.168E+06
7	60.96	29123	4.168E+06
8	60.96	29123	4.168E+06
9	60.96	29123	4.168E+06
10	60.96	29123	4.168E+06
11	60.96	29123	4.168E+06
12	60.96	29123	4.168E+06
13	60.96	29123	4.168E+06
14	60.96	29123	4.168E+06
15	60.96	29123	4.168E+06
16	60.96	29123	4.168E+06
17	60.96	29123	4.168E+06
18	60.96	29123	4.168E+06
19	60.96	29123	4.168E+06
20	60.96	29123	4.168E+06
21	60.96	29123	4.168E+06
22	60.96	29123	4.168E+06
23	60.96	29123	4.168E+06
24	60.96	29123	4.168E+06
25	60.96	29123	4.168E+06
26	60.96	29123	4.168E+06
27	60.96	29123	4.168E+06
28	60.96	29123	4.168E+06
29	60.96	29123	4.168E+06
30	60.96	29123	4.168E+06

TABLE 6.3

WWL MODE	DMJM MODE	WR(RPS)	DR	MT	MRAT
1	1	0.306	0.006	1.000	0.849
2	2	0.542	0.006	2.000	0.501
3	3	0.702	0.006	1.000	1.000
4	4	0.808	0.006	2.000	0.795
5	5	0.836	0.006	2.000	0.271
6	6	1.029	0.006	2.000	0.773
7	7	1.153	0.006	3.000	0.730
8	8	1.230	0.006	1.000	0.813
9	9	1.244	0.006	2.000	0.728
10	10	1.278	0.006	1.000	0.930

MT=1 FOR SWAY, 2 FOR VERTICAL, 3 FOR TORSION
MRAT IS THE RATIO OF GENERALIZED MASS ASSOCIATED WITH DECK MOTION TO THE TOTAL GENERALIZED MASS

TABLE 6.4

WWL MODE 1
DMJM MODE 1

NODE	RX	RY	RZ
1	-0.0004	0.0000	-0.0000
2	-0.0009	0.0000	-0.0000
3	-0.0013	0.0000	-0.0000
4	-0.0015	0.0000	-0.0000
5	-0.0016	0.0000	-0.0000
6	-0.1461	0.0000	0.0000
7	-0.3033	0.0000	-0.0000
8	-0.4506	-0.0000	-0.0001
9	-0.5844	0.0000	-0.0001
10	-0.7023	0.0000	-0.0002
11	-0.8022	0.0000	-0.0002
12	-0.8827	0.0000	-0.0002
13	-0.9424	-0.0000	-0.0001
14	-0.9813	-0.0000	-0.0001
15	-1.0000	-0.0000	-0.0000
16	-1.0000	0.0000	-0.0000
17	-0.9814	0.0000	-0.0001
18	-0.9426	0.0000	-0.0002
19	-0.8830	-0.0000	-0.0002
20	-0.8025	-0.0000	-0.0002
21	-0.7025	-0.0000	-0.0002
22	-0.5843	-0.0000	-0.0001
23	-0.4503	-0.0000	-0.0001
24	-0.3031	-0.0000	-0.0000
25	-0.1459	-0.0000	0.0000
26	-0.0015	-0.0000	-0.0000
27	-0.0014	-0.0000	-0.0000
28	-0.0012	-0.0000	-0.0000
29	-0.0008	-0.0000	-0.0000
30	-0.0003	-0.0000	-0.0000

TABLE 6.5

WWL MODE 2
DMJM MODE 2

NODE	RX	RY	RZ
1	0.0001	0.0254	0.0000
2	0.0001	0.0535	-0.0000
3	0.0000	0.0642	-0.0000
4	0.0000	0.0573	-0.0000
5	0.0000	0.0334	-0.0000
6	-0.0000	0.2809	0.0000
7	-0.0001	0.5575	-0.0000
8	-0.0001	0.7770	0.0000
9	-0.0000	0.9262	0.0000
10	-0.0001	0.9951	0.0000
11	-0.0000	0.9772	0.0000
12	-0.0001	0.8732	0.0000
13	-0.0000	0.6896	0.0000
14	-0.0000	0.4406	0.0000
15	-0.0000	0.1487	0.0000
16	0.0000	-0.1579	0.0000
17	0.0001	-0.4495	0.0000
18	0.0001	-0.6978	-0.0000
19	0.0002	-0.8806	-0.0000
20	0.0003	-0.9834	-0.0000
21	0.0003	-1.0000	-0.0000
22	0.0002	-0.9299	0.0000
23	0.0001	-0.7794	-0.0000
24	0.0001	-0.5588	-0.0000
25	0.0000	-0.2813	-0.0000
26	-0.0000	-0.0329	-0.0000
27	-0.0000	-0.0564	-0.0000
28	-0.0000	-0.0633	0.0000
29	-0.0000	-0.0526	-0.0000
30	-0.0000	-0.0250	-0.0000

TABLE 6.6

WWL MODE 3
DMJM MODE 3

NODE	RX	RY	RZ
1	-0.0011	0.0000	0.0001
2	-0.0023	0.0000	0.0001
3	-0.0031	0.0000	0.0001
4	-0.0034	0.0000	0.0001
5	-0.0032	0.0000	0.0000
6	-0.2843	0.0000	0.0007
7	-0.5664	0.0001	0.0007
8	-0.7893	-0.0001	0.0007
9	-0.9352	-0.0000	0.0005
10	-0.9951	-0.0000	0.0004
11	-0.9660	-0.0001	0.0003
12	-0.8528	-0.0001	0.0001
13	-0.6658	-0.0001	0.0000
14	-0.4231	-0.0002	-0.0001
15	-0.1467	-0.0003	-0.0003
16	0.1418	-0.0001	-0.0004
17	0.4208	-0.0001	-0.0004
18	0.6662	0.0000	-0.0003
19	0.8557	0.0000	-0.0002
20	0.9704	0.0001	-0.0001
21	1.0000	0.0001	-0.0002
22	0.9393	0.0001	-0.0004
23	0.7921	0.0001	-0.0005
24	0.5681	0.0001	-0.0007
25	0.2849	0.0001	-0.0006
26	0.0029	0.0000	-0.0000
27	0.0030	0.0000	-0.0001
28	0.0028	0.0000	-0.0001
29	0.0021	0.0000	-0.0001
30	0.0010	0.0000	-0.0000

TABLE 6.7

WWL MODE 4
DMJM MODE 4

NODE	RX	RY	RZ
1	0.0003	0.1316	0.0000
2	0.0003	0.2810	-0.0000
3	0.0003	0.3397	-0.0000
4	0.0002	0.3019	-0.0000
5	0.0001	0.1743	0.0000
6	-0.0000	0.1171	-0.0000
7	-0.0000	0.1911	-0.0000
8	-0.0000	0.1798	-0.0000
9	0.0001	0.0826	0.0000
10	0.0001	-0.0863	-0.0000
11	0.0001	-0.3035	-0.0000
12	0.0001	-0.5373	-0.0000
13	0.0000	-0.7526	-0.0000
14	-0.0001	-0.9157	-0.0000
15	-0.0001	-1.0000	-0.0000
16	0.0004	-0.9920	0.0000
17	0.0003	-0.8922	0.0000
18	0.0001	-0.7158	0.0000
19	0.0000	-0.4906	0.0000
20	-0.0001	-0.2516	0.0000
21	-0.0003	-0.0343	0.0000
22	-0.0003	0.1297	0.0000
23	-0.0001	0.2178	0.0000
24	-0.0001	0.2171	0.0000
25	-0.0000	0.1297	0.0000
26	0.0001	0.1678	0.0000
27	0.0001	0.2905	-0.0000
28	0.0001	0.3268	-0.0000
29	0.0002	0.2703	-0.0000
30	0.0001	0.1265	0.0000

TABLE 6.8

WWL MODE 5
DMJM MODE 5

NODE	RX	RY	RZ
1	0.0003	0.1121	0.0000
2	0.0003	0.2396	-0.0000
3	0.0002	0.2899	-0.0000
4	0.0002	0.2575	-0.0000
5	0.0001	0.1484	0.0000
6	0.0000	-0.2509	-0.0000
7	0.0001	-0.5174	-0.0000
8	0.0002	-0.7477	-0.0000
9	0.0001	-0.9115	-0.0000
10	0.0001	-0.9845	-0.0000
11	0.0000	-0.9537	-0.0000
12	0.0001	-0.8220	-0.0000
13	0.0000	-0.6054	-0.0000
14	-0.0001	-0.3310	-0.0000
15	-0.0002	-0.0287	-0.0000
16	-0.0003	0.2734	0.0000
17	-0.0006	0.5499	0.0000
18	-0.0007	0.7769	0.0000
19	-0.0009	0.9327	0.0000
20	-0.0009	1.0000	0.0000
21	-0.0009	0.9733	0.0000
22	-0.0007	0.8585	0.0000
23	-0.0003	0.6747	0.0000
24	-0.0002	0.4493	0.0000
25	-0.0001	0.2117	0.0000
26	-0.0001	-0.1914	-0.0000
27	-0.0001	-0.3320	0.0000
28	-0.0002	-0.3736	0.0000
29	-0.0002	-0.3088	0.0000
30	-0.0001	-0.1443	-0.0000

TABLE 6.9

WWL MODE 6
DMJM MODE 6

NODE	RX	RY	RZ
1	0.0007	0.2673	0.0000
2	0.0008	0.5797	0.0000
3	0.0007	0.7064	-0.0000
4	0.0005	0.6265	-0.0000
5	0.0002	0.3581	0.0000
6	-0.0000	-0.3399	0.0000
7	0.0001	-0.6736	0.0000
8	0.0001	-0.9080	0.0000
9	-0.0001	-0.9962	-0.0000
10	-0.0001	-0.9206	-0.0000
11	-0.0001	-0.6961	0.0000
12	-0.0001	-0.3728	0.0000
13	-0.0000	-0.0233	0.0000
14	0.0001	0.2700	0.0000
15	0.0002	0.4362	-0.0000
16	-0.0007	0.4358	-0.0000
17	-0.0005	0.2687	-0.0000
18	-0.0001	-0.0255	-0.0000
19	0.0002	-0.3758	-0.0000
20	0.0005	-0.6997	-0.0000
21	0.0006	-0.9245	-0.0000
22	0.0006	-1.0000	-0.0000
23	0.0002	-0.9111	-0.0000
24	0.0002	-0.6757	-0.0000
25	0.0001	-0.3408	-0.0000
26	0.0001	0.3625	0.0000
27	0.0002	0.6340	0.0000
28	0.0003	0.7149	-0.0000
29	0.0003	0.5866	0.0000
30	0.0002	0.2705	0.0000

TABLE 6.10

WWL MODE 7
DMJM MODE 7

NODE	RX	RY	RZ
1	0.0027	-0.0000	-0.0003
2	0.0049	-0.0000	-0.0006
3	0.0059	-0.0000	-0.0007
4	0.0058	-0.0000	-0.0006
5	0.0045	-0.0000	-0.0004
6	-0.1171	0.0001	0.0221
7	-0.1827	0.0000	0.0412
8	-0.2264	0.0004	0.0568
9	-0.2438	0.0001	0.0677
10	-0.2375	-0.0002	0.0729
11	-0.2111	-0.0002	0.0718
12	-0.1692	-0.0002	0.0645
13	-0.1160	-0.0001	0.0517
14	-0.0571	0.0005	0.0346
15	0.0030	0.0015	0.0145
16	0.0507	0.0007	-0.0072
17	0.0865	0.0003	-0.0286
18	0.1138	0.0001	-0.0474
19	0.1335	0.0001	-0.0618
20	0.1467	0.0001	-0.0704
21	0.1549	0.0001	-0.0725
22	0.1570	0.0001	-0.0678
23	0.1486	0.0002	-0.0572
24	0.1243	-0.0000	-0.0417
25	0.0875	-0.0000	-0.0223
26	-0.0008	-0.0001	-0.0003
27	-0.0008	-0.0002	-0.0004
28	-0.0006	-0.0003	-0.0005
29	-0.0002	-0.0002	-0.0004
30	0.0003	-0.0001	-0.0002

TABLE 6.11

WWL MODE 8
DMJM MODE 8

NODE	RX	RY	RZ
1	0.0608	-0.0000	-0.0103
2	0.0982	0.0001	-0.0194
3	0.1124	0.0004	-0.0228
4	0.1052	0.0005	-0.0205
5	0.0756	0.0006	-0.0128
6	-0.3503	0.0001	-0.0012
7	-0.6804	0.0002	-0.0002
8	-0.8943	0.0001	0.0049
9	-0.9601	-0.0004	0.0140
10	-0.8780	-0.0009	0.0260
11	-0.6736	-0.0012	0.0399
12	-0.3958	-0.0012	0.0540
13	-0.1041	-0.0008	0.0669
14	0.1376	-0.0006	0.0769
15	0.2742	-0.0003	0.0832
16	0.2786	0.0001	0.0850
17	0.1453	0.0005	0.0819
18	-0.1002	0.0007	0.0741
19	-0.4021	0.0008	0.0625
20	-0.6935	0.0006	0.0487
21	-0.9111	0.0003	0.0344
22	-1.0000	-0.0002	0.0214
23	-0.9320	-0.0005	0.0111
24	-0.7094	-0.0005	0.0043
25	-0.3672	-0.0003	0.0012
26	0.0770	0.0002	-0.0131
27	0.1074	-0.0002	-0.0210
28	0.1149	-0.0004	-0.0233
29	0.1005	-0.0005	-0.0198
30	0.0622	-0.0003	-0.0105

TABLE 6.12

WWL MODE 9
DMJM MODE 9

NODE	RX	RY	RZ
1	0.0011	0.3666	0.0000
2	0.0014	0.8117	-0.0000
3	0.0013	1.0000	-0.0000
4	0.0010	0.8854	-0.0000
5	0.0005	0.5005	0.0000
6	0.0001	0.0469	-0.0000
7	0.0003	0.0835	-0.0000
8	0.0003	0.0915	-0.0000
9	0.0004	0.0704	-0.0000
10	0.0004	0.0289	-0.0000
11	0.0003	-0.0190	-0.0000
12	0.0001	-0.0572	-0.0000
13	-0.0000	-0.0724	-0.0000
14	-0.0001	-0.0591	-0.0000
15	-0.0002	-0.0227	-0.0000
16	-0.0002	0.0226	-0.0000
17	-0.0002	0.0590	0.0000
18	-0.0000	0.0721	0.0000
19	0.0001	0.0568	0.0000
20	0.0003	0.0185	0.0000
21	0.0004	-0.0295	0.0000
22	0.0005	-0.0710	0.0000
23	0.0004	-0.0919	0.0000
24	0.0003	-0.0838	0.0000
25	0.0001	-0.0470	0.0000
26	-0.0002	-0.4968	-0.0000
27	-0.0004	-0.8790	0.0000
28	-0.0005	-0.9928	0.0000
29	-0.0005	-0.8061	0.0000
30	-0.0003	-0.3642	-0.0000

TABLE 6.13

WWL MODE 10
DMJM MODE 10

NODE	RX	RY	RZ
1	0.0585	-0.0004	-0.0095
2	0.0960	-0.0008	-0.0179
3	0.1106	-0.0008	-0.0210
4	0.1035	-0.0006	-0.0189
5	0.0740	-0.0001	-0.0118
6	0.4239	0.0008	-0.0019
7	0.7931	0.0012	0.0010
8	0.9919	0.0016	0.0079
9	0.9917	0.0009	0.0178
10	0.8015	-0.0001	0.0297
11	0.4594	-0.0009	0.0421
12	0.0320	-0.0015	0.0537
13	-0.3981	-0.0017	0.0635
14	-0.7451	-0.0012	0.0706
15	-0.9370	-0.0003	0.0741
16	-0.9374	0.0007	0.0738
17	-0.7448	0.0016	0.0696
18	-0.3954	0.0020	0.0621
19	0.0383	0.0016	0.0521
20	0.4688	0.0008	0.0403
21	0.8116	-0.0003	0.0279
22	1.0000	-0.0013	0.0160
23	0.9976	-0.0019	0.0062
24	0.7972	-0.0016	-0.0003
25	0.4264	-0.0009	-0.0026
26	0.0738	0.0007	-0.0121
27	0.1037	0.0008	-0.0193
28	0.1110	0.0007	-0.0215
29	0.0967	0.0004	-0.0183
30	0.0591	0.0001	-0.0097

Figure 6.1

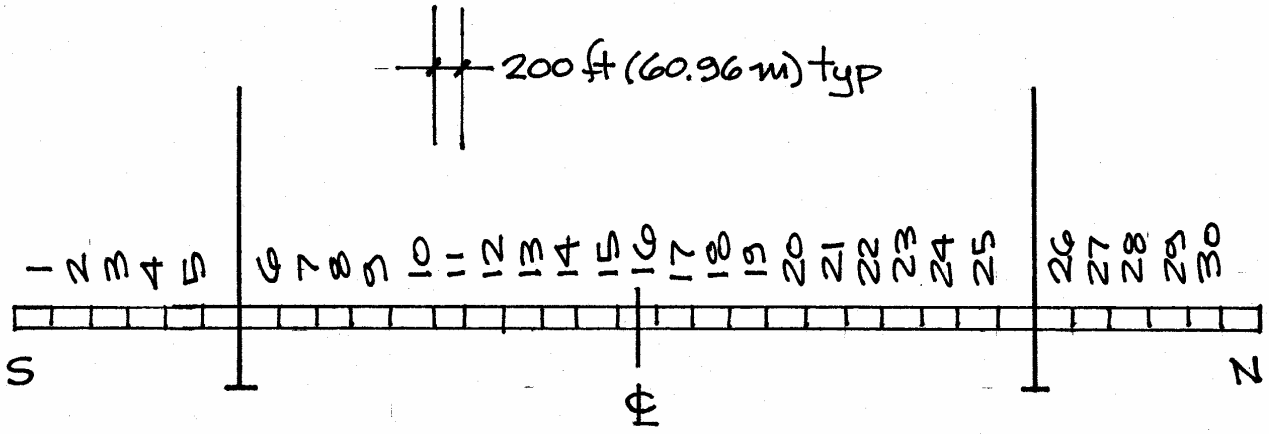

WEST WIND LABORATORY NODE NUMBERS

Figure 6.2

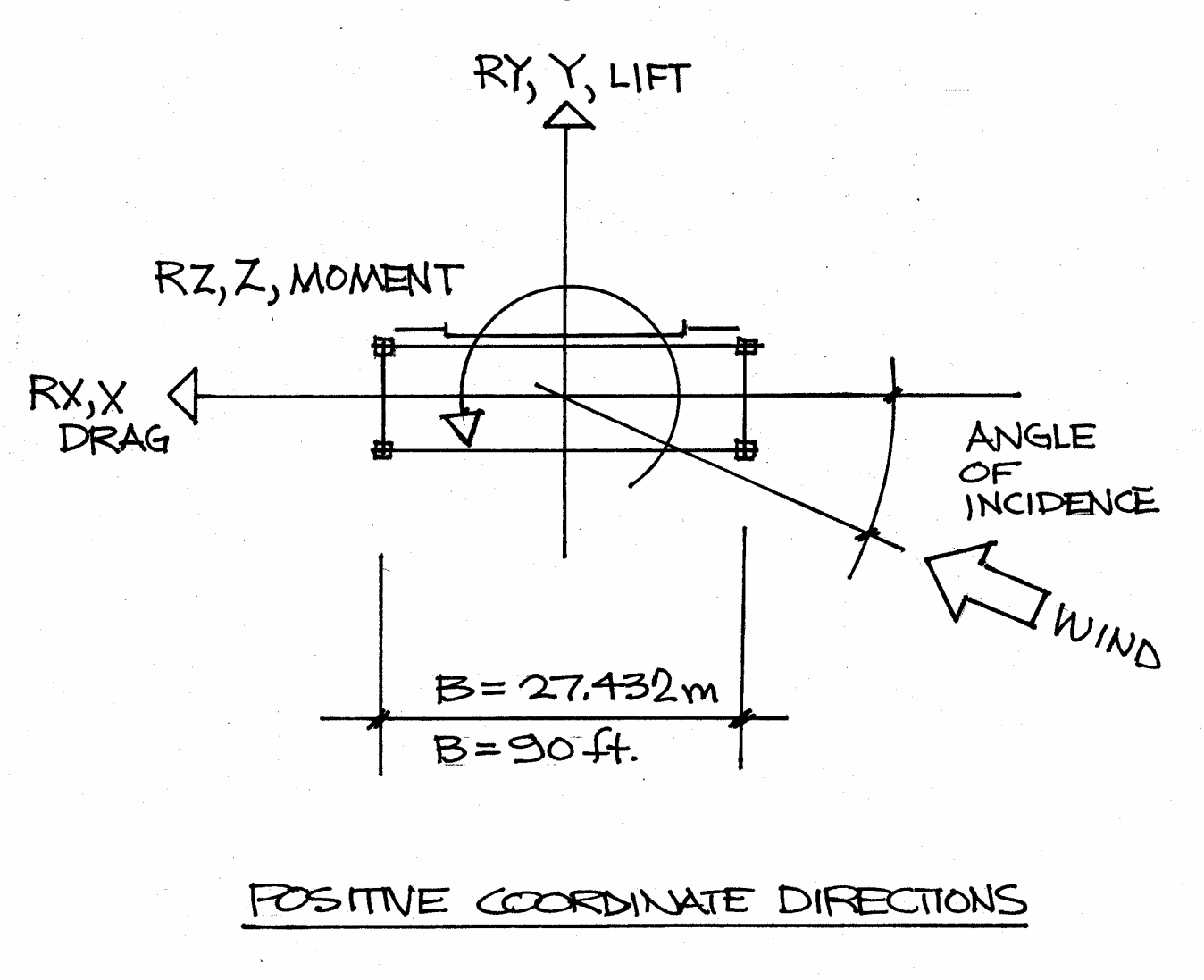
RY, Y, LIFT
RZ, Z, MOMENT
RX, X
DRAG
ANGLE
OF
INCIDENCE
WIND
B = 27.432m
B = 90 ft.
POSITIVE COORDINATE DIRECTIONS

APPENDIX 7
REFERENCES

1. Simiu, E., and Scanlan, R. H. Wind Effects on Structures, Third Edition, John Wiley & Sons, New York, 1996.

2. Raggett, J. D., West Wind Laboratory, Inc., "Section Model Wind Tunnel Studies Golden Gate Bridge Seismic and Wind Retrofit, San Francisco, California", Job No. W920421, June 1995

3. Yinghong Cao, Haifan Xiang, and Ying Zhou, "Simulation of Stochastic Wind Velocity Field on Long-Span Bridges", Journal of Engineering Mechanics, Vol. 126, No. 1, ASCE, January, 2000

4.. Xinzhong Chen, Masaru Matsumoto, and Ahsan Kareem, "Time Domain Flutter and Buffeting Response Analysis of Bridges", Journal of Engineering Mechanics, Vol. 126, No. 1, ASCE, January, 2000

5. Xie, J., Dunn, G., Irwin, P. A., Rowan Williams Davies & Irwin Inc., "Wind Tunnel Studies for the Golden Gate Bridge, San Francisco, California", Report 93-144F-5, April 20, 1994

6. British Highways Agency, Design Manual for Roads and Bridges, BD 37/01, Loads for Highway Bridges.

7. Raggett, J. D., "Stabilizing Winglet Pair for Slender Bridge Decks", Proceedings of the 6th Annual ASCE Structural Division Structures Congress, August 17-20, 1987

This report was developed by the following organizations with much support from the Golden Gate Bridge, Highway and Transportation District:

DMJM Harris
Oakland CA

Maunsell
Hong Kong China

CirclePoint
San Franciso CA

JRP Historical Consultants
Davis CA

Macdonald Architects
San Francisco CA

West Wind Laboratory
Marina CA

24 May 2007